



National Library
of Canada

Acquisitions and
Bibliographic Services Branch

395 Wellington Street
Ottawa, Ontario
K1A 0N4

Bibliothèque nationale
du Canada

Direction des acquisitions et
des services bibliographiques

395, rue Wellington
Ottawa (Ontario)
K1A 0N4

Your file - Votre référence

Our file - Notre référence

NOTICE

The quality of this microform is heavily dependent upon the quality of the original thesis submitted for microfilming. Every effort has been made to ensure the highest quality of reproduction possible.

If pages are missing, contact the university which granted the degree.

Some pages may have indistinct print especially if the original pages were typed with a poor typewriter ribbon or if the university sent us an inferior photocopy.

Reproduction in full or in part of this microform is governed by the Canadian Copyright Act, R.S.C. 1970, c. C-30, and subsequent amendments.

AVIS

La qualité de cette microforme dépend grandement de la qualité de la thèse soumise au microfilmage. Nous avons tout fait pour assurer une qualité supérieure de reproduction.

S'il manque des pages, veuillez communiquer avec l'université qui a conféré le grade.

La qualité d'impression de certaines pages peut laisser à désirer, surtout si les pages originales ont été dactylographiées à l'aide d'un ruban usé ou si l'université nous a fait parvenir une photocopie de qualité inférieure.

La reproduction, même partielle, de cette microforme est soumise à la Loi canadienne sur le droit d'auteur, SRC 1970, c. C-30, et ses amendements subséquents.

University of Alberta

**LOADING AND STRAIN DISTRIBUTION FROM OSSEOINTEGRATED
CRANIOFACIAL IMPLANTS**

By

VICTOR DEL VALLE



A thesis submitted to the Faculty of Graduate Studies and Research in partial fulfillment of the requirements for the degree of Master of Science.

Department of Mechanical Engineering

Edmonton, Alberta

Fall 1995



National Library
of Canada

Acquisitions and
Bibliographic Services Branch

395 Wellington Street
Ottawa, Ontario
K1A 0N4

Bibliothèque nationale
du Canada

Direction des acquisitions et
des services bibliographiques

395, rue Wellington
Ottawa (Ontario)
K1A 0N4

Your file *Votre référence*

Our file *Notre référence*

THE AUTHOR HAS GRANTED AN IRREVOCABLE NON-EXCLUSIVE LICENCE ALLOWING THE NATIONAL LIBRARY OF CANADA TO REPRODUCE, LOAN, DISTRIBUTE OR SELL COPIES OF HIS/HER THESIS BY ANY MEANS AND IN ANY FORM OR FORMAT, MAKING THIS THESIS AVAILABLE TO INTERESTED PERSONS.

L'AUTEUR A ACCORDE UNE LICENCE IRREVOCABLE ET NON EXCLUSIVE PERMETTANT A LA BIBLIOTHEQUE NATIONALE DU CANADA DE REPRODUIRE, PRETER, DISTRIBUER OU VENDRE DES COPIES DE SA THESE DE QUELQUE MANIERE ET SOUS QUELQUE FORME QUE CE SOIT POUR METTRE DES EXEMPLAIRES DE CETTE THESE A LA DISPOSITION DES PERSONNE INTERESSEES.

THE AUTHOR RETAINS OWNERSHIP OF THE COPYRIGHT IN HIS/HER THESIS. NEITHER THE THESIS NOR SUBSTANTIAL EXTRACTS FROM IT MAY BE PRINTED OR OTHERWISE REPRODUCED WITHOUT HIS/HER PERMISSION.

L'AUTEUR CONSERVE LA PROPRIETE DU DROIT D'AUTEUR QUI PROTEGE SA THESE. NI LA THESE NI DES EXTRAITS SUBSTANTIELS DE CELLE-CI NE DOIVENT ETRE IMPRIMES OU AUTREMENT REPRODUITS SANS SON AUTORISATION.

ISBN 0-612-06461-1

Canada

University of Alberta

Release Form

Name of Author: **Victor Raymond del Valle**
Title of Thesis **Loading and Strain Distribution from Osseointegrated
Craniofacial Implants**
Degree: **Master of Science**
Year This Degree Granted: **1995**

Permission is hereby granted to the University of Alberta Library to reproduce single copies of this thesis and to lend or sell such copies for private, scholarly or scientific research purposes only.

The author reserves all other publication and other rights in association with the copyright in the thesis, and except as hereinbefore provided neither the thesis nor any substantial portion thereof may be printed or otherwise reproduced in any material form whatever without the author's prior written permission.



Victor del Valle

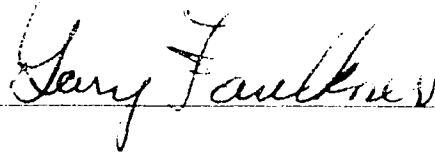
#306 12015 25 Avenue
Edmonton, Alberta
T6H-3C9

Date: July 21/95

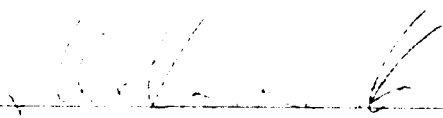
University of Alberta

Faculty of Graduate Studies and Research

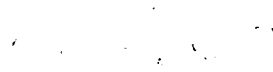
The undersigned certify that they have read and recommend to the Faculty of Graduate Studies and Research for acceptance, a thesis entitled **Loading and Strain Distribution from Osseointegrated Craniofacial Implants** submitted by **Victor Raymond del Valle** in partial fulfillment of the requirements for the degree of **Master of Science**



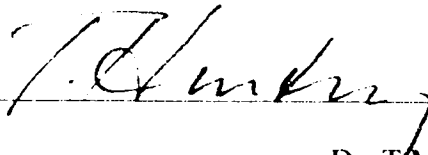
Dr. M.G. Faulkner (Supervisor)



Dr. J. Wolfaardt (Co-supervisor)



Dr. A.W. Lipsett



Dr. T.M. Hruddy

Date: July 21 / 95

To my wife Michele.

ABSTRACT

It is generally felt that the success rate of craniofacial osseointegrated implants is partially based on the loading of the implants and the resulting strain placed on the surrounding bone.

In this thesis a study of the loads placed on the implants due to the removal of the prosthesis for various attachment devices was examined. Two bar and clip, two ball and socket and five magnetic systems were examined. These results were compared with the retentive strength provided by two medical adhesives that also have been used to retain prostheses.

In addition a finite element study was done to determine how factors such as the bone configuration and implant design affect the load transfer and the state of strain in the bone. To this end three different implants designs were examined in three bone configurations with two loading conditions. The models represented typical clinical situations found in the craniofacial environment.

ACKNOWLEDGMENTS

Completing a thesis is never a one person job and I am indebted to many people for their help and encouragement.

I would like to thank Mr. Richard Hall of Technovent LTD, Leeds, England and Noblepharma Canada Inc. for supplying the materials for the experimental side of the project. I also appreciate the assistance of Mrs. Angelika Kleta-Kaden of the Dental Aesthetics Laboratory in Edmonton in setting up the experiment.

Thanks to Dr. Wolfaardt for his suggestions and comments that helped to keep my thesis on the right track. His dedication and commitment to his field will always be an inspiration. I would also like to say thank-you to the COMPRU staff at the Misericordia Hospital for their assistance.

I am also very grateful to Dr. Faulkner whose knowledge and experience is easily recognized. He not only provided me with invaluable insight and feedback on my work but also provided an enjoyable work environment with his personable nature and desire to get to know his students. I would also like to thank Al, Max, Albert, Ian, Wayne, Helen and Doris and a large number of other people employed by the university and the mechanical engineering department for their assistance.

On a personal note I would like to thank my lab mates and class mates Don, Vince, Pat, Rob, Paul and others for supplying many of the good times that are a part of completing a masters thesis. I would also like to thank my cousin Graham and my mother for suppling me with the computer at home that proved to be an valuable resource. A very special thank-you goes to my wife Michele who has been by my side from start to finish and has always provided me with love and encouragement.

Finally I would like to thank the Alberta Heritage Foundation for Medical Research for their financial support.

TABLE OF CONTENTS

	<u>Page #</u>
CHAPTER 1: INTRODUCTION	1
1.1 History	1
1.2 Craniofacial Implants: Introduction and Literature Review	2
1.2.1 Bone and Implant Integration.....	2
1.2.2 Implant Location and Bone Structure.....	3
1.2.3 Material Properties of the Bone.....	4
1.2.4 Implant Design.....	5
1.2.5 Maintaining an Osseointegrated Bond	6
1.2.6 Implant to Prosthesis Attachment.....	9
1.3 Thesis Outline	9
1.3.1 Experimental Study.....	10
1.3.2 Computer Model.....	10
CHAPTER 2: EVALUATION OF IMPLANT RETENTION SYSTEMS	12
2.1 Introduction	12
2.2 Material and Method.....	12
2.2.1 Testing Apparatus.....	13
2.2.2 Implant Retention Systems.....	17
2.2.3 Adhesive Systems	20
2.2.4 Testing procedure - Implant systems	20
2.2.5 Testing procedure - Adhesive Systems	22
2.3 Results and Discussion	22
CHAPTER 3: FINITE ELEMENT MODELS	31
3.1 Introduction	31
3.2 Background on the Finite Element Method	31

3.3 Model Parameters	37
3.3.1 The Implants.....	37
3.3.2 Loading Configurations.....	38
3.3.3 Bone Properties.....	39
3.3.4 The Bone Configurations	40
3.3.5 Boundary Conditions	43
3.4 Computer Finite Element Software	44
3.4.1 Pre-Processing	44
3.4.2 Analysis and Post Processing	46
CHAPTER 4: FINITE ELEMENT RESULTS AND DISCUSSION	49
4.1 Introduction	49
4.2 Vertical Force Axisymmetric Loading Condition	49
4.2.1 Implant design: Vertical Load	51
4.2.2 Bone Configuration: Vertical Load	54
4.2.2.1 Unicortical, Bicortical and Solid Bone Comparison.....	55
4.2.2.2 Effects of Cancellous bone for the Unicortical and Bicortical Bone Configurations.....	60
4.2.2.3 Effects of Intervening Soft Tissue	61
4.2.3 Flange: Vertical Load.....	65
4.3 Vertical Load and Moment Loading Condition	66
4.3.1 Implant Design: Force and Moment	70
4.3.2 Bone Configuration: Force and Moment	71
4.3.2.1 Unicortical, Bicortical and Solid Bone Comparison.....	71
4.3.2.2 Effects of the Cancellous Bone for the Unicortical and Bicortical Bone Configurations.....	75
4.3.2.3 Effect of Intervening Soft Tissue	79
4.3.3 Flange: Vertical load and Moment.....	79
4.3.4 Comparison of the Two Loading Conditions	83
4.4 Discussion	84

4.4.1 Examination of Stress in the Bone.....	84
4.4.2 Overall Effects of Variables.....	86
4.4.3 Discussion of Model Limitations	92
CHAPTER 5: CONCLUSION AND IMPLICATIONS	95
5.1 Conclusion	95
5.2 Implications of the Results.....	96
REFERENCES	98

LIST OF TABLES

Table 2-1:	Retention Systems and Instrument Specifications.....	18
Table 2-2:	Single Retention Point Vertical Withdrawal	23
Table 2-3:	Symmetric 3 Retention Point Vertical Withdrawal	23
Table 2-4:	Unsymmetric 3 Retention Point Vertical Withdrawal.....	24
Table 2-5:	Horizontal Pull Test in Negative X Direction	27
Table 2-6:	Horizontal Pull Test in Positive Y Direction.....	27
Table 2-7:	Horizontal Pull Test in Negative Y Direction	27
Table 2-8:	Adhesive Pull Test Results.....	28
Table 3-1:	Material Properties	40
Table 4-1:	Summary of the Maximum Tensile and Compressive Principal Strains for all of the Models Loaded with a Vertical Force.....	50
Table 4-2:	Summary of the Maximum Tensile and Compressive Principal Strains for all of the Models Loaded with a Force and a Moment.....	71

LIST OF FIGURES

Figure 1-1:	Typical Installation of Craniofacial Implants for an Auricular Prosthesis....	3
Figure 1-2:	Cross Sectional Schematic of the Bone and Implant	4
Figure 1-3:	Frost's Theory on Bone Remodeling (in micro strain).....	7
Figure 2-1:	Overall View of Testing Apparatus.....	13
Figure 2-2:	Test Bases.....	14
Figure 2-3:	Test Jigs.....	15
Figure 2-4:	Test Jig Keeper.....	16
Figure 2-5:	Symmetric 3 Retention Point Clip Activation Test for the Prefabricated Bar Jig 1.....	25
Figure 2-6:	Unsymmetric 3 Retention Point Clip Activation Test for the Prefabricated Bar Jig 1.....	26
Figure 2-7:	Average Retention Strength for the Single Retention Point Vertical Test	29
Figure 2-8:	Average Retention Strength for the Symmetric Three Retention Point Vertical Test.....	30
Figure 3-1:	Axisymmetric Element.....	33
Figure 3-2:	Dimensions of the Brånemark, Bud and IMZ Implants.....	38
Figure 3-3:	Solid Bone Configuration with the Branemark Implant	41
Figure 3-4:	Bicortical Configuration with an IMZ Implant.....	41
Figure 3-5:	Unicortical Configuration with a Bud Implant.....	42
Figure 3-6:	Boundary Conditions for the Cortical Bone.....	44
Figure 3-7:	3-D Element Mesh for the Solid Bone Configuration for the Brånemark Implant.....	45
Figure 3-8:	Cylinder Under Pure Shear	48
Figure 4-1:	Minimum Principal Strain Distribution of the Brånemark Implant in Solid Bone.....	52
Figure 4-2:	Maximum Principal Strain Distribution for the Brånemark Implant in	

	Solid Bone.....	52
Figure 4-3:	Minimum Principal Strain Distribution of the IMZ Implant in Solid Bone	53
Figure 4-4:	Minimum Principal Strain Distribution for the Bud Implant in Solid Bone.....	53
Figure 4-5:	Maximum Magnitude of Minimum Principal Strain for the Vertical Force Loading Condition	56
Figure 4-6:	Minimum Strain Distribution for the Bud Implant in Unicortical Bone with a Vertical Load.	56
Figure 4-7:	Radial Strain Distribution for the Brånemark Implant with a Vertical Load in Solid Bone.....	57
Figure 4-8:	Hoop Strain Distribution for the Brånemark Implant with a Vertical Load in Solid Bone.....	57
Figure 4-9:	Vertical Strain Distribution for the Brånemark Implant with a Vertical Load in Solid Bone.....	58
Figure 4-10:	Radial Strain Distribution for the Brånemark Implant with a Vertical Load in Unicortical Bone.....	58
Figure 4-11:	Hoop Strain for the Brånemark Implant with a Vertical Load in Unicortical Bone.....	59
Figure 4-12:	Vertical Strain Distribution for the Brånemark Implant with a Vertical Load in Unicortical Bone.....	59
Figure 4-13:	Display of General Areas of Radial and Hoop Compression and Tension using the IMZ Implant in Unicortical Bone (Displacement exaggerated).....	62
Figure 4-14:	Evaluation of the Impact of Cancellous Bone for the Unicortical Bone Configuration, the Vertical Loading Condition and the Three Implant Types.	62
Figure 4-15:	Evaluation of the Effects of Cancellous Bone for the Bicortical Bone Configuration, the Vertical Load Loading Condition and the Three Implant Types.....	63

Figure 4-16: Minimum Principal Strain for the Brånemark Implant with a Vertical Load in the Bicortical and an Air Space Bone Configuration.....	63
Figure 4-17: Minimum Principal Strain for the Brånemark Implant with a Vertical Load in the Bicortical and Cancellous Bone Configuration.....	64
Figure 4-18: Evaluation of the Effects of Soft Tissue on the Minimum Principal Stress for the Solid Bone Configuration and the three Implants with a Vertical Load.....	64
Figure 4-19: Evaluation of the Effects of Soft Tissue on the Minimum Principal Strain for the IMZ Implant in three Different Bone Configurations.....	67
Figure 4-20: Minimum Principal Strain for the Bud Implant in Solid Bone with Soft Tissue and the Vertical Force Loading Condition.....	67
Figure 4-21: Comparison of the Minimum Principal Strain for the three Implants in Solid Bone with a Vertical Load with and without the Flange	68
Figure 4-22: Comparison of the Minimum Principal Strain for the three Implants in Bicortical Bone with a Vertical Load with and without the Flange	68
Figure 4-23: Comparison of the Minimum Principal Strain for the Three Implants in Unicortical Bone with a Vertical Load with and without the Flange	69
Figure 4-24: Minimum Principal Strain for the Brånemark Implant in Solid Bone with a Vertical Load and No Flange	69
Figure 4-25: Sample View of the Finite Element Mesh of Cortical Bone for the Brånemark Implant in Solid Bone.....	72
Figure 4-26: Sample View of the Finite Element Mesh of Cortical Bone for the Bud Implant in Bicortical Bone.....	72
Figure 4-27: Sample View of the Finite Element Mesh of Cortical Bone for the Bud Implant in Bicortical Bone	73
Figure 4-28: Minimum Principal Strain for the Three Implants in the Three Bone Configurations for the Force and Moment Loading Condition.....	73
Figure 4-29: Minimum Principal Strain for the Brånemark Implant in Solid Bone with the Force and Moment Loading Condition.....	74

Figure 4-30: Minimum Principal Strain for the Bud Implant in Solid Cortical Bone with a Force and Moment Loading Condition.	74
Figure 4-31: Minimum Principal Strain for the IMZ Implant in Solid Cortical Bone with a Force and Moment Loading Condition.	76
Figure 4-32: Minimum Principal Strain for the IMZ Implant in Bicortical Bone with a Force and Moment Loading Condition.....	76
Figure 4-33: Minimum Principal Strain for the IMZ Implant in Unicortical Bone with a Force and Moment Loading Condition.	77
Figure 4-34: Displacement of the Bicortical Bone with an IMZ implant and a force and moment loading condition with regions of compression (-) and tension (+) highlighted. (Scale Exaggerated by a 1000).....	77
Figure 4-35: Radial Strain for the Brånemark Implant in Bicortical Bone with a Force and Moment Loading Condition.	78
Figure 4-36: Hoop Strain for the Brånemark Implant in Bicortical Bone with a Force and Moment Loading Condition.	78
Figure 4-37: Vertical Strain for the Brånemark Implant in Bicortical Bone with a Force and Moment Loading Condition.....	80
Figure 4-38: Minimum Principal for the Brånemark Implant in Bicortical Bone with Cancellous and a Force and Moment Loading Condition.....	80
Figure 4-39: Soft Tissue Comparison for the IMZ Implant in the three Bone Configurations for the Force and Moment Loading Condition.....	81
Figure 4-40: Comparison of the Minimum Principal Strain with and without the Flange for the Three Implants in Solid Bone with the Force and Moment Loading Condition.....	81
Figure 4-41: Comparison of the Minimum Principal Strain with and without the Flange for the Three Implants in Bicortical Bone with the Force and Moment Loading Condition.....	82
Figure 4-42: Comparison of the Minimum Principal Strain with and without the Flange for the Three Implants in Unicortical Bone with the Force and Moment Loading Condition.....	82

Figure 4-43: Minimum Principal Strain for the Brånemark Implant in Solid Bone with the Flange Removed for the Force and Moment Loading Condition.	85
Figure 4-44: Vertical Stress for the Brånemark Implant in Bicortical Bone with the Flange in Contact and the Vertical Force only Loading Condition	85
Figure 4-45: Von Mises Stress Picture for the Brånemark Implant in Bicortical Bone with a Cancellous Bone Layer and the Force and Moment Loading Condition.	88
Figure 4-46: Axial Stress Placed on a Beam in Pure Bending	88
Figure 4-47: Minimum Principal Strain for the Modified Bud Implant in Solid Bone with the force and Moment Loading Condition	91
Figure 4-48: Minimum Principal Strain for the 5.0 mm diameter (at the neck) Brånemark Implant in Solid Bone with a Force and Moment Loading Condition	91

1. INTRODUCTION

1.1 History

The absence or loss of part of the face may cause functional disability as well as serious emotional stress for individuals who may feel alienated and reclusive due to their loss. Medical professionals have tried to aid patients that have suffered such a loss by providing them with a prosthesis that attempts to functionally and aesthetically replace the missing facial structure. The success of such devices depends on the design of the prosthesis and the method used to retain the prosthesis. In the past, inadequate methods of retaining facial prostheses and inferior prosthesis design resulted in a poor success rate for this form of treatment. In the 1960's silicone elastomers were first used in facial prostheses and they greatly improved the appearance of the prosthesis not only in shape but color as well. To the casual observer a properly constructed silicone facial prosthesis is almost indistinguishable from a real facial part. Initially these silicone prostheses were attached to the face using extrinsic mechanical retention (such as attaching the prosthesis to spectacle frames) or by using medical adhesives that attached the prosthesis directly to the face. Having the prosthesis attached to spectacle frames was not an ideal solution because it often provided poor retention, was inconvenient to the patient and was aesthetically compromising. Adhesives were also not an ideal way of attaching the prosthesis to the face since they were often unreliable and unpredictable in the retention

that they provided to the prosthesis. In addition the adhesives had to be applied daily and would often caused irritation of the skin especially where the tissue had been exposed to therapeutic radiation. Furthermore the adhesives and solvents often damaged the prosthesis and reduced its durability.

In the early 1950's experimental work began on the technique of using tissue integrated prostheses. The initial clinical applications for the technique occurred in the area of dentistry. In this application titanium screws were implanted into the jaw bones and used to anchor bridges and dentures for edentulous or partially edentulous patients. In 1979 this bone anchoring technique was applied to craniofacial (skull and face) applications. Missing facial parts could now be replaced with silicone prostheses that attached to the face with the use of craniofacial implants. This provided a more reliable and predictable method of facial prosthesis retention.

1.2 Craniofacial Implants: Introduction and Literature Review

1.2.1 Bone and Implant Integration

The success of permanent hard tissue integrated implants depends largely on the type of interface that is developed between the implant and the bone. The ideal type of interface for long term implant success has been termed *osseointegration* where osseointegration has been defined as the direct structural and functional connection between ordered, living bone and the surface of a load carrying implant [1]. This type of interface is remarkably strong and it has been shown that the bone near the implant would fail before the interface between the bone and implant. Other interfaces such as a fibrous

tissue interface, which is typified by a growth of fibrous material between the implant and the bone, has also been observed to occur clinically. It is generally accepted that this type of interface is inferior to the osseointegrated type interface and usually indicates impending loss of the implant. It is therefore desirable for the implant and the biological and mechanical conditions at the implant site to promote an osseointegrated interface.

1.2.2 Implant Location and Bone Structure

Currently craniofacial implants have been successfully placed in several locations on the skull and face. Typical sites include the orbital area (around the eye), the mastoid region (behind the ear) and the nasal region. Figure 1-1 displays a schematic of a typical

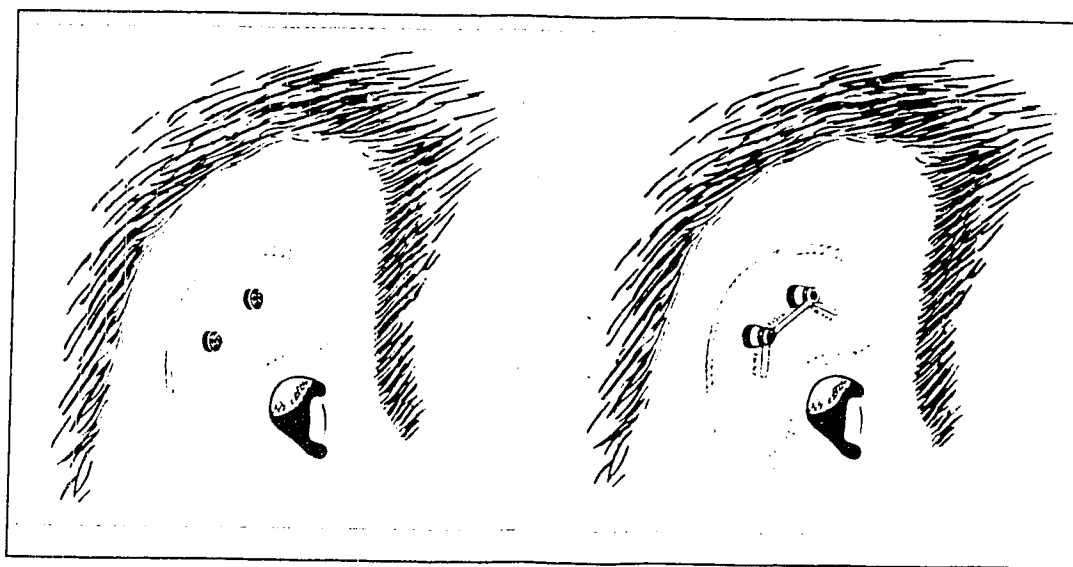


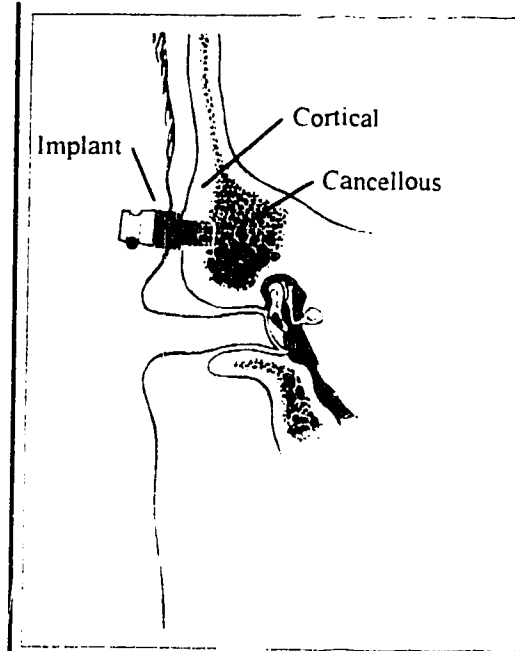
Figure 1-1: Typical Installation of Craniofacial Implants for an Auricular Prosthesis

installation for a patient missing the external ear. The two implants shown on the left side of this figure are placed in the mastoid region of the skull. The right side of the figure displays the implants connected with a gold bar that would be used to attach the prosthesis. The bone in the various implant regions on the face and skull can differ

substantially for the same patient and between patients. Figure 1-2 displays a cross sectional schematic view of an implant and the bone in the mastoid region. This example

shows the implant embedded in a solid cortical bone layer, where cortical bone is the stiff and compact outer tissue of a bony structure.

Depending on the patient and the location, the thickness of this layer could vary from approximately 2 mm to 5 or 6 mm. Therefore in clinical applications it is possible for the implant to pass through the first cortical layer and have the end of the implant protrude into



the cancellous bone region. Cancellous or trabecular bone is the porous inner bone layer

Figure 1-2: Cross Sectional Schematic of the Bone and Implant.

that is composed of various individual trabecular plates and rods. Also, there are bone structures that would cause the implant to pass through the first cortical bone layer and a thin cancellous layer and engage a second cortical layer. Therefore there are three general cortical bone configurations that can be present at an implant site, a solid, a single plate or unicortical, and a two plate or bicortical configuration. These three general configurations could, however, have a large number of various bone layer thickness for the cortical and cancellous bone depending on the patient and location.

1.2.3 Material Properties of the Bone

As indicated above there are two general types of bone, cortical bone and cancellous bone, that are present in the craniofacial environment. Cortical bone is the solid outer layer bone which provides the strength and rigidity for the skeleton. The elastic symmetry of cortical bone is based on the textural symmetry and geometry of the bone structure. For example the long bones of the leg develop a transversely isotropic structure with a higher stiffness and strength in the longitudinal direction. As a result the elastic properties can vary from individual to individual and for different locations within one person.

While cortical bone is known to be a viscoelastic material, however it has often been considered as a linear elastic isotropic solid for the purpose of quasi-static stress analysis [2]. Measured values for the stiffness of cortical bone have varied considerably but an approximate value found in the literature has a modulus of 14.0 GPa [2] [3][4][5][6].

Cancellous bone which is the porous type of bone has very different material properties. There is much less known about the material properties of cancellous bone as opposed to cortical bone. The individual trabecular rods and plates that make up cancellous bone are aligned in a complex type structure with various structural densities. Currently there are theories that relate the elastic modulus and shear modulus of cancellous bone to the density of the bone structure. A typical value of 0.5 GPa is used for the stiffness of cancellous bone[5].

1.2.4 Implant Design

Currently there are a large number of choices for the type and size of implants to use. The implants vary in their thread design, diameter, length and surface treatment. It may be postulated that all of these variables could affect the biological and mechanical state of the bone-implant interface. Typically the choice of material properties of the implant is restricted as only certain materials have been found to osseointegrate with the bone[1]. Large variations in the thread design including those which appear to be mechanical bolt threads, rounded or rectangular threads and no threads have been developed. The designers of these implants promises an improved osseointegration with bone. Manufacturer's of implants will also usually provide them in a variety of lengths (from 3 mm - 20 mm or longer) and sometimes offer them in a variety of diameters (approximately 3 mm - 6 mm)

1.2.5 Maintaining an Osseointegrated Interface

The osseointegrated interface is commonly considered the ideal type of interface to have between the bone and implant and the success of maintaining an implant retained prosthesis depends upon the integrity of the bone-implant interface. There are a number of biological and physiological factors, many of which are still unknown, that determine the success of the osseointegrated interface. The biocompatibility of implant materials, the physiology of the bone, the health and lifestyle of the patient and the mechanical loading on the implant are a few of the factors that may influence the success of the bone-implant interface. The loading at the interface is believed to be a major influence in the development and maintenance of osseointegration.

There are many theories that attempt to predict bone growth or resorption (bone loss) based on the mechanical stress or strain in the bone. For example Frost proposed a theory that attempts to relate the strain placed on the bone to the increase or loss of bone[7]. This theory suggests that there are ranges of strain that promote bone growth, loss and equilibrium. As shown in Figure 1-3 the strain range from -200 to 200 microstrain promotes bone loss while the ranges of -200 to -2500 microstrain

Over Load	Formation	Equilibrium	Resorption	Equilibrium	Formation	Over Load
	-3000	-2500	-200	200	1500	?

Figure 1-3: Frost's Theory on Bone Remodeling (in microstrain)

(compressive) and 200 to 1500 microstrain (tensile) are believed to be an equilibrium state while strains from -2500 to -3000 and above 1500 microstrain promote bone formation. The theory also states that there exists a pathological overload zone for excessively high magnitudes of strains. This is a rather simple theory that predicts some of the bone responses for certain loading conditions but not all responses. Many other theories have expanded upon this basic idea but none of them to date are able to predict all of the clinical responses observed. Most of the theories seem to agree that it is the strain and not the stress that determines the remodeling response of the bone. The theories disagree on what type of strain is the most significant, i.e. the principal strain, the strain energy density, the sum of the principal strains, etc.. In addition these theories are for a general response of bone under loading and are rarely applied to the craniofacial region or the bone implant interfaces. The theories do provide some useful insight into how mechanical straining due to implant loading may influence local bone formation or

resorption. It is believed that local bone resorption and the loss of osseointegration eventually leads to a loss of the implant.

Currently there are a number of finite element models that deal with the loading on bone anchored implants for dental applications. These types of models are only of limited use for craniofacial applications as the bone structure and implant length used vary substantially. Rieger et al. examined various bone anchored implants in solid cortical bone type configurations [6][8]. These dental implants were much longer (7 mm or more) than what is normally used in craniofacial applications. Also, these studies were limited to only vertical loading on the implant and used bone thickness and boundary conditions that would not be appropriate for craniofacial applications. Other studies have examined dental implants with other types of loading and bone structures. Clelland et al. examined the stress on solid cortical bone due to an implant that is loaded with a force and moment [9]. This study, however, also used an implant with a length of 6 mm and a bone thickness which is more applicable to dental situations. Other studies include a model by Matsushita et al. that examined dental implants loaded with a vertical and a lateral force placed in a cortical and cancellous bone model of the mandible (lower jaw) [10]. This study was useful in that it provided a bone configuration that was more indicative of what might occur clinically but again was focused on the dental application. A study by Hoshaw et al. examined a finite element and experimental model of dental implants placed in the tibia of a dog [3]. This examined the formation of the bone around implants that were subjected to experimental loading. The results were compared to a finite element

model, however, only vertical loading with one type of implant and bone configuration was examined.

1.2.6 Implant to Prosthesis Attachment

Once the implants provide a base the three general mechanisms used to attach a prosthesis to the implant are a ball and socket, a magnet and keeper and a bar and clip. For the ball and socket arrangement a small metal ball is affixed to the implant and a socket is attached to the prosthesis. The ball snaps into the socket and the prosthesis is held firmly in place. In a similar manner the magnetic systems have magnet secured to the prosthesis and a magnetic or ferromagnetic keeper fastened to the implant. The bar and clips arrangements are slightly different, in that the prosthesis is not fastened directly onto the implants but rather onto a bar that is attached to the implants (as shown in Figure 1-1). The clips are attached to the back of the prosthesis and fit firmly around the bar. Usually two or more implants are used to attach a single prosthesis and a mixture of the various retention systems can be used. Details on these attachments and their retentive strengths have been described by del Valle et al.[11].

1.3 Thesis Outline

The objective of the present study was firstly to improve the understanding of the mechanical loads which are typically applied to craniofacial implants and secondly how these loads are carried by the hard tissue. To this end an experimental study was performed in a attempt to ascertain the loading that is placed on the implant through the

removal and attachment of a typical auricular prosthesis. In addition a finite element computer analysis was performed of the bone and implant to examine how these loads are carried by the bone in several situations which are believed to approximate those encountered in craniofacial osseointegrated reconstruction.

1.3.1 Experimental Study

For the experimental study, outlined in Chapter 2, nine different mechanisms for attaching prostheses to implants were investigated. The study sought to classify the retentive strength of each of the mechanisms. Each of the devices was tested as a single unit and as a functional group that would be typical of a standard clinical application. To date there has been little work done to classify the various strengths of the retentive systems. This work is necessary to determine the magnitudes of loads that would pass from the implant to the bone. Since the use of adhesives to attach facial prosthesis has been criticized for its poor retention strength and consistency, the present study also compared the retentive strength placed on a prosthesis for the various implant systems with two commonly used medical adhesives. The testing of the adhesives followed previous work by Tam et al. [12][13]. The results of this study can be compared to the loading applied to osseointegrated implants in the oral environment. Glantz et al. found that during mastication that the experimental peak loads on dental implants reached to about 25 N [14].

1.3.2 Computer Model

The second part of the study involved modeling the bone and implant to determine how forces placed on the implant are transferred to the bone. Previous studies did not include any work on craniofacial osseointegrated implants and examined a limited number of loading conditions and/or bone configurations. In the current work the strain distribution in the bone was examined for a number of purely craniofacial applications. For this reason two different loading conditions, three implant types and three different general bone configurations were examined. It was hoped that by performing a large number of variations with a computer model that general relationships between implant design and bone strain for craniofacial bone configurations could be developed. The details of the finite element modeling are given in Chapter 3 while the results are given and discussed in Chapter 4.

2. EVALUATION OF IMPLANT RETENTION SYSTEMS

2.1 Introduction

In this chapter the retentive strengths of the superstructure of the various systems which have been designed to attach the prosthesis to the implants is examined. While it is difficult to predict or design for various accidental loading situations on the implant, it is useful to appreciate the loads occurring during normal removal and placement of the prostheses. This information is important in the evaluation of the loads being applied through the implants to the underlying hard tissue. Also, to appreciate some of the differences associated with retaining prostheses with implants as compared to adhesives, an evaluation of some currently used facial prosthetic adhesives was conducted.

2.2 Material and Methods

The evaluations included nine different mechanical and magnetic retention systems which have been used in conjunction with craniofacial osseointegration implants as well as two facial prosthetic adhesives.

2.2.1 Testing Apparatus

The loading/measuring apparatus used was a custom built system which was modified from one originally designed to measure both tensile and shearing strengths of

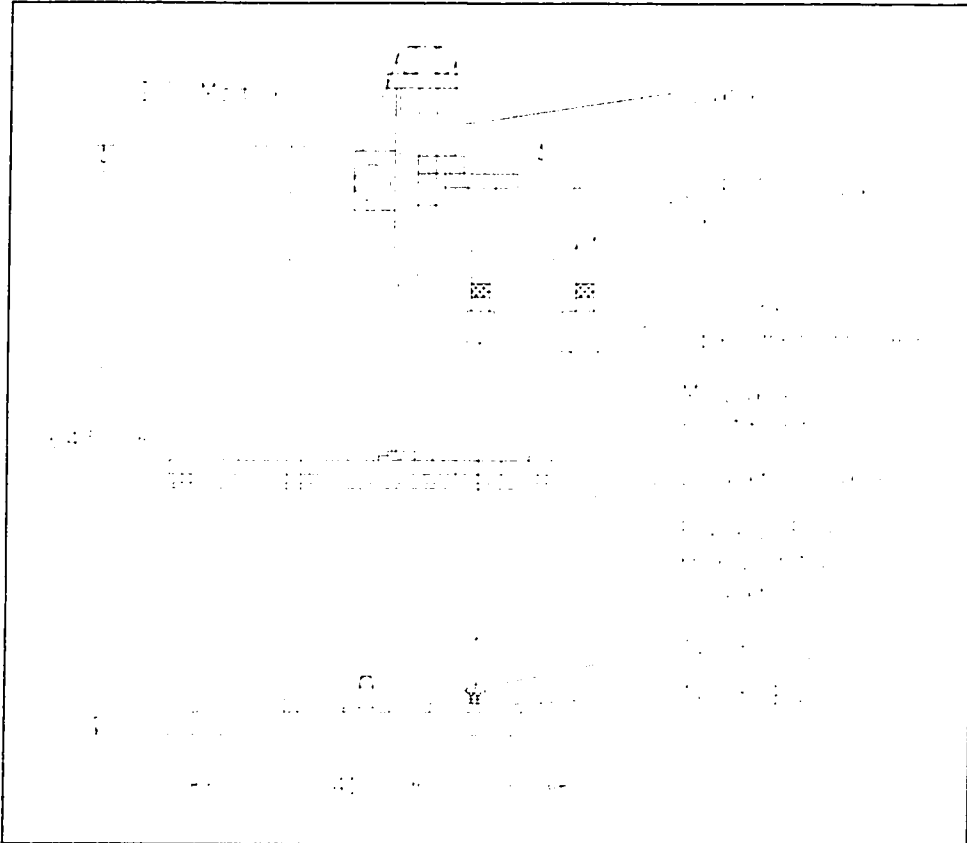


Figure 2-1: Overall View of Testing Apparatus

biomedical adhesives [12]. The system is shown schematically in Figure 2-1. The evaluation of the implant retention systems was accomplished in vitro using a series of test bases and test jigs. The plexiglass test bases, shown in Figure 2-2, simulating the bone or skull, was secured to the apparatus base and had Brånemark 4.0 mm flange fixtures mounted in it. The retention system to be evaluated was constructed on these fixtures. The test jig, simulating the prosthesis, attached to the implants by means of the retention

system. The loading of the system was accomplished through the use of the DC motor, cable and pulley system which applied upward force to the test jig. The variable speed DC

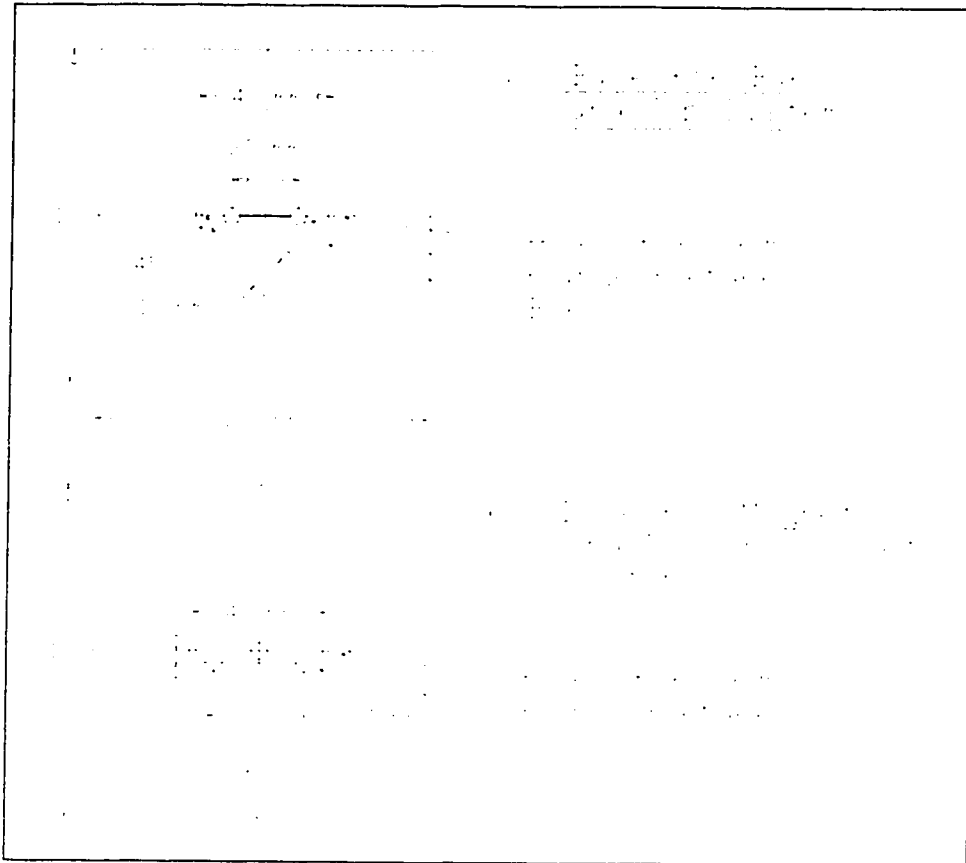


Figure 2-2: Test Bases

motor was set to provide a testing speed of between 28 to 44 mm/min.

The test jigs, shown in Figure 2-3, permitted the loading to be applied at any one of four locations including directly above the center retention point as well as horizontal loads in the negative x direction or in either the positive or negative y direction. For certain cases of the vertical loading, the test jig was held in a keeper, displayed in Figure 2-4, which was in turn loaded by the motor drive. The keeper was used so that the loading point could be placed either at the centroid of the three retention points to allow

symmetric loading or 17 mm to the left of the centroid to provide an unsymmetric loading condition. In all cases the loading cable was attached to the jig or keeper by means of a simple hook to allow the retention mechanism to be self-aligned.

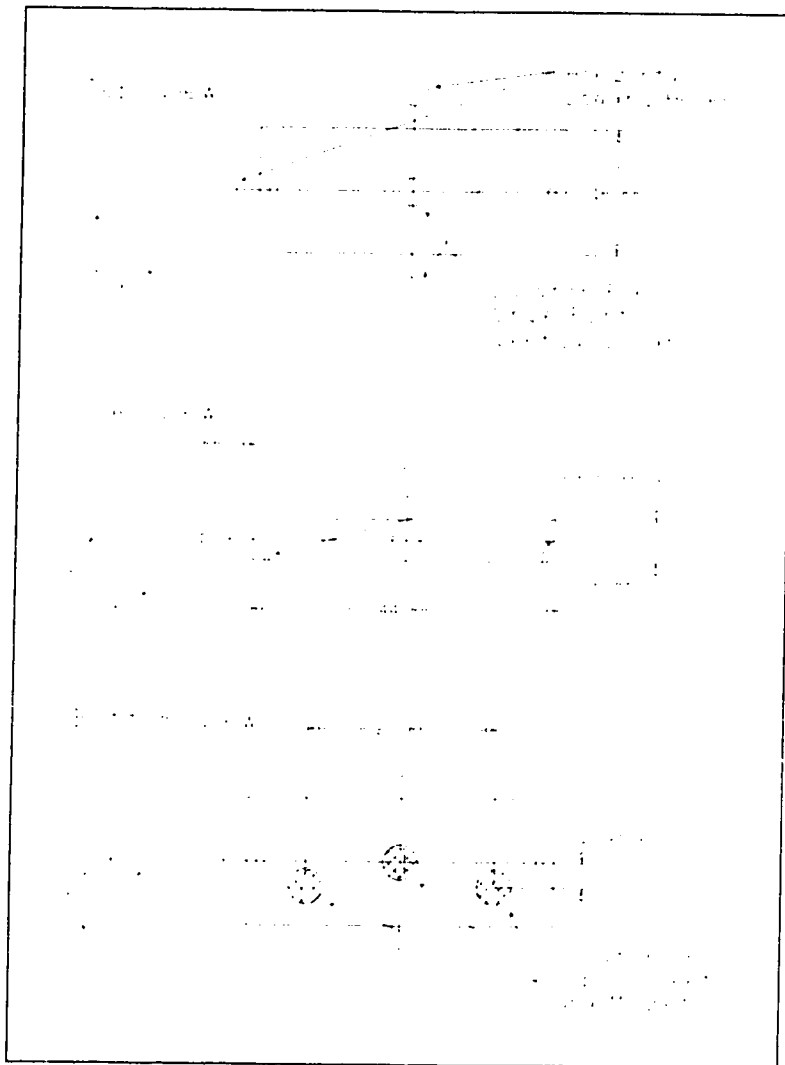


Figure 2-3: Test Base

As described, the test jigs could also be loaded horizontally to simulate the removal of a prosthesis using a shearing force. This horizontal loading was accomplished by mounting pulleys to the apparatus base as shown schematically in Figure 2-1. This capability was only used for the magnetic retention systems.

The measurement of the loads was done using an Omega LCF-5 (Omega Engineering Inc. One Omega Drive, Box 4047, Stamford, CT 069078-0047) miniature tension/compression load cell which had a 0-22 Newton range. When the loads required

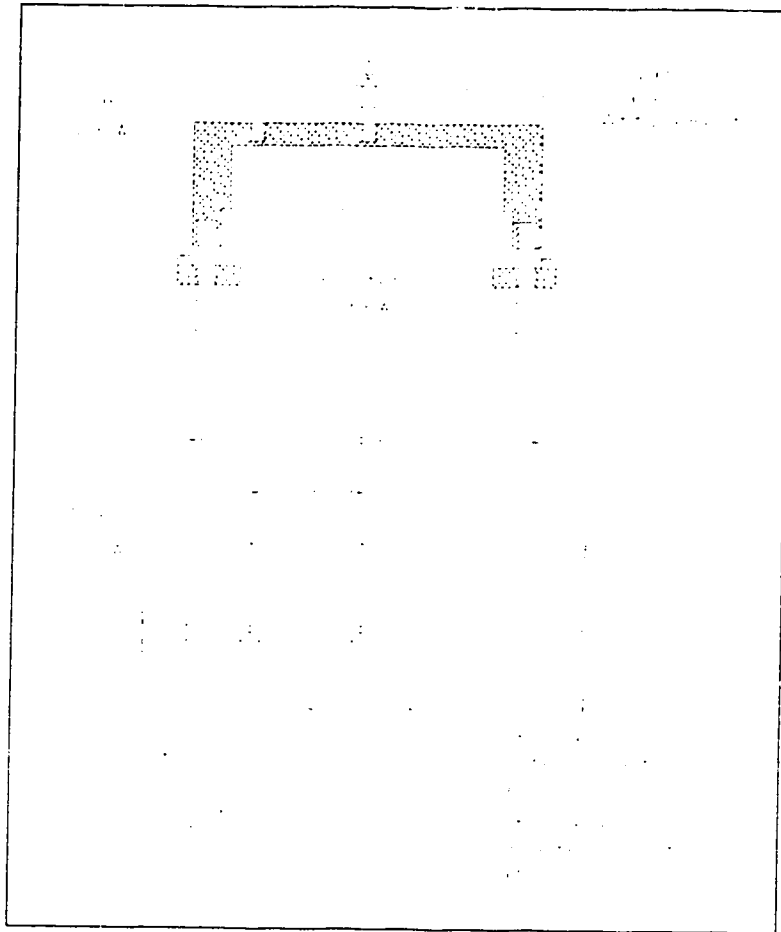


Figure 2-4: Test Jig Keeper

to remove the test jig went beyond the capacity of the load cell a pulley system which provided a mechanical advantage of 2 was used. The strain gauge load cell was monitored using a custom built signal conditioner and an Omega Model 585 (Omega Engineering Inc. One Omega Drive, Box 4047, Stamford, CT 06907-0047) strip chart recorder. This allowed a continuous record of the loads to be made.

For the evaluation of the retention loads of the adhesives, the loading apparatus was modified to use a silicone specimen holder at the bottom of the load cell, as shown in Figure 2-1. The conically shaped silicone prosthesis specimen provided a 5 mm wide annulus at an average diameter of 27.5 mm over which the adhesive could be applied. For these tests the test base and jigs were removed to provide direct access to an area of the skin. The prosthesis was then applied to the skin and loaded in the same manner as the implants.

2.2.2 Implant Retention Systems

The details of manufacture and model of the nine different mechanical and magnetic systems used in conjunction with the implants are given in Table 1. These include the two ball and socket systems (A & B), two bar and clip systems (C & D) and five magnetic systems (E, F, G, H & I). To rationalize the variations in these systems, four test bases, two of each of those shown in Figure 2-2 were made with the Brånemark flange fixtures (SEC 002) mounted in the positions indicated. The ball and socket systems were used in conjunction with one of the test bases using three flange fixtures (Figure 2-2 b). The attachments connected to these fixtures were Nobelpharma 4.0 mm ball attachment abutments for the Nobelpharma system (Table 1, B) and Dalla Bona 3.0 mm ball abutments for the Dalla Bona system (Table 1, A).

The bar and clip systems (Table 1, C and D) were developed on the two test bases shown in Figure 2-3a which used only two Brånemark flange fixtures. Both of these systems used Brånemark 4.0 mm craniofacial fixture abutments (SEC 008) which secured the gold bars configured as shown in the figure.

Table 1: Retention Systems and Instrumentation Specifications

Label	Type	Model	Supplier	Comments
A1	Dalla Bona Ball and Socket (unactivated)	42-43020 3 mm size	Swiss NF Metals Inc.	(1) (3)
A	Dalla Bona Ball and Socket (activated)	42-430230 3 mm size	Swiss NF Metals Inc.	(1) (3)
B	Nobelpharma Ball Attachment and Socket	SDCA 116 4 mm size	Nobelpharma Canada Inc.	(2) (4)
C	Nobelpharma Overdenture Bar (Gold Bar) and Clips (unactivated)	DCA 110	Nobelpharma Canada Inc.	(2) (4)
D	Nobelpharma Overdenture Bar (Plastic Bar) and Clips (unactivated)	DCA 130 Bar cast with type 4 Gold	Nobelpharma Canada Inc.	(2) (4)
E	Dynamag Magnets	99-20026 Medium	Swiss NF metals Inc.	(2) (3)
F	Neomag Magnets	71-361015 Medium	Swiss NF metals Inc.	(2) (3)
G	Neo-maxi Magnets	#M4	Innovadent Technics Ltd.	(2) (5)
H	Neo-midi Magnets	#M3	Innovadent Technics Ltd.	(2) (5)
I	Neo-mini Magnets	#M1	Innovadent Technics Ltd.	(2) (5)
J	Pros-Aide Adhesive	-----	ADM Tronics, Inc.	(6)
K	Hollister Medical Adhesive	-----	Hollister Incorporated	(7)

(1) For all ball and socket systems 4.0 mm flange fixtures were used. The abutments for the Nobelpharma ball attachments were 4.0 mm abutments (SDCA 116) while the abutments used for the Dalla Bona were 3.0 mm abutments (420430230). The tool used for Dalla Bona is an activator/deactivator for the Dalbo Anchor, Cendres and Métaux SA, Biel Bienne, Switzerland

(2) For the bar and clips systems and the magnetic systems, 4.0 mm flange fixtures (SEC 002) and 4.0 mm craniofacial abutments were used. These components were supplied by Nobelpharma Canada Inc.

(3) Swiss NF Metals Inc, P.O. Box 644 Station B, Willodale, Ontario, Canada, M2K 2P6

(4) Nobelpharma Canada Inc, 284 Consumers Road, Willodale, Ontario, Canada, M2J 1P8

(5) Innovadent Technics Ltd., 26 Primley Park Mount, Leeds, England, LS17 7JS

(6) ADM Tronics Inc, Northvale, New Jersey, USA

(7) Hollister Incorporated 200 Hollister Drive Libertyville, Illinois, U.S.A. 60048

The six magnetic systems were all used in conjunction with the second test base that had three flange fixtures (Figure 2-3b) connected to Nobelpharma Standard 4.0 mm abutments.

The test jigs which corresponded to each of the bases held either three sockets (Table 1, A and B), three clips (Table 1, C and D) or three magnets (Table 1, E - I). The jigs and bases were kept in alignment for mounting these retention points using the alignment hole and shims shown in Figures 2-2 and 2-3. The mounting of the retentive components on the jigs and the bars was carried out by a dental laboratory (Dental Aesthetics Laboratory, Edmonton, Alberta).

The three clips for systems C and D (Table 1) were aligned so that one attached to the midpoint of the bar while the other two engaged the 45° wings (Figures 2-2a). These clips were all positioned so that their centers corresponded to the locations of the abutments of the ball and socket and magnetic systems. This meant that the three retention points for all nine systems were placed in the same relative positions. In order to evaluate intrasystem variability, three jigs were constructed for each of the retention systems. Because of the positions of the retention points, it was also possible to test a single clip, ball and socket or magnet by simply reversing the test jig and engaging the center component only.

These systems, including the common three retention points, were chosen as being representative of an installation for auricular reconstruction. By having all systems with three retention points allowed for comparisons between them.

2.2.3 Adhesive Systems

The two adhesives tested (Table 1, J and K) were Pros-Aide and Hollister Medical Adhesive. The adhesive was applied between the silicone specimen with a contact area of 432.6 mm² and the shaved inner forearm of five subjects. Each adhesive was applied according to manufacturer's specifications and tested five times for each adhesive on each of the five individuals for a total of 50 tests. Each test used a different silicone specimen placed onto a new skin site to help ensure that the tests were independent.

To develop a means for comparing the loads measured for the implant and adhesive retention systems, the bond area for a typical replacement ear was evaluated. The base perimeter of 10 adult male ears was measured and the bond area of a typical prosthesis was estimated to be 1200 mm². This meant that the silicone test specimens had 432.6/1200 or approximately one-third the bond area of a typical adult male ear prosthesis.

2.2.4 Testing Procedure - Implant Systems

For each system, the retentive strength was measured by pulling the jigs from the test base in the vertical direction in three different modes. First, with only the center socket, clip or magnet engaged, data was collected for a single retention point. Secondly all three retention points were engaged and pulled from the centroid of the three units. A third series of tests was done in which the loading point of the jig was placed at a position 17 mm in the negative x-direction from the centroid of the three units (see Figure 2-4). These were termed the unsymmetric vertical tests.

Each of the jigs was tested 20 times for each of the loading scenarios above and for each retention system considered. This meant that there was a total of 60 tests (3 jigs tested 20 times each) conducted for each system and for each loading situation.

For the magnetic systems only, a further series of tests in which the jig was subjected to a horizontal forces was done. Each jig was pulled in the negative x direction (Figure 2-3) and in both the positive and negative y directions. Again each system, jig and loading direction was evaluated 20 times.

All of the systems were initially tested in the condition received from the manufacturer. However, as the mechanical systems are normally activated before being installed, an attempt was made to understand the influence this activation has on the retentive forces produced. For the Dalla Bona ball and socket, the activation was accomplished using the tool supplied (Dalbo Anchor, Table 1). This system (Table 1.A) was then evaluated in the same manner as the unactivated case (Table 1, A1). The bar and clip systems had no standard activation procedure, so a series of tests was done using the Nobelpharma prefabricated bar and clip (Table 1, C) at various amounts of activation. In particular, the clips were activated by first installing them over the bar and then closing the ends by approximately 0.15 mm. The retentive force was then evaluated 90 times to first determine the change in force level and second to evaluate the degradation which might occur due to creeping or fatigue in the clips. These 90 tests were done both for the symmetric and the unsymmetric pull tests. A similar series of tests was done for the cast bar and clip (Table 1, D) as well.

2.2.5 Testing Procedure - Adhesive Systems

For the adhesive tests, the silicone specimen prosthesis was attached to the shaved inner forearm of the subjects. The skin surface was prepared with ethyl alcohol prior to applying the adhesive. The procedure of skin loading with the adhesive used was as described by Wolfaardt et al. [13]. Each individual had five tests done with each adhesive. For each measurement a new silicone specimen and area of skin was used.

The force necessary to break the adhesive bond was measured in the same manner as was done for the implant based systems.

2.3 Results and Discussion

The results of the three vertical load testing configurations are shown in Tables 2, 3 and 4 for the mechanical and magnetic systems evaluated. This includes the results for a single retention point (Table 2), three retention points symmetrically withdrawn (Table 3) and three retention points unsymmetrically withdrawn (Table 4). For the Dalla Bona system all the tables include results for the as received case (A1) and the case in which the attachment was activated using the manufacturer's tool (A). The average value for each of the three jigs tested for each system are shown along with the standard deviation (σ) for the 20 tests done on each jig. The final mean value shown is for all three tests on a particular system along with the 95% confidence interval on this mean.

Table 2: Single Retention Point Vertical Withdrawal

	Retention System	Jig #1 Force (N) $\pm\sigma$	Jig #2 Force (N) $\pm\sigma$	Jig #3 Force (N) $\pm\sigma$	Average Force (N) with 95% confidence interval
A1	Dalla Bona B & C	7.87 \pm 0.67	7.10 \pm 0.73	10.57 \pm 0.9	8.51 \pm 0.44
A	Dalla Bona B & C (Activated)	12.28 \pm 0.80	9.04 \pm 0.69	11.87 \pm 0.85	11.06 \pm 0.42
B	Nobelpharma B & C	7.83 \pm 0.20	8.32 \pm 0.16	7.14 \pm 0.13	7.77 \pm 0.13
C	Prefabricated Gold Bar (unactivated)	10.34 \pm 0.30	11.24 \pm 0.50	8.67 \pm 0.45	10.08 \pm 0.26
D	Cast Gold Bar (unactivated)	5.51 \pm 0.55	7.55 \pm 0.80	8.22 \pm 0.71	7.10 \pm 0.35
E	Dynamag	1.32 \pm 0.04	1.60 \pm 0.03	1.52 \pm 0.02	1.48 \pm 0.03
F	Neomag	1.21 \pm 0.05	1.11 \pm 0.03	1.27 \pm 0.02	1.20 \pm 0.02
G	Neo-maxi	6.00 \pm 0.27	7.40 \pm 0.15	5.60 \pm 0.38	6.34 \pm 0.19
H	Neo-midi	5.51 \pm 0.53	5.94 \pm 0.59	6.22 \pm 0.18	5.89 \pm 0.13
I	Neo-mini	4.51 \pm 0.17	4.41 \pm 0.33	4.14 \pm 0.10	4.35 \pm 0.08

Table 3: Symmetric 3 Retention Point Vertical Withdrawal

	Retention System	Jig #1 Force (N) $\pm\sigma$	Jig #2 Force (N) $\pm\sigma$	Jig #3 Force (N) $\pm\sigma$	Average Force (N) with 95% confidence interval
A1	Dalla Bona B & C	14.57 \pm 2.14	18.12 \pm 1.14	20.69 \pm 2.27	17.80 \pm 0.82
A	Dalla Bona B & C (Activated)	30.13 \pm 2.13	25.18 \pm 0.88	25.11 \pm 2.61	27.19 \pm 0.80
B	Nobelpharma B & C	23.99 \pm 1.14	23.07 \pm 1.07	19.17 \pm 0.74	22.28 \pm 0.54
C	Prefabricated Gold Bar (unactivated)	26.90 \pm 1.29	21.75 \pm 1.29	21.32 \pm 0.85	23.42 \pm 0.72
D	Cast Gold Bar (unactivated)	15.90 \pm 1.22	12.85 \pm 1.29	16.40 \pm 2.29	15.17 \pm 0.61
E	Dynamag	3.71 \pm 0.07	4.57 \pm 0.12	3.88 \pm 0.06	4.05 \pm 0.10
F	Neomag	3.49 \pm 0.16	3.43 \pm 0.10	3.37 \pm 0.12	3.43 \pm 0.04
G	Neo-maxi	22.60 \pm 0.27	22.12 \pm 0.24	21.34 \pm 0.47	22.02 \pm 0.14
H	Neo-midi	19.51 \pm 0.46	19.47 \pm 0.20	16.79 \pm 0.57	18.58 \pm 0.32
I	Neo-mini	15.08 \pm 0.24	16.61 \pm 0.25	14.87 \pm 0.16	15.51 \pm 0.21

Table 4: Unsymmetric 3 Retention Point Vertical Withdrawal

	Retention System	Jig #1 Force (N) $\pm\sigma$	Jig #2 Force (N) $\pm\sigma$	Jig #3 Force (N) $\pm\sigma$	Average Force (N) with 95% confidence interval
A1	Dalla Bona B & C	5.34 \pm 0.30	6.97 \pm 0.36	6.63 \pm 0.24	6.32 \pm 0.19
A	Dalla Bona B & C (Activated)	9.14 \pm 0.22	8.57 \pm 0.42	7.73 \pm 0.53	8.48 \pm 0.16
B	Nobelpharma B & C	9.40 \pm 0.52	8.52 \pm 0.26	7.25 \pm 0.18	9.39 \pm 0.26
C	Prefabricated Gold Bar (unactivated)	12.00 \pm 0.80	7.94 \pm 0.39	9.75 \pm 0.55	8.85 \pm 0.47
D	Cast Gold Bar (unactivated)	6.77 \pm 0.63	2.71 \pm 0.49	6.73 \pm 0.78	5.39 \pm 0.52
E	Dynamag	1.26 \pm 0.07	1.51 \pm 0.06	0.85 \pm 0.07	1.21 \pm 0.07
F	Neomag	1.22 \pm 0.09	1.30 \pm 0.03	1.30 \pm 0.07	1.27 \pm 0.02
G	Neo-maxi	10.47 \pm 0.14	9.91 \pm 0.30	10.88 \pm 0.12	10.42 \pm 0.10
H	Neo-midi	5.95 \pm 0.28	7.81 \pm 0.19	6.94 \pm 0.22	6.90 \pm 0.19
I	Neo-mini	7.09 \pm 0.10	6.94 \pm 0.53	6.65 \pm 0.24	6.89 \pm 0.09

Table 2 indicates that while there is an almost 10:1 ratio between the largest and the smallest forces generated, that the strongest magnetic systems (G and H) produced levels very close to many of the mechanical clip/bar and ball/socket systems. The variations between different samples of the same system were larger for the mechanical than for the magnetic ones. The large variations in the mechanical systems are undoubtedly due the sensitivity of the retention force to the detail of the clip or socket configuration. Comparison of the values shown for the Dalla Bona ball/socket between the as received and the activated cases (A1 and A) shows an increase of 30% to 50% in retention forces that occurred for what appeared to be minor alterations in the configuration of the retentive component. These large variations between the three jigs of the same mechanical system are again seen for the case of all three retention points being simultaneously withdrawn (Table 3).

The results of the additional testing of the prefabricated bar and clips (Table 1.C) when they were activated is shown in Figures 2-5 and 2-6 for the symmetric and unsymmetric vertical pull configurations. Comparisons of the force levels in these figures with those in Tables 3 and 4 indicates that the relatively small changes in activation (0.15 mm) resulted in changes in the retentive force by a factor of 2 to 3. This means that large variation in the retentive force are possible by small variations in the activation of the clips. Figures 2-5 and 2-6 also confirm that the mechanical bar and clip system retains its retentive force even after 90 applications and withdrawals. In fact for the symmetric withdrawal the force actually rose slightly as the testing sequence progressed.

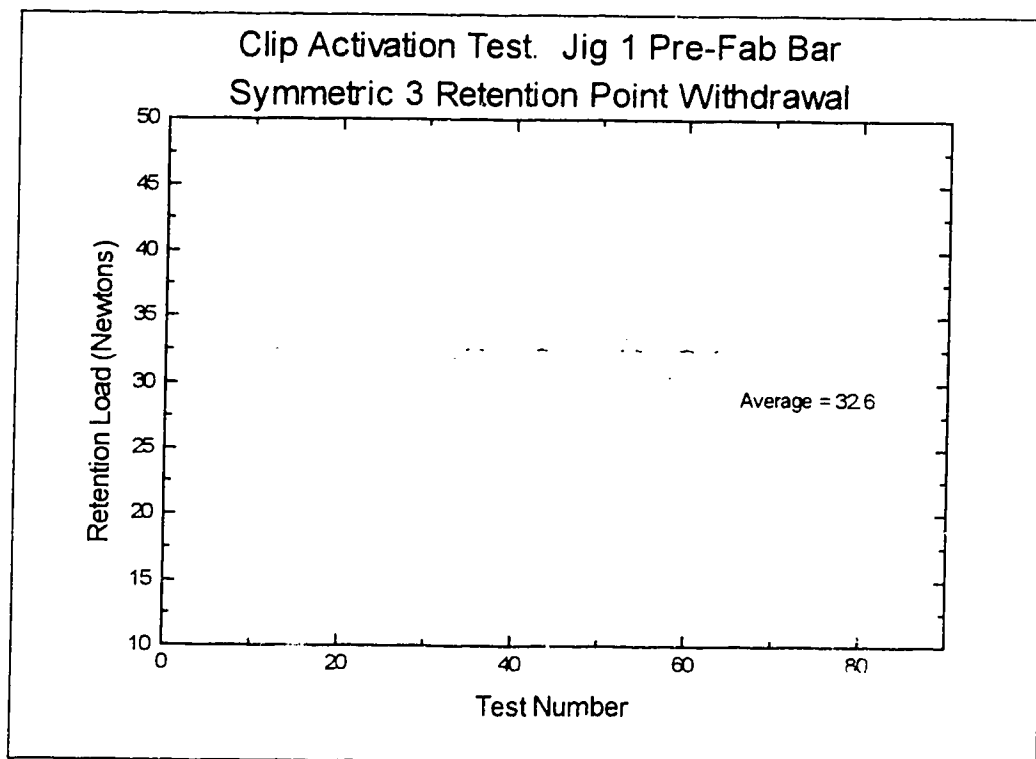


Figure 2-5: Symmetric 3 Retention Point Clip Activation Test for the Prefabricated Bar Jig 1.

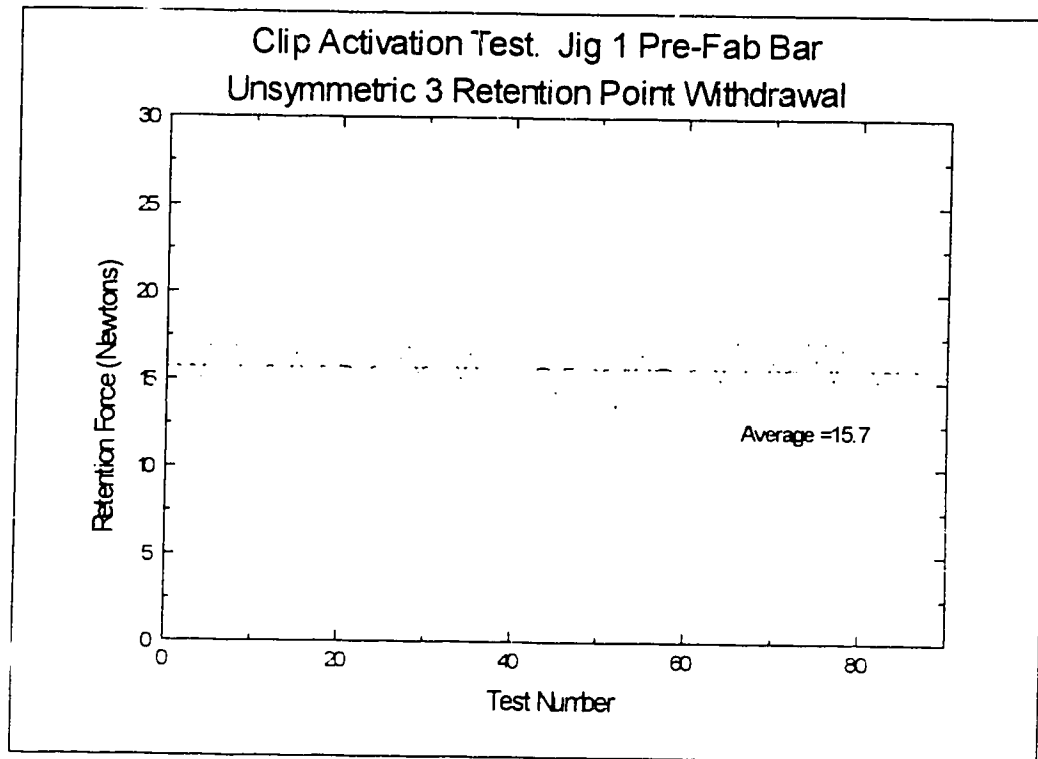


Figure 2-6: Unsymmetric 3 Retention Point Clip Activation Test for the Prefabricated Bar Jig1.

The results of Tables 3 and 4 also include the effects of alignment variations. For the unsymmetric vertical pull tests (Table 4), the stronger magnetic systems produced force levels comparable and greater than those of the mechanical ones. This is not unexpected as the jigs were essentially rigid and therefore unsymmetrical loading would not allow any realignment of the retention points for the magnetic cases while there may be some bending and realignment in the mechanical clips or sockets.

The horizontal or shearing withdrawal tests done on the magnetic systems are summarized in Tables 5, 6 and 7 for the three different directions of pull. In general, the results for the three different directions are very similar and are in approximately the same

relation to each other as they were for the vertical withdrawal tests. The absolute values are between 1/3 and 1/5 of those for the symmetric vertical retention values (Table 3).

Table 5: Horizontal Pull Test in Negative X Direction

	Retention System	Jig #1 Force (N) $\pm\sigma$	Jig #2 Force (N) $\pm\sigma$	Jig #3 Force (N) $\pm\sigma$	Average Force (N) with 95% confidence interval
E	Dynamag	1.47 \pm 0.05	1.62 \pm 0.03	1.37 \pm 0.05	1.49 \pm 0.03
F	Neomag	1.29 \pm 0.03	1.20 \pm 0.03	1.30 \pm 0.04	1.27 \pm 0.01
G	Neo-maxi	3.81 \pm 0.10	4.23 \pm 0.16	3.81 \pm 0.11	3.95 \pm 0.06
H	Neo-midi	3.07 \pm 0.12	3.04 \pm 0.16	3.04 \pm 0.23	3.05 \pm 0.04
I	Neo-mini	2.98 \pm 0.11	3.21 \pm 0.22	2.56 \pm 0.11	2.91 \pm 0.08

Table 6: Horizontal Pull Test in Positive Y Direction

	Retention System	Jig #1 Force (N) $\pm\sigma$	Jig #2 Force (N) $\pm\sigma$	Jig #3 Force (N) $\pm\sigma$	Average Force (N) with 95% confidence interval
E	Dynamag	1.97 \pm 0.05	1.23 \pm 0.02	1.14 \pm 0.04	1.11 \pm 0.03
F	Neomag	1.09 \pm 0.03	0.83 \pm 0.03	0.97 \pm 0.02	0.96 \pm 0.03
G	Neo-maxi	4.60 \pm 0.59	4.22 \pm 0.08	4.25 \pm 0.14	4.35 \pm 0.12
H	Neo-midi	2.96 \pm 0.10	3.34 \pm 0.09	2.70 \pm 0.09	3.00 \pm 0.07
I	Neo-mini	2.29 \pm 0.09	2.79 \pm 0.16	2.41 \pm 0.10	2.48 \pm 0.06

Table 7: Horizontal Pull Test in Negative Y Direction

	Retention System	Jig #1 Force (N) $\pm\sigma$	Jig #2 Force (N) $\pm\sigma$	Jig #3 Force (N) $\pm\sigma$	Average Force (N) with 95% confidence interval
E	Dynamag	1.97 \pm 0.05	1.23 \pm 0.02	1.14 \pm 0.04	1.11 \pm 0.03
F	Neomag	1.09 \pm 0.03	0.83 \pm 0.03	0.97 \pm 0.02	0.96 \pm 0.03
G	Neo-maxi	4.60 \pm 0.59	4.22 \pm 0.08	4.25 \pm 0.14	4.35 \pm 0.12
H	Neo-midi	2.96 \pm 0.10	3.34 \pm 0.09	2.70 \pm 0.09	3.00 \pm 0.07
I	Neo-mini	2.29 \pm 0.09	2.79 \pm 0.16	2.41 \pm 0.10	2.48 \pm 0.06

The results for each of the adhesives evaluated is given in Table 8. Each group of five are the results from one subject. As expected the results are not only quite variable from one subject to another but also within a particular individual. The differences between the two adhesives also produced average force values with a 3:1 ratio.

Table 8: Adhesive Pull Test Results

Individual	Pros-Aide Adhesive Force (N) (J, Table 1)		Hollister Medical Adhesive Force (N) (K, Table 1)	
	Test Result	Mean \pm σ	Test Result	Mean \pm σ
1	4.12 3.33 4.41 5.69 1.77	3.86 \pm 1.45	10.59 10.98 13.37 8.83 10.00	10.83 \pm 1.82
2	5.49 1.57 5.30 1.57 3.33	3.45 \pm 1.71	12.36 13.93 12.16 15.10 12.75	13.26 \pm 1.11
3	5.10 3.14 4.51 6.08 3.14	4.39 \pm 1.14	10.59 12.55 13.53 15.30 10.79	12.55 \pm 1.76
4	2.75 5.69 11.18 3.73 6.28	5.92 \pm 2.92	13.14 10.40 17.06 10.79 11.18	12.51 \pm 3.03
5	1.77 12.55 3.33 5.30 2.75	5.14 \pm 3.88	15.30 8.63 14.91 11.96 17.26	13.53 \pm 2.46
Overall Based on 433 mm ²	4.55 \pm 2.64		12.55 \pm 2.35	
Overall Based on 1200 mm ²	12.63 \pm 7.33		34.82 \pm 6.53	

In order to summarize the comparisons of the 4 mechanical, 5 magnetic and 2 adhesive systems evaluated, the results from the single retention unit and the three unit

symmetrical vertical test are given in Figure 2-7 and 2-8. Also included in Figure 2-7 are the adhesive test results which have been normalized to 1/3 of the area of the nominal ear

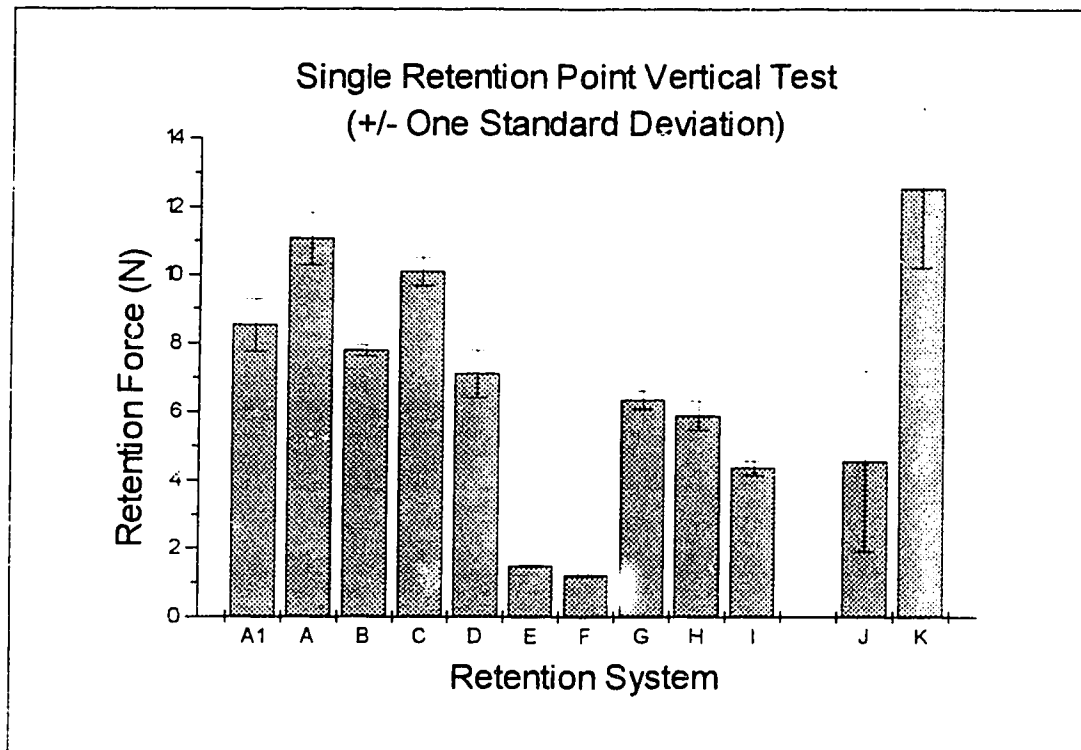


Figure 2-7: Average Retention Strength for the Single Retention Point Vertical Test.

or 400 mm^2 . Figure 2-8 includes the adhesive force expected for the 1200 mm^2 ear. As this ratio is 3/1, Figure 2-7 shows the comparison for a single unit while Figure 2-8 shows that approximate results for a system used to retain a typical ear prosthesis. For comparisons, the vertical scale of Figure 2-8 is 3 times that of Figure 2-7 so that if the 3 retention point tests yielded exactly 3 times the single unit value, they appear alike on the two graphs.

Figure 2-7 and 2-8 generally show the same relative strengths of all 12 systems evaluated. In fact for the three retention unit tests (Figure 2-7), the 4 mechanical systems

(2 ball/socket, 2 clip/bar unactivated) and the stronger magnetic ones (G,H,I) provide forces which are quite comparable. All of these systems have retention values intermediate to the two adhesives tested. These figures also show that the magnetic systems provided the least amount of variations between individual tests and between different installations of the same systems (i.e. between jigs). The mechanical systems

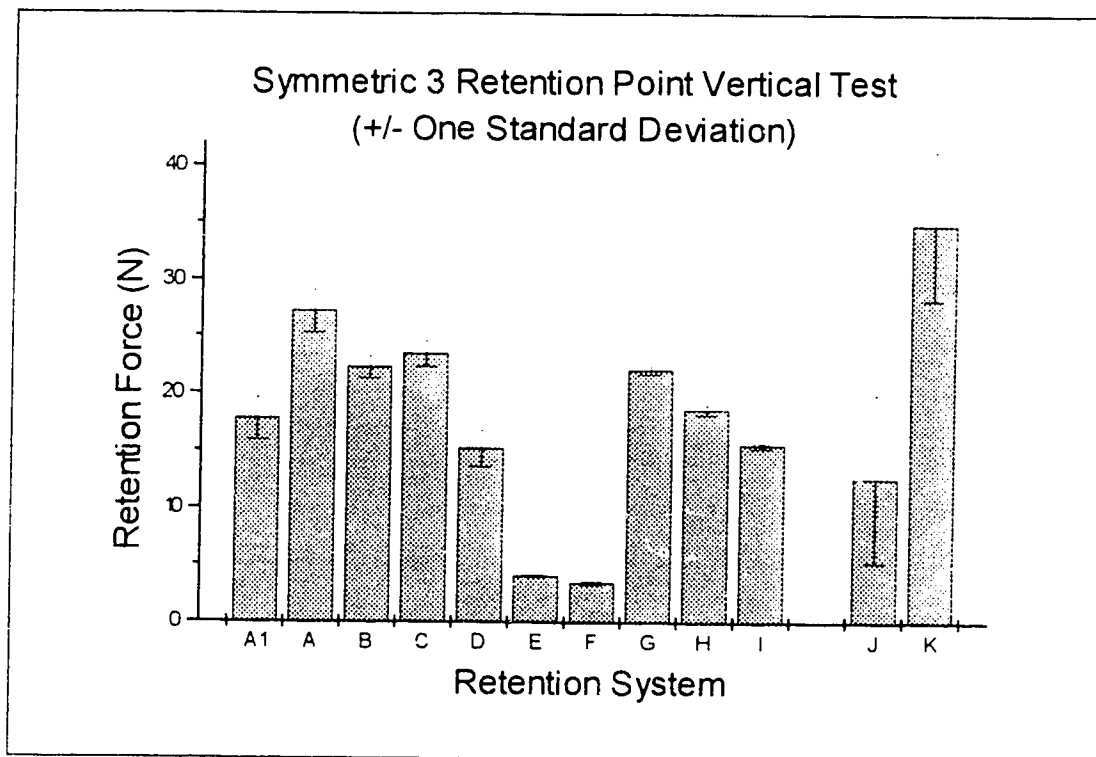


Figure 2-8: Average Retention Strength for the Symmetric Three Retention Point Vertical Test

showed somewhat more variations than the magnetic systems but were still much more consistent than the adhesives. The adhesives showed considerable variation not only between subjects but also in the repeat testing done on one subject using the same adhesives.

3. FINITE ELEMENT MODELS

3.1 Introduction

To examine how the loads measured in chapter 2 are carried by the tissue, a numerical model was developed to estimate the stress and strain distribution in the region surrounding the craniofacial osseointegrated implants. The stress analysis was done using the finite element method. A description of this technique applied to linear elastic materials is first outlined. In addition, a complete description of the specific model parameters for the bone configurations, the loading conditions and the implant design will also be given. Details of the commercial software used to perform the modeling and the types of results or outputs that were available will also be discussed.

3.2 Background on the Finite Element Method

The basis for the finite element technique is to consider a complex system broken into numerous small finite pieces or elements as a complete analytical model of the entire system cannot be found. The physical characteristics of the system are then defined as a mathematical model that can be applied to each of the elements. In general the equations for each of the elements are much simpler than for the entire problem, as the elements can be selected to have a known distribution of properties and are of simpler geometry. The

equations for each of the elements of the complex model are then combined into a large system of equations that can be solved simultaneously. Various elements can be employed to provide systems which model the original system to a high degree of precision.

For this investigation the finite element method was applied to the problem of a loaded craniofacial osseointegrated titanium implant in bone. This system was modeled with isotropic linearly elastic solids using axisymmetric and three-dimensional stress elements. From the assembly of elements a relationship between the displacements and the forces applied on the system is developed. This relationship is represented by the relationship

$$\{F\} = [k_G]\{u\} \quad (3.1)$$

in which the $\{F\}$ vector represents all the forces applied to the elements at their nodes and the $\{u\}$ vector represents the displacement of the nodes. The matrix $[k_G]$ represents the global stiffness matrix for the system. In general the force vector is usually known and the displacement vector is unknown, while the global stiffness matrix is determined from assembling the element stiffness matrixes. There are a number of methods that can be used to determine the element stiffness matrixes and to assemble the global stiffness matrix. These include direct, energy/variational, and residual methods. For descriptive purposes an outline of the formation of the element matrixes using the energy technique for an axisymmetric stress element is given below.

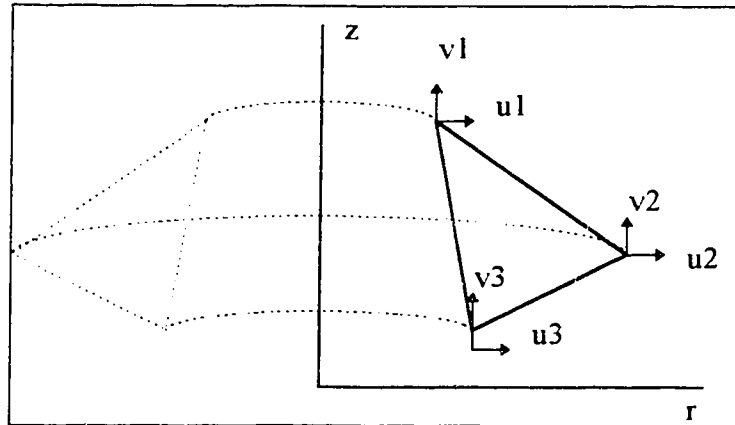


Figure 3-1: Axisymmetric Element

Figure 3-1 displays a triangular axisymmetric element. This type of element is rotated around the z axis by 360° and the nodes on the corner elements are described as nodal circles. For this element there are only two degrees of motion for the nodes. These motions are radial displacement, which is represented by u , and vertical displacement, which is represented by v . The displacements of any node can be related to its position in the z - r plane with the equations:

$$\begin{aligned} u &= a + br + cz \\ v &= d + er + fz \end{aligned} \quad (3.2)$$

where a , b , c , d , e and f are constants. Equation (3.2) can be rewritten in matrix format for all of the three nodes as:

$$\begin{Bmatrix} u_1 \\ u_2 \\ u_3 \\ v_1 \\ v_2 \\ v_3 \end{Bmatrix} = \begin{bmatrix} 1 & r_1 & z_1 & 0 & 0 & 0 \\ 1 & r_2 & z_2 & 0 & 0 & 0 \\ 1 & r_3 & z_3 & 0 & 0 & 0 \\ 0 & 0 & 0 & 1 & r_1 & z_1 \\ 0 & 0 & 0 & 1 & r_2 & z_2 \\ 0 & 0 & 0 & 1 & r_3 & z_3 \end{bmatrix} \begin{Bmatrix} a \\ b \\ c \\ d \\ e \\ f \end{Bmatrix} \quad (3.3)$$

Where u_1 and v_1 are the displacements in the radial and vertical direction for node 1 and r_1 and z_1 are the coordinates of node 1. Equation (3.3) can be simplified to the expression:

$$\{u\} = [T]\{\alpha\} \quad (3.4)$$

and

$$\{\alpha\} = [T^{-1}]\{u\}. \quad (3.5)$$

The relationship between the strain and the displacement for a solid using Equation (3.2) is given as:

$$\begin{aligned} \varepsilon_r &= \frac{\partial u}{\partial r} = b \\ \varepsilon_z &= \frac{\partial v}{\partial z} = f \\ \varepsilon_{\theta} &= \frac{u}{r} = \frac{a + br + cz}{r} \\ \gamma_{rz} &= \frac{\partial u}{\partial z} + \frac{\partial v}{\partial r} = c + e. \end{aligned} \quad (3.6)$$

These strains can be rewritten in matrix format as:

$$\begin{Bmatrix} \varepsilon_r \\ \varepsilon_z \\ \varepsilon_{\theta} \\ \gamma_{rz} \end{Bmatrix} = \begin{bmatrix} 0 & 1 & 0 & 0 & 0 & 0 \\ 0 & 0 & 0 & 0 & 0 & 1 \\ 1/r & 1 & z/r & 0 & 0 & 0 \\ 0 & 0 & 1 & 0 & 1 & 0 \end{bmatrix} \begin{Bmatrix} a \\ b \\ c \\ d \\ e \\ f \end{Bmatrix} \quad (3.7)$$

or

$$\{\varepsilon\} = [G]\{\alpha\}. \quad (3.8)$$

The strains can then be related to the displacements of the nodes by using (3.5) and (3.8).

$$\{\varepsilon\} = [G][T^{-1}]\{u\}. \quad (3.9)$$

The G and T^{-1} matrix can be combined to form a single B matrix so that equation (3.9) becomes:

$$\{\varepsilon\} = [B]\{u\} \quad (3.10)$$

From Hooke's law a relationship between the strain and the stress can be formulated. For an axisymmetric element that assumes the material is homogeneous, isotropic and linearly elastic the strain stress relationship is

$$\begin{aligned} \sigma_r &= \frac{E}{(1+\nu)(1-2\nu)} ((1-\nu)\varepsilon_r + \nu\varepsilon_\theta + \nu\varepsilon_z) \\ \sigma_\theta &= \frac{E}{(1+\nu)(1-2\nu)} (\nu\varepsilon_r + (1-\nu)\varepsilon_\theta + \nu\varepsilon_z) \\ \sigma_z &= \frac{E}{(1+\nu)(1-2\nu)} (\nu\varepsilon_r + \nu\varepsilon_\theta + (1-\nu)\varepsilon_z) \\ \tau_{rz} &= \frac{E}{(1+\nu)(1-2\nu)} \frac{1-2\nu}{2} \gamma_{rz} \end{aligned} \quad (3.11)$$

or in matrix format

$$\begin{Bmatrix} \sigma_r \\ \sigma_\theta \\ \sigma_z \\ \tau_{rz} \end{Bmatrix} = \frac{E}{(1+\nu)(1-2\nu)} \begin{bmatrix} 1-\nu & \nu & \nu & 0 \\ \nu & 1-\nu & \nu & 0 \\ \nu & \nu & 1-\nu & 0 \\ 0 & 0 & 0 & (1-2\nu)/2 \end{bmatrix} \begin{Bmatrix} \varepsilon_r \\ \varepsilon_\theta \\ \varepsilon_z \\ \gamma_{rz} \end{Bmatrix}. \quad (3.12)$$

This expression can be simplified as

$$\{\sigma\} = [D]\{\varepsilon\}. \quad (3.13)$$

It is then possible to determine the strain energy of the element from these stress and strain components using

$$U_e = \frac{1}{2} \int_V \{\epsilon\}^T \{\sigma\} dv. \quad (3.14)$$

In this expression $dv = 2\pi r dr dz$. This equation can be expanded using (3.10) and (3.12) to form

$$U_e = \frac{1}{2} \{u\}^T 2\pi \int_V [B]^T [D][B] r dr dz \{u\}. \quad (3.15)$$

From this expression the stiffness matrix for the element can be developed as

$$U_e = \frac{1}{2} \{u\}^T [k_e] \{u\} \quad (3.16)$$

so that

$$[k_e] = 2\pi \int_V [B]^T [D][B] r dr dz. \quad (3.17)$$

The element stiffness matrix, $[k_e]$, for each element is combined for all of the elements to give the global stiffness matrix, $[k_g]$, for the entire system. This global stiffness matrix allows the calculation of the nodal displacements using (3.1). The element displacements are then used in (3.10) to determine the strains which in turn using (3.13) allows calculation of the stresses. The formulation of the element stiffness matrix for the three dimensional block element is similar and can be found in Robinson [15].

3.3 Model Parameters

3.3.1 The Implants

For this investigation three different clinically applied craniofacial osseointegrated implants were modeled. They were the Brånemark, the Bud and the IMZ 4 mm implants. These implants along with their specific dimensions are shown in Figure 3-2. All of the implants were made from titanium which was assumed to have a Young's modulus of 103.4 GPa . The implants were assumed to be solid except for the flange on the Brånemark implant. Part of the Brånemark flange was given a reduced modulus of 25 GPa to better represent the fact that the flange has a series of holes in it. When available the implant dimensions were taken from drawings supplied from the manufacturer, otherwise the dimensions were obtained from measuring the actual implants.

To obtain a better understanding of the load transfer between the implant and the bone, each implant was examined in its standard design, shown in Figure 3-2, and in a modified design with the flange removed. The implants were modified because in the clinical applications the flange can complicate implant placement. It should be noted that the threads on the implants were not modeled as helical threads but rather as circular rings or steps in order to reduce the complexity of the model.

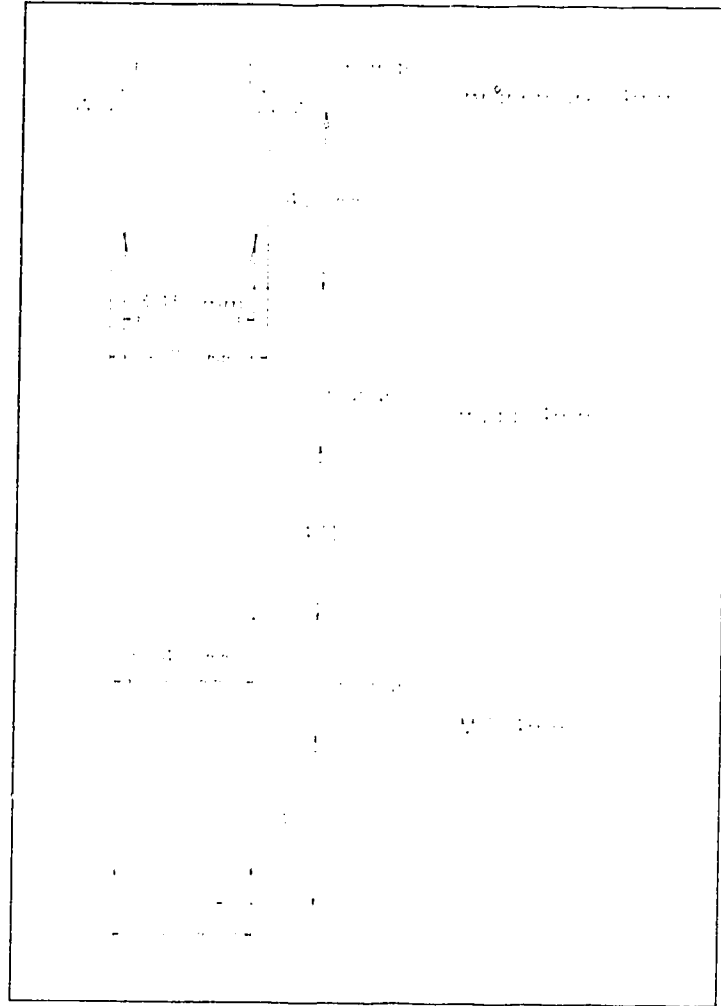


Figure 3-2: Dimensions of the Brånemark, Bud and IMZ Implants

3.3.2 Loading Configuration

There were two loading conditions applied to the implants. The first was a vertical load of 10 N placed on the center of the implant and the second condition was a 10 N load and a moment of 100 Nmm. The 10 N vertical on the implant represents a reasonable implant load based on the single and three point retention strengths as shown in Chapter 2.

The 100 Nmm couple represents the additional effect of having this load displaced a distance of 10 mm from the center of the implant. It should be noted that although these loads are representative of those found in clinical applications, the main intention of this study is not to obtain exact values of strain in the bone but, to compare the loading of the three implants in various bone configurations. As the analysis is strictly linearly elastic, a change in load magnitude would result in a proportional change in the stresses and strain.

It should be noted that the strain analysis for all of the models that were loaded vertically with no moment were done with axisymmetric elements, while the models loaded vertically with a moment were done with 3 dimensional block elements.

3.3.3 Bone Properties

The bone which surrounds the implant was modeled as consisting of two general types, cortical bone and cancellous bone. Cortical bone is the stiffer, more solid, surface type bone, while cancellous bone is the less stiff porous type bone. While these types of tissues are known not to be isotropic, homogenous or linearly elastic they were modeled as such for this study. Previous investigators [3][4][5][6] have used similar assumptions in implant model studies. While these assumptions will undoubtedly limit the accuracy it is believed the results are acceptable for general comparisons to illustrate large percentage variations between the situations considered. The stiffness of the cortical bone was prescribed at 14.0 GPa and 0.5 GPa for the cancellous bone. These values were the average values found from the literature.

In addition to this modeling for hard tissue, a third type of softer material was modeled. This soft tissue was an attempt to represent tissue that could develop around the implant in a clinical application. It is usually accepted that the formation of this soft tissue between the bone and the implant indicates a failure of the interface. The soft tissue layer was included to model its effects on the distribution of stress in the bone as compared to the standard case. The Young's Modulus for the soft tissue was estimated to be 3.5 GPa and was also assumed to be linearly elastic, homogeneous and isotropic. Table 1 summarizes all of the properties for the materials used.

Table 1: Material Properties

Material	Poisson's Ratio	Young's Modulus (GPa)
Titanium	0.35	103.4
Branemark Flange	0.35	26.0
Cortical Bone	0.3	14.0
Soft Tissue	0.3	3.5
Cancellous Bone	0.3	0.5

3.3.4 The Bone Configurations

Each of the three implants were examined in three different bone configurations which were deemed to be representative of situations in the craniofacial region. These configurations were the solid cortical bone, shown in Figure 3-3, the bicortical (two solid plates), shown in Figure 3-4, and the unicortical (single solid plate), shown in Figure 3-5. Each of these bone configurations were modeled as a circular bone "plug" of a radius of 6.5 mm with the implant placed in its center.

For the solid cortical bone plate the depth of the plate was prescribed as 0.5 mm greater than the implant's length. For example, the Brånemark implant, which had a length of 4.2 mm, was modeled in cortical bone with a depth of 4.7 mm. The cortical bone depths for the Bud and IMZ implant were 4.6 mm and 4.5 mm respectively.

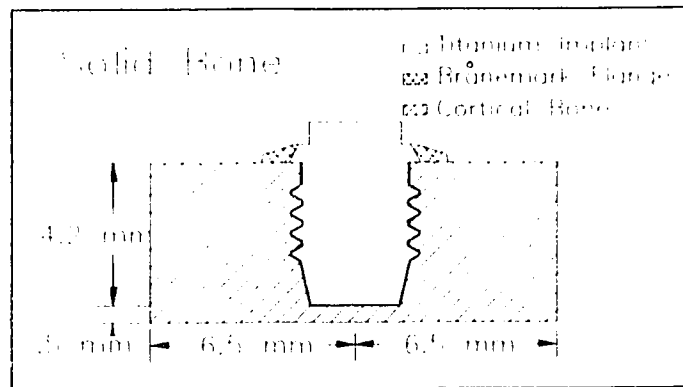


Figure 3-3: Solid Bone Configuration with the Brånemark Implant

For the bicortical configuration each of the cortical bone plates was given a thickness of 1.5 mm. The bottom plate was positioned vertically so that the implant would engage 1 mm deep into the second plate and leave 0.5 mm of untouched bone beneath it, therefore the space between the plates varied slightly for each implant. For the axisymmetric vertical load loading condition this space between the plates was either filled

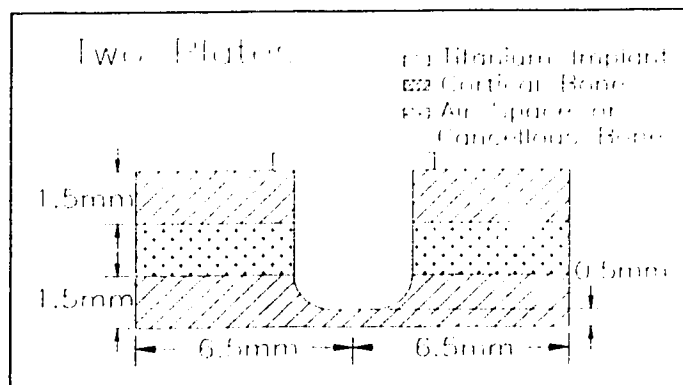


Figure 3-4: Bicortical Configuration with an IMZ Implant

with cancellous bone or left as an air space. For the three dimensional load and moment configurations the space was only modeled as cancellous bone and as an air space for the Brånemark implant. The other two implants were modeled only with the air space in order to limit the extent of the study.

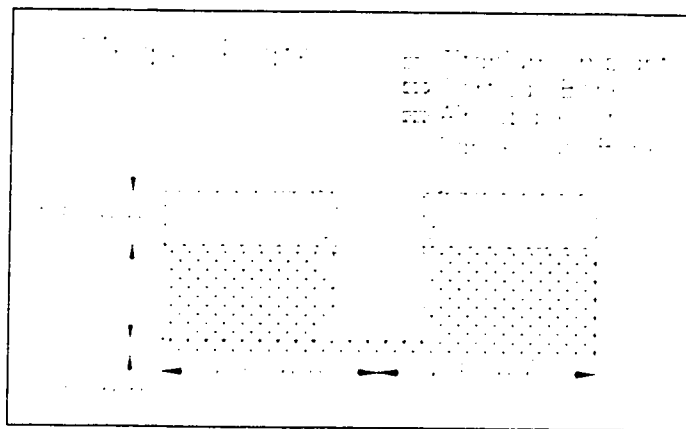


Figure 3-5: Unicortical Configuration with a Bud Implant

The unicortical configuration had single cortical plate with a thickness of 1.5 mm. As with the bicortical configuration the space beneath the implant was either cancellous bone or an air space for the vertical load situation. For the force and moment loading condition the space was modeled only as an air space with the exception of the Brånemark implant which was modeled with an air space and cancellous bone. Again not all of the implants were modeled with the force and moment and cancellous bone in order to limit the extent of the study.

The soft tissue that was modeled around the implant where it contacted the bone was given a thickness of 0.05 mm. This thickness was significantly greater than the

thickness that would occur clinically however, constraints of the finite element code limited the minimum thickness which could be accommodated. This crude approximation of the soft tissue was examined for all of the implants with a vertical load in the solid bone configuration, for the IMZ implant with a vertical load in the bicortical and unicortical configuration, and the IMZ implant with a vertical load and moment in the solid, bicortical and unicortical configuration. The soft tissue was not examined for all of the implants in all of the bone configurations in order maintain constraints on the study.

3.3.5 Boundary Conditions

The boundary conditions for the bone plates in the three configurations were free along the bottom and fixed in radial, hoop and vertical directions along the outside circumferential edges. In Figure 3-6, which displays a picture of the solid bone with the implant removed, the triangles indicate where the bone was fixed for the finite element models. This type of boundary condition assumes that the material under the bone plates is considerably softer than the bone. The interface conditions between the implant and bone elements were assumed to be joined. This implies that any node on the bone that was next to a node on the implant would be equally displaced under load. It has been suggested that this “welded” bond is representative of an osseointegrated interface [6]

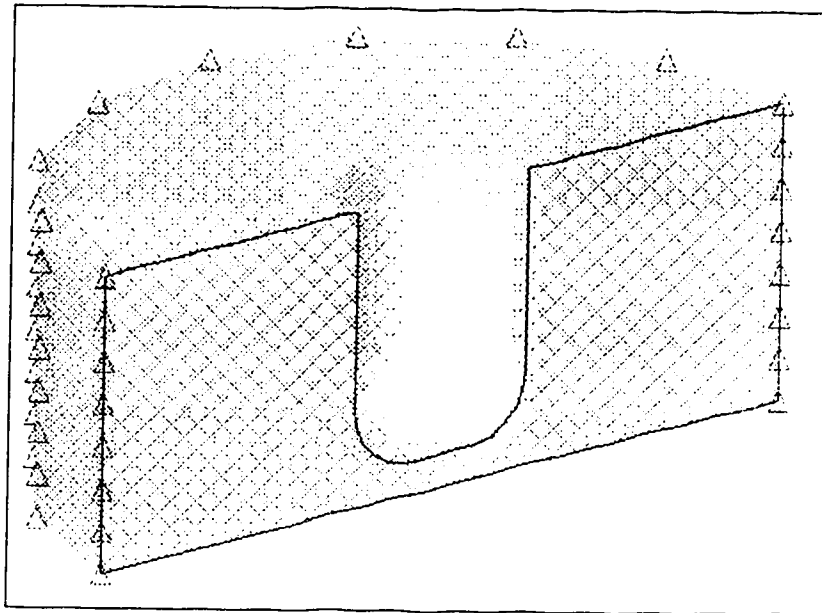


Figure 3-6: Boundary Conditions for the Cortical Bone

3.4 Computer Finite Element Software

The finite element analysis was done using the commercial software ALGOR (Algor Inc., Pittsburgh, PA, USA) which included the preprocessing, analysis and post processing steps.

3.4.1 Pre-Processing

The pre-processing for these models was done with ALGOR's software Super Draw version 3.16. This software was used to generate the models with a drawing type interface. It provided a function for meshing enclosed objects with a two dimensional mesh. This mesh could be made up of triangles or quadrilaterals or a combination. The density of the mesh could be globally or locally refined using built in functions. The three dimensional models that used brick elements were formed from the 2-D meshes by rotating and copying them around the vertical axis every 22.5 degrees. Figure 3-7 displays

the 3-D element mesh for the solid bone configuration and the Brånemark implant. In the figure the implant has been removed for clarity.

A typical 3-D model would have approximately 2624 elements and 2932 nodes while a 2-D model would have about 1389 elements and 1383 nodes. The elements for both types of models had a single node at each of their corners. Therefore a 3-D element would have 8 or 6 nodes per element depending on whether or not the element had a triangular or square base and a 2-D element would have 3 or 4 nodes. It should be noted that elements would share common nodes with other elements that were next to them.

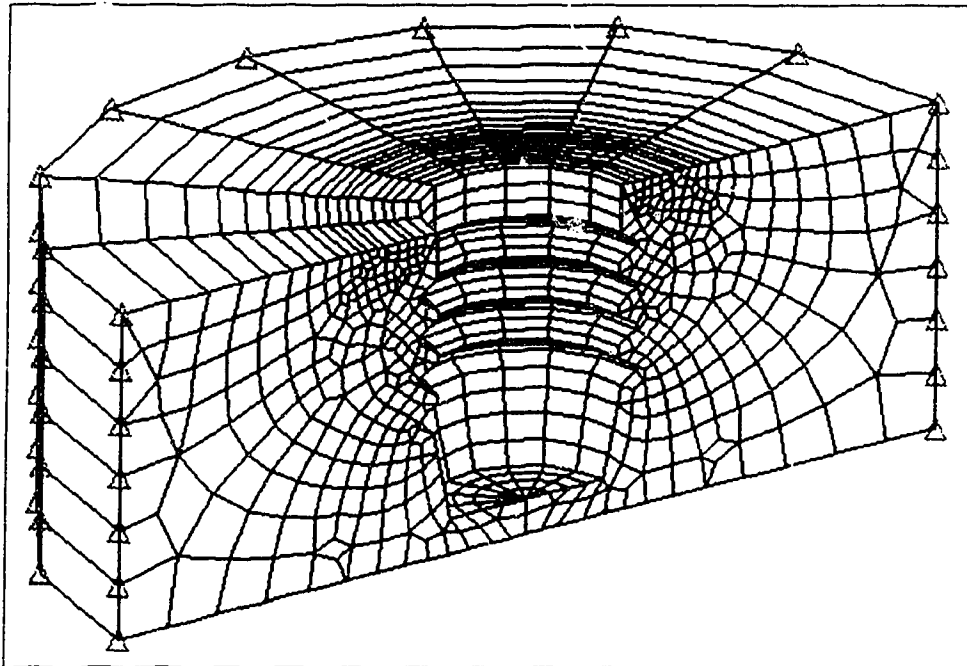


Figure 3-7: 3-D Element Mesh for the Solid Bone Configuration for the Brånemark Implant

As indicated above, all of the 3-D models were subjected to a vertical force and a moment. Due to the plane of symmetry in this type of loading only half of the model was used in the finite element solution.

Each of the meshed objects and the loading and boundary conditions were “decoded” or assigned their material strengths and element parameters using the DecodS stress decoder version 2.06.

3.4.2 Analysis and Post Processing

The solver used was ALGOR’s Linear Stress Analysis SSAP0 version 11.06. This program solved the system given the input file name from the decoder.

The results were displayed using ALGOR’s Super View program version 4.12. This program displayed the stress state as a standard graphical dithered picture or allowed the information to be stored as a file. This program allowed the display of the magnitude of two of the three principal stresses (σ_1 and σ_3) and principal strains (ϵ_1 and ϵ_3). It also displayed the stresses and strains corresponding to the hoop, radial and vertical stresses. In addition the Von Mises stress,

$$(\sigma_1 - \sigma_2)^2 + (\sigma_2 - \sigma_3)^2 + (\sigma_1 - \sigma_3)^2 = 2\sigma_{Von\ Mises}^2, \quad (3.18)$$

which is often used as a failure criteria for typical engineering materials, could be calculated and displayed. The program could also substitute the principal stress values for equation 3.16 with principal strain values to provide a view of Von Mises type strains in the bone.

For comparisons purposes the absolute maximum for any given strain or stress state was not used due to numerical errors that could occur at a single point. Instead the maximum value was determined from the average stress or strain that occurred over 5%

of the highest stressed or strained volume in the cortical bone. This was accomplished by collecting all of the bone elements in the model and sorting them from largest to smallest based on their average strain values. The average strain of the element was then weighted against its volume and the values from the highest strained elements were averaged until a volume of 5% of the total volume was reached. This provided a good means of comparing the overall magnitude of the strains that occurred in the bone. This 5% average was also used to compare the various stress states that were examined.

The overall error in the numerical solution was minimized by a trial and error technique. The model was solved with an initial guess for the mesh density. This mesh density was then increased and the results were compared to the initial case. If very small or no difference was noticed results were considered numerically accurate. If a large difference was noticed the density was increased again until the results converged to a set stress state. The software did provide a precision dither that was of some use in refining the mesh at critical points. This technique was not used as an estimate of the numerical error, but simply to suggest locations for mesh refinements.

The overall accuracy of the computer code was tested by examining the situation of a infinitely long cylinder under pure shear as displayed in Figure 3-8. This problem was chosen due to its similarity to the implant geometry and loading. The analytical solution to the shear stress at any point in the cylinder was compared to the numerical results of a finite element model of a cylinder under shear where the length of the cylinder was at least 10 times longer than the diameter. It was found there was less than 2% variation in the two solutions.

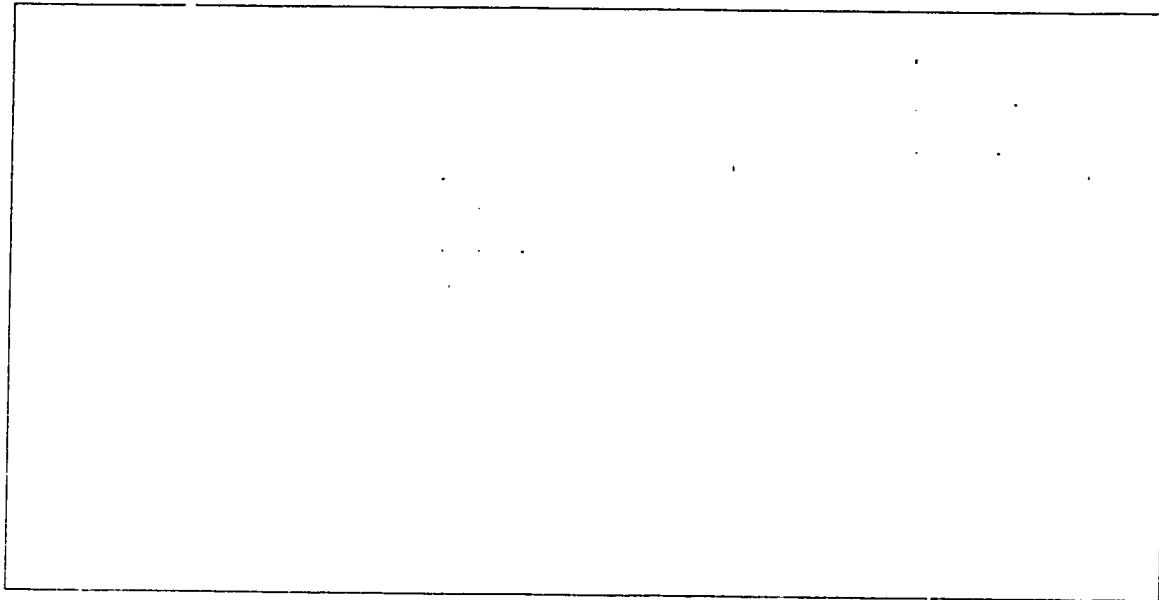


Figure 3-8: Cylinder Under Pure Shear

4. FINITE ELEMENT RESULTS AND DISCUSSION

4.1 Introduction

In order to organize the findings of the present study this chapter will be broken down into three main sections. The first section will give results from all of the axisymmetric models where the implant was loaded with a force only. This section also examines the effects that the various implant and bone configurations and flanges had on the state of strain in the cortical bone. The second section will provide similar results for the above variables for the three dimensional force and moment loading condition. An additional section will give results of a comparison between the two loading conditions. The final section discusses and analyzes all of the results including consideration of the uncertainty that is present in the computer models.

4.2 Vertical Force Axisymmetric Loading Condition

As mentioned in Chapter 3 the vertical load with no moment loading condition was modeled as an axisymmetric model. The strain pictures that are shown in this section display a two dimensional slice which is representative of any axisymmetric cut through the model. For clarity the implant was removed from all of the pictures and only the bone was displayed. The units used to display the strain in the diagrams are unitless (mm/mm).

Table 4-1 displays the maximum value of the tensile and compressive principal strains for all of the models discussed in this section. From the table it can be seen that the two principal strains had similar magnitudes for all of the models. It can also be seen from Figures 4-1 and 4-2 that the general distribution of the tensile and compressive strain fields

Table 4-1: Summary of the Maximum Tensile and Compressive Principal Strains for all of the Models Loaded with a Vertical Force.

Implant Type	Bone Configuration	Flange	Cancellous Bone	Soft Tissue	Tensile Principal Strain ($\mu\epsilon$)	Compressive Principal Strain ($\mu\epsilon$)
Branemark	solid	yes	no	no	15.0	-23.0
Branemark	solid	no	no	no	18.2	-27.9
Branemark	solid	yes	no	yes	16.7	-24.6
Branemark	unicortical	yes	no	no	80.0	-85.9
Branemark	unicortical	no	no	no	100.2	-103.1
Branemark	unicortical	yes	yes	no	61.0	-64.6
Branemark	unicortical	no	yes	no	75.9	-80.6
Branemark	bicortical	yes	no	no	47.4	-57.3
Branemark	bicortical	no	no	no	57.2	-67.4
Branemark	bicortical	yes	yes	no	40.0	-50.0
Branemark	bicortical	no	yes	no	48.5	-59.4
Bud	solid	yes	no	no	18.6	-30.5
Bud	solid	no	no	no	21.0	-31.9
Bud	solid	yes	no	yes	19.3	-32.8
Bud	unicortical	yes	no	no	87.1	-103.8
Bud	unicortical	no	no	no	101.5	-109.7
Bud	unicortical	yes	yes	no	72.8	-81.8
Bud	unicortical	no	yes	no	80.0	-85.4
Bud	bicortical	yes	no	no	50.6	-65.0
Bud	bicortical	no	no	no	51.1	-66.7
Bud	bicortical	yes	yes	no	47.3	-62.1
Bud	bicortical	no	yes	no	50.6	-61.4
IMZ	solid	yes	no	no	16.6	-23.8
IMZ	solid	no	no	no	19.2	-27.4
IMZ	solid	yes	no	yes	26.5	-34.8
IMZ	unicortical	yes	no	no	84.3	-91.7
IMZ	unicortical	no	no	no	102.5	-105.1
IMZ	unicortical	yes	no	yes	80.1	-93.6
IMZ	unicortical	yes	yes	no	65.6	-75.6
IMZ	unicortical	no	yes	no	76.8	-83.7
IMZ	bicortical	yes	no	no	49.8	-61.5
IMZ	bicortical	no	no	no	55.4	-63.5
IMZ	bicortical	yes	no	yes	45.7	-62.9
IMZ	bicortical	yes	yes	no	43.1	-54.9
IMZ	bicortical	no	yes	no	48.4	-58.6

in cortical bone was also similar. Also, it should be noted that if the load placed on the implant was reversed, so that it was directed vertically upward, that the magnitudes for the compressive and tensile principal strains would be reversed. As a result all comparisons done between models only the compressive principal strain was used. Since the compressive principal strain had a slightly higher magnitude for the given loading condition it also represents the maximum magnitude of the principal strain (compressive or tensile) that would be present if the load on the implant was cycled from positive to negative.

4.2.1 Implant design: Vertical Load

Overall the implant design did not greatly affect the maximum magnitude of the strain or the general strain field of the cortical bone for the vertical load with no moment load case. Figures 4-1, 4-3 and 4-4 display the compressive principal strain field for the Brånemark, Bud and IMZ implants in the solid cortical bone configuration. The magnitude and distribution of the strains were quite similar for the three implants in this bone configuration. For all of the implants the maximum strain occurred where the edge of the flange contacted the bone as well as along the first thread. The strains along the threads tended to decrease as the depth from the surface increased. Some small variations however can be noticed. For example the Bud implant generally induced a slightly higher maximum strain in the bone while the strains for the IMZ and Brånemark implant were slightly more uniformly distributed down the threads of the implant. It is difficult to determine whether or not these small differences would influence the success rate of the implant since the variations are quite small and the properties of solid cortical bone could

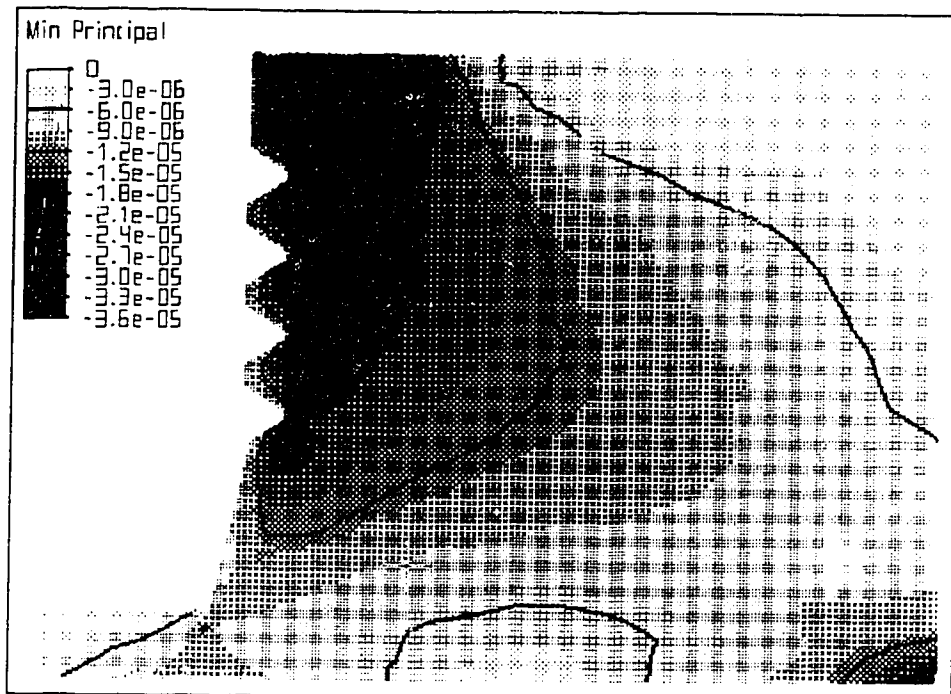


Figure 4-1: Compressive Principal Strain Distribution of the Brånemark Implant in Solid Bone

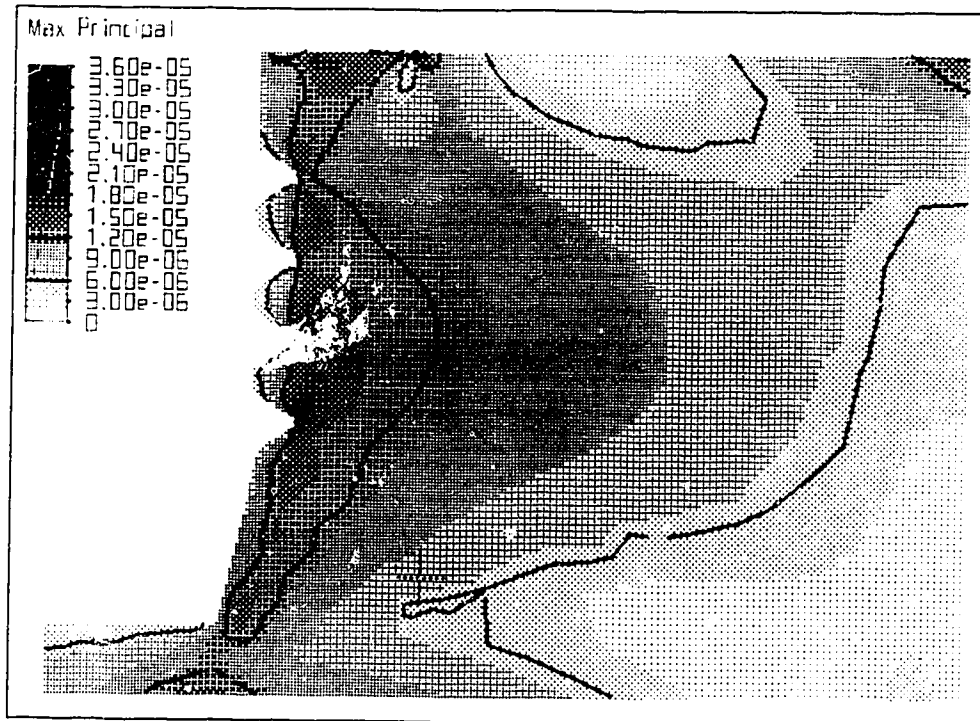


Figure 4-2: Tensile Principal Strain Distribution for the Brånemark Implant in Solid Bone.

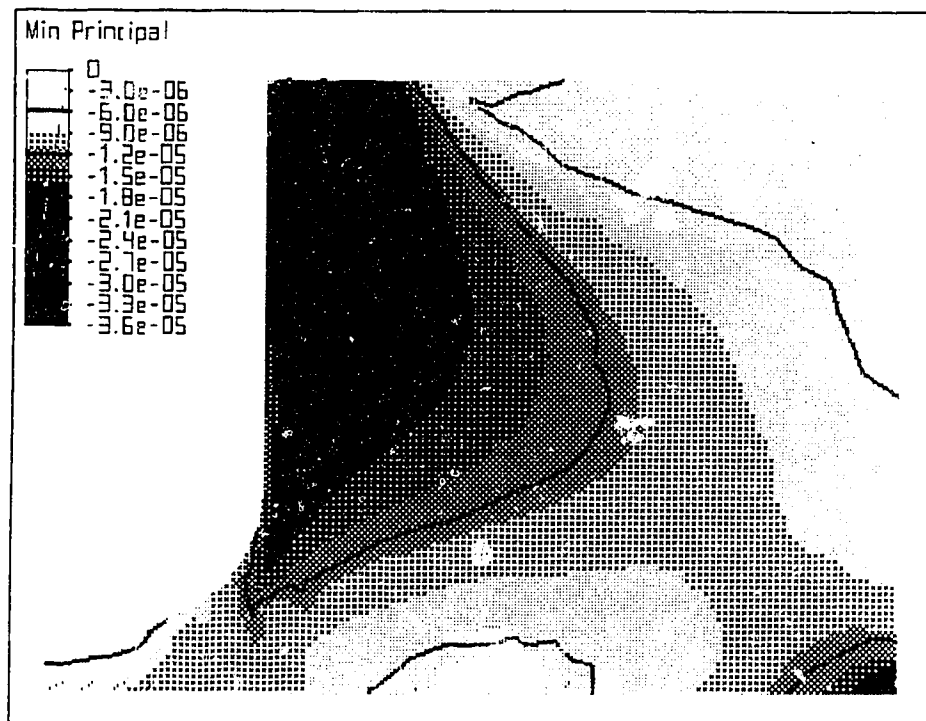


Figure 4-3: Compressive Principal Strain Distribution of the IMZ Implant in Solid Bone

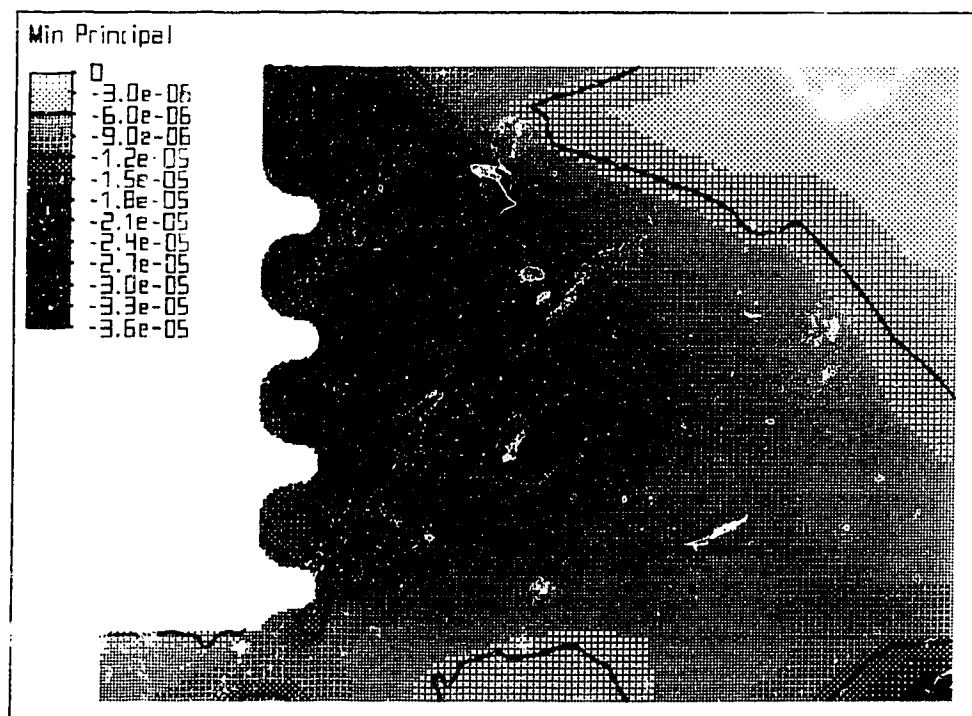


Figure 4-4: Compressive Principal Strain Distribution for the Bud Implant in Solid Bone.

vary substantially between patients. A similar comparison of the strain field for the three implants could also be described for the unicortical and bicortical configurations and although there would be differences noticed between the bone configurations (which will be described below) there was very little difference noticed between the implants for a given bone configuration. For example Figure 4-5 shows that the maximum values of the compressive principal strain for the three implants in each of the three general bone configuration were about equal. It should be noted that since the strain patterns are similar for all of the models that the maximum average value of the strain, as described in chapter 3 section 4.2, gives a good indication of the overall magnitudes of the strains in the bone. For Figure 4-5 the maximum compressive principal strain were taken for each implant with the flange in contact with the bone and did not include the cancellous bone for the unicortical and the bicortical bone configurations.

4.2.2 Bone Configuration: Vertical Load

The comparison of the strain states for the various bone configurations is further broken down into three sections: the first section examines the differences between the unicortical, bicortical and solid cortical type bone configurations, the second examines the effects of replacing cancellous bone into the air space for the unicortical and bicortical configurations, the last section explores the effect of the intermediate soft tissue that was placed between the bone and the soft tissue

4.2.2.1 Unicortical, Bicortical and Solid Bone Comparison

Not surprisingly, the amount of cortical bone present had the largest influence on the state of strain in the bone for the vertical load only loading condition. Figure 4-5 shows that the principal strain was substantially higher for the unicortical configuration when compared with the solid configuration. On average for the three implants the bicortical bone configuration had a maximum strain that was 2.3 times greater than the solid bone configuration while the unicortical bone had a maximum value that was on average 3.6 times higher than the solid bone and was 1.6 times higher than the bicortical bone. Figure 4-4 and Figure 4-6 display an overall view of the compressive principal strain for the Bud implant in the solid cortical bone and the unicortical configuration. It should be noted that for the unicortical picture that the scale for the strain is four times that of the solid case.

When the strain levels in the radial, hoop and vertical directions are compared, it is generally noticed that the magnitudes of the strains in these directions changed, relative to each bone configuration, in the same proportion as the compressive principal strain changed for each bone configuration. Therefore if the principal strain increased by a factor of two between the two bone configurations generally the hoop, radial and vertical strain also increased by a factor of two. Overall the pattern of the strain in the bone for each bone configuration stayed the same but the magnitude increased. For example Figures 4-7 to 4-9 display the radial, hoop and vertical strain for the Brånemark implant in solid bone, while Figures 4-10 to 4-12 display the radial hoop and vertical strain for the Brånemark implant in unicortical bone. The figures show that for both bone configurations that the bone was under compressive stress in the hoop and radial

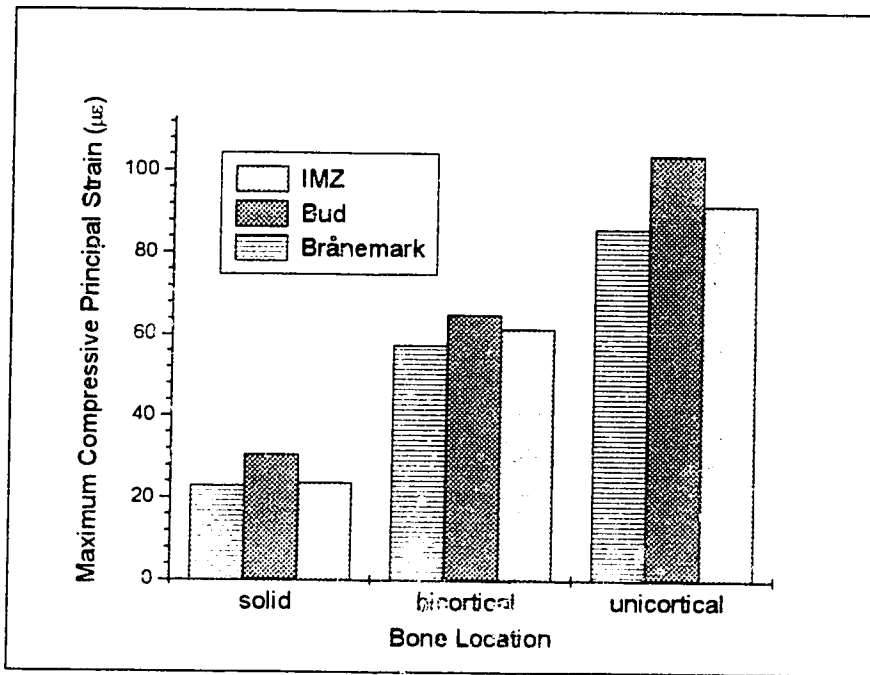


Figure 4-5: Maximum Magnitude of Compressive Principal Strain for the Vertical Force Loading Condition

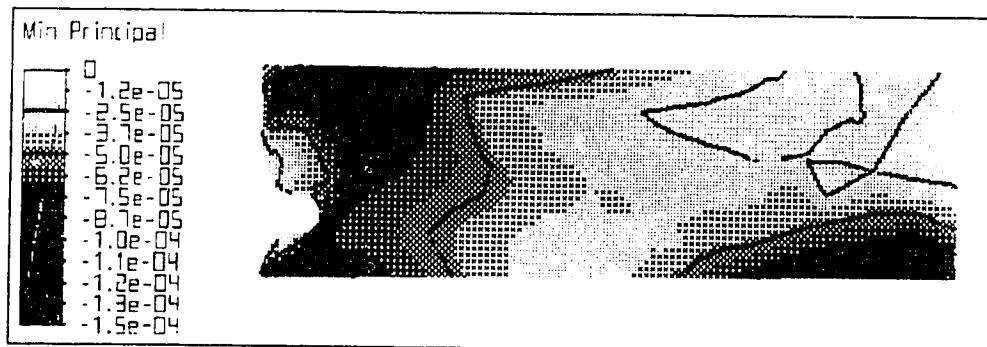


Figure 4-6: Minimum Strain Distribution for the Bud Implant in Unicortical Bone with a Vertical Load.

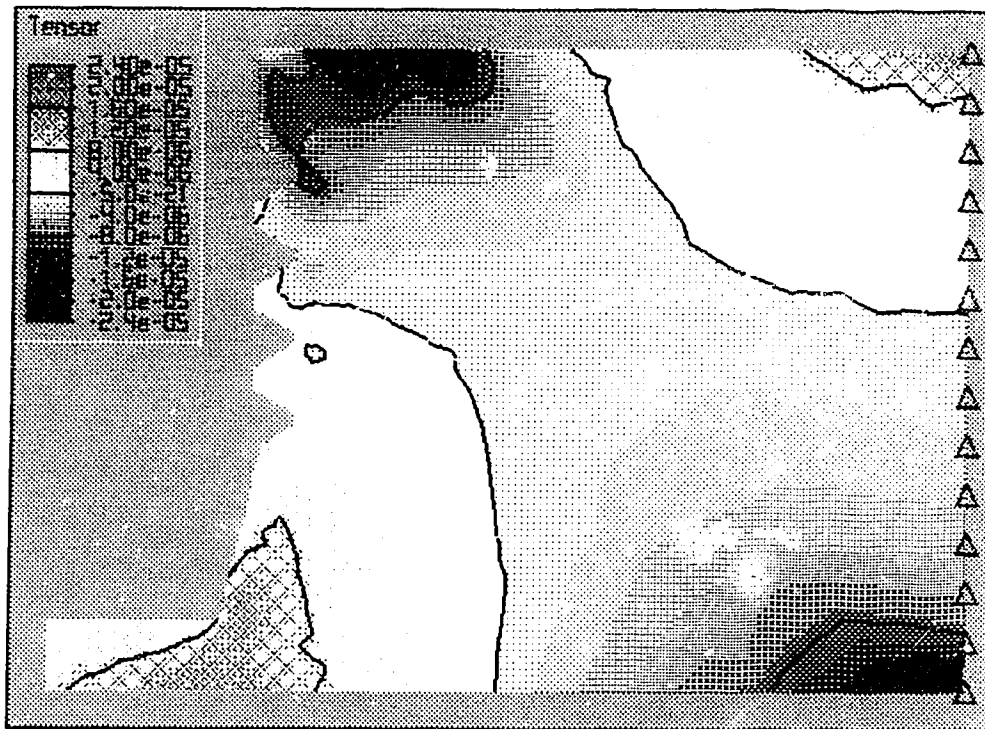


Figure 4-7: Radial Strain Distribution for the Brånemark Implant with a Vertical Load in Solid Bone.

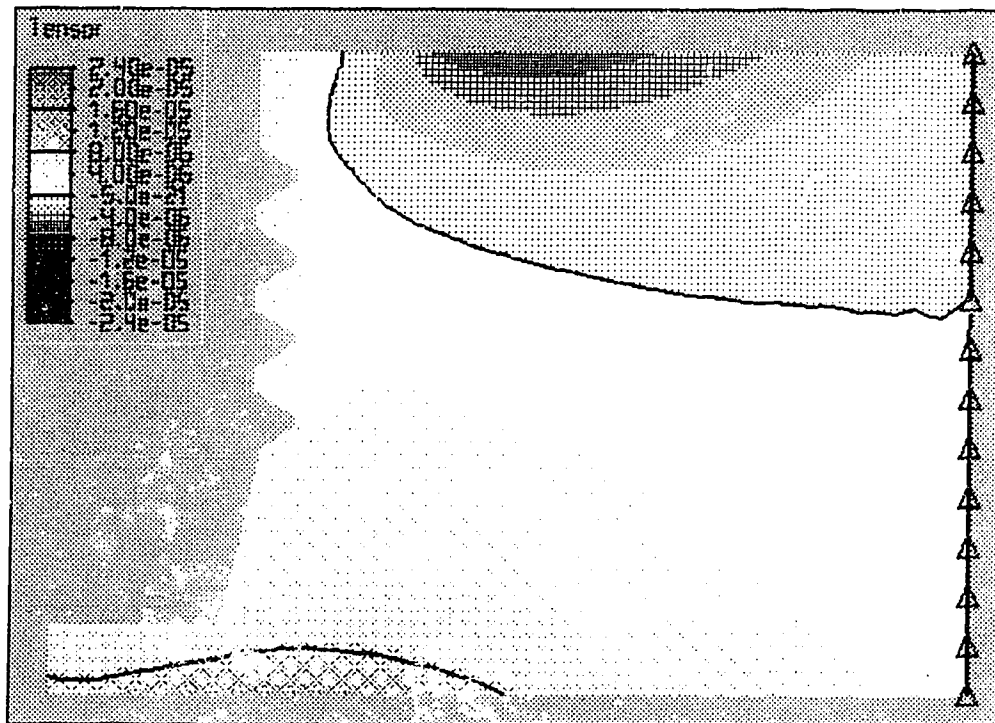


Figure 4-8: Hoop Strain Distribution for the Brånemark Implant with a Vertical Load in Solid Bone.

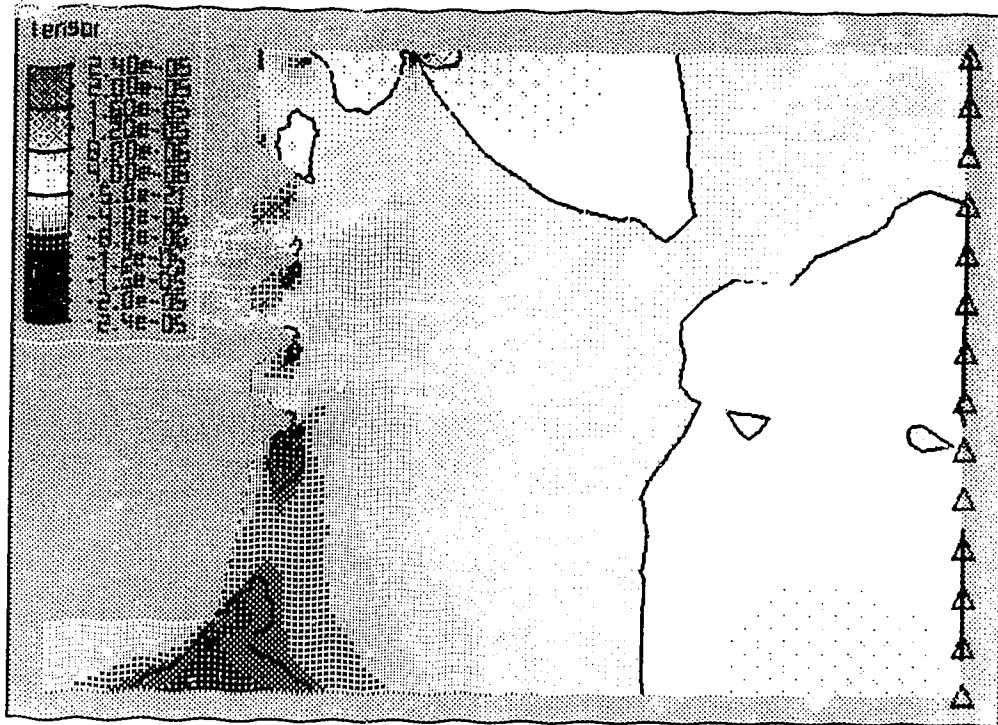


Figure 4-9: Vertical Strain Distribution for the Brånemark Implant with a Vertical Load in Solid Bone

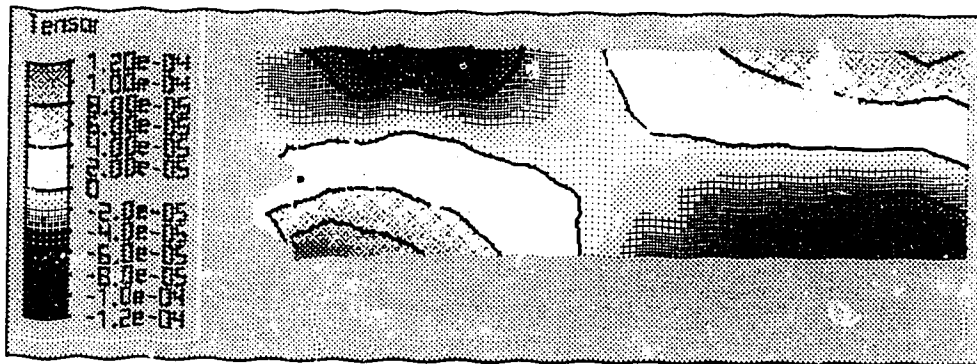


Figure 4-10: Radial Strain Distribution for the Brånemark Implant with a Vertical Load in Unicortical Bone.

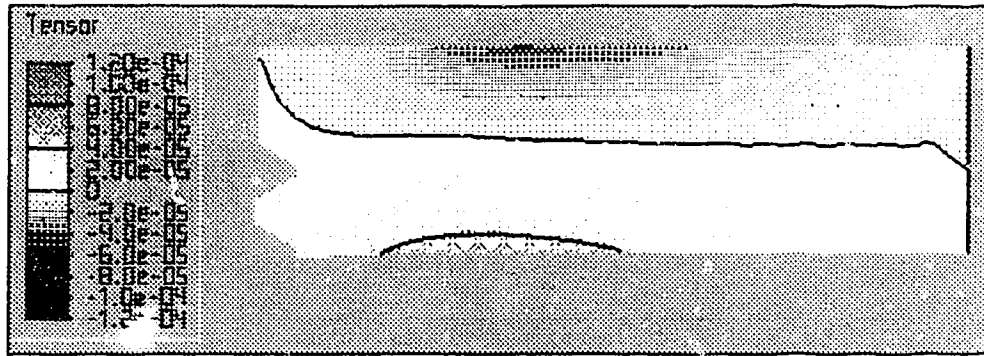


Figure 4-11: Hoop Strain for the Brånemark Implant with a Vertical Load in Unicortical Bone.

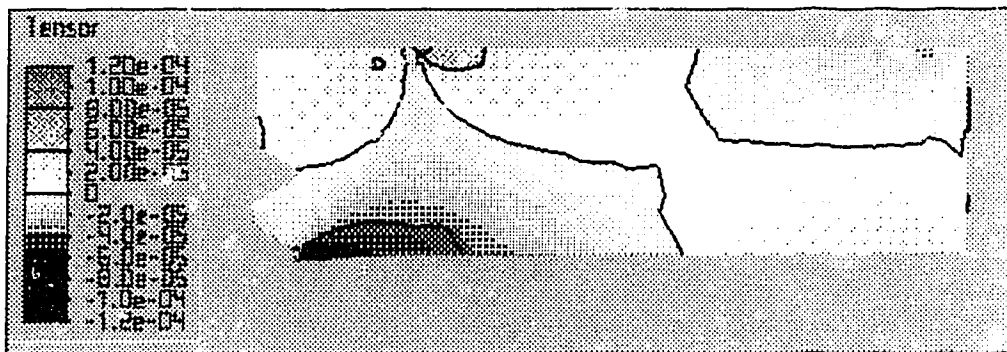


Figure 4-12: Vertical Strain Distribution for the Brånemark Implant with a Vertical Load in Unicortical Bone

directions in the top left corner under the flange and the bottom right corner. While the bone is under tensile stress in the hoop and radial directions in the bottom right and top left corner. This pattern is expected given the loading and boundary conditions and can be appreciated by examining Figure 4-13. This figure displays the exaggerated displacement of the bone for the IMZ implant in the unicortical bone configuration. From this figure it is evident why the maintenance of contact assumption between the implant and the bone along with the fixed boundary condition at the edge of the bone produces the hoop and radial stress patterns described above under the vertical load. Although the pattern of the strains were similar for the three bone configurations, the magnitudes of the strains in the three directions were quite different. The strains were approximately four times higher in the unicortical case as compared to the solid case.

4.2.2.2 Effects of Cancellous Bone for the Unicortical and Bicortical Bone Configurations.

Figures 4-14 and 4-15 display the effect that replacing the air space with cancellous bone had on the maximum value of the compressive principal strain for the unicortical and bicortical bone configurations. As expected the addition of the cancellous bone did decrease the magnitude of the principal strain in the cortical bone. Also, this decrease was more noticeable for the unicortical than the bicortical configuration. On average, for the three implants, the strain was reduced by 21% for the unicortical configuration and by 8% for the bicortical bone configuration. As an example of the reduction of strain, Figure 4-16 displays the compressive principal strain for the Brånemark implant in the bicortical bone with an air space configuration and Figure 4-17

displays the Brånemark implant in bicortical bone with a cancellous bone layer. It can be seen from the figure that the amount of strain in the cortical bone did decrease but in general the addition of the cancellous bone did not greatly affect the location of maximum strain in the cortical bone. It is also apparent from the Figure 4-17 that the cancellous bone was strained to a much higher degree than the cortical bone. In general the high strain in the cancellous bone was noticed for all of the implants in both the unicortical and bicortical bone configurations. It should be noted that the high strains in the cancellous bone does not indicate that the cancellous bone was carrying a large proportion of the load, since the strain in the cortical bone was not notably effected, but rather it was a result of the fact that the elastic modulus or stiffness of the cancellous bone was much less than the cortical bone.

4.2.2.3 Effect of Intervening Soft Tissue

As mentioned in chapter 3, the soft tissue used in this study was intended to be an approximation of the soft tissue that might develop between the bone and the implant. It should again be noted that the soft tissue thickness of 0.05 mm was significantly larger than what is speculated to occur normally and that the material properties for the tissue were only roughly estimated. In all, despite the large thickness there was very little influence from the addition of the soft tissue on the distribution and magnitude of strains in the bone. Figure 4-18 displays the compressive principal strain with and without the soft tissue for each of the three implants in solid bone. This graph shows, except for the IMZ implant, that there was very little difference in the compressive principal strain when the soft tissue was introduced for the solid bone configuration. Figure 4-19 displays the

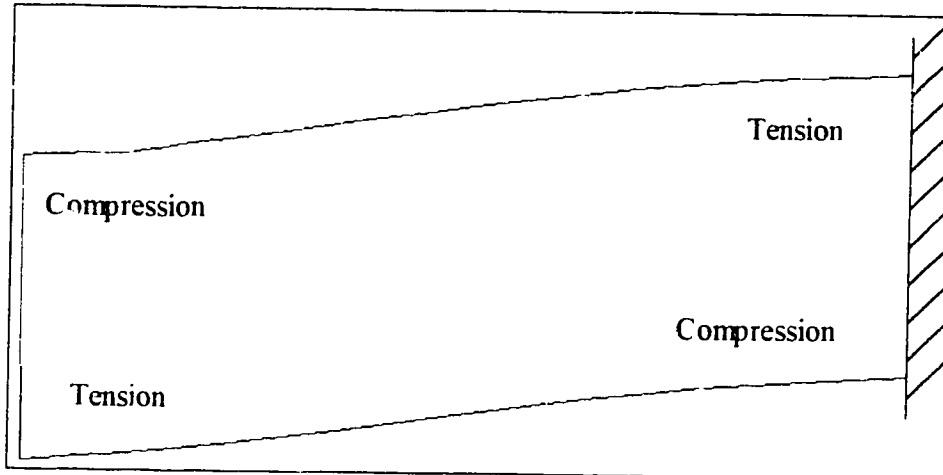


Figure 4-13: Display of General Areas of Radial and Hoop Compression and Tension using the IMZ Implant in Unicortical Bone (Displacement exaggerated).

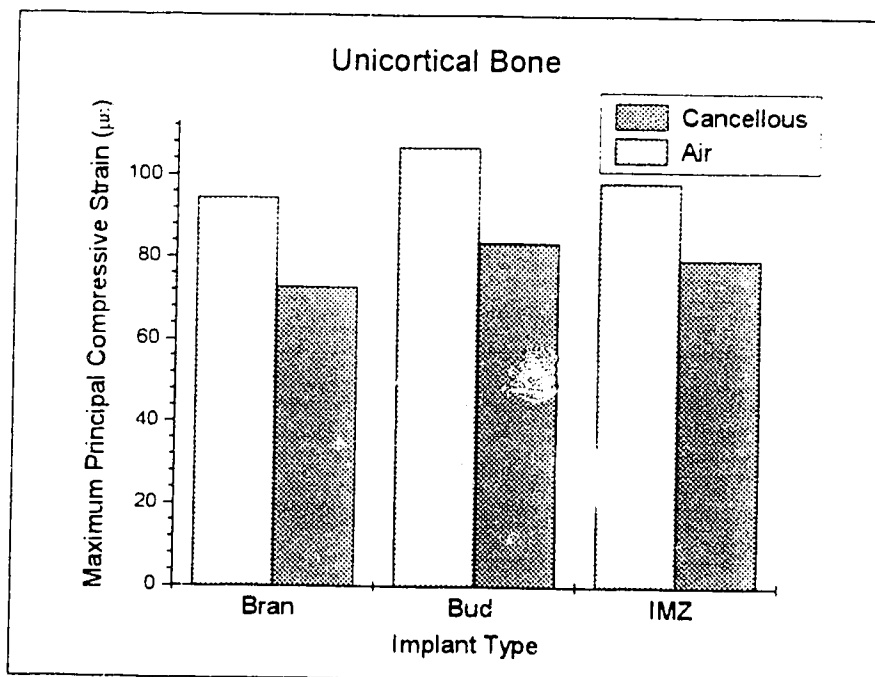


Figure 4-14: Evaluation of the Impact of Cancellous Bone for the Unicortical Bone Configuration, the Vertical Loading Condition and the Three Implant Types.

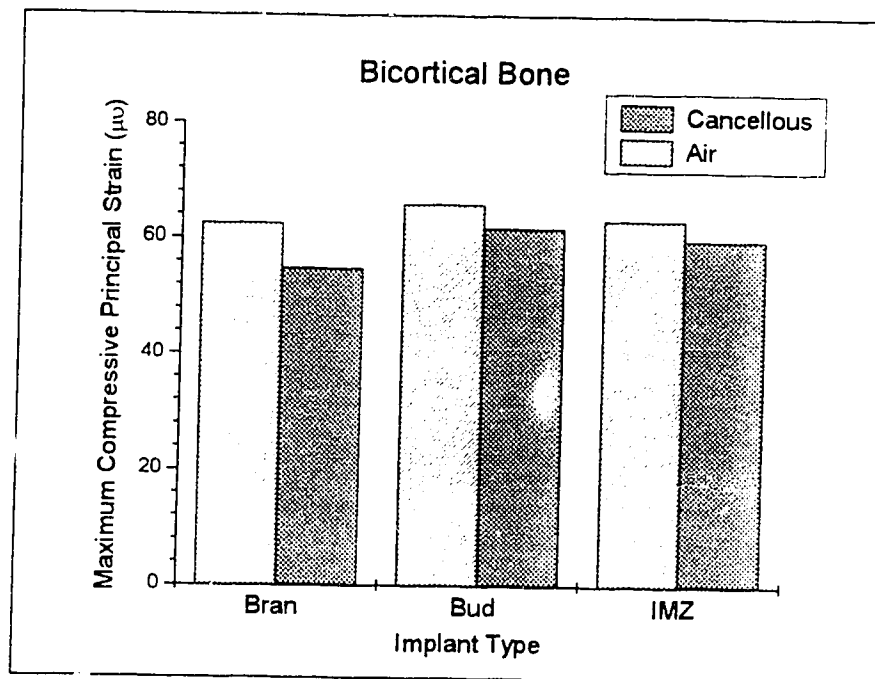


Figure 4-15: Evaluation of the Effects of Cancellous Bone for the Bicortical Bone Configuration, the Vertical Load Loading Condition and the Three Implant Types.

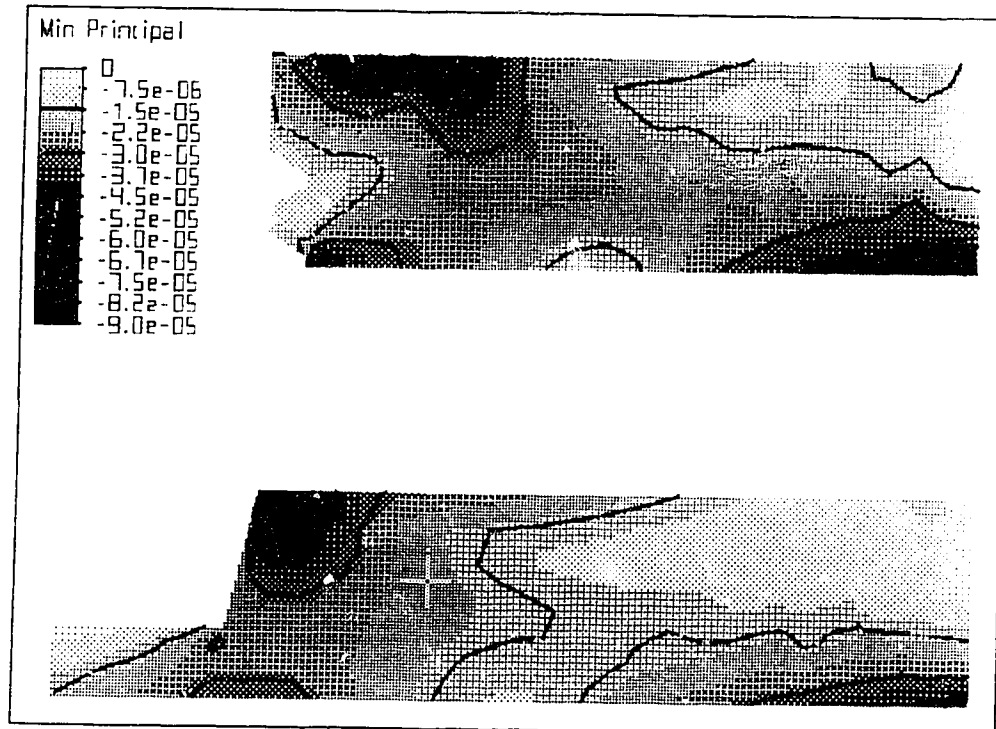


Figure 4-16: Compressive Principal Strain for the Brånemark Implant with a Vertical Load in the Bicortical and an Air Space Bone Configuration.

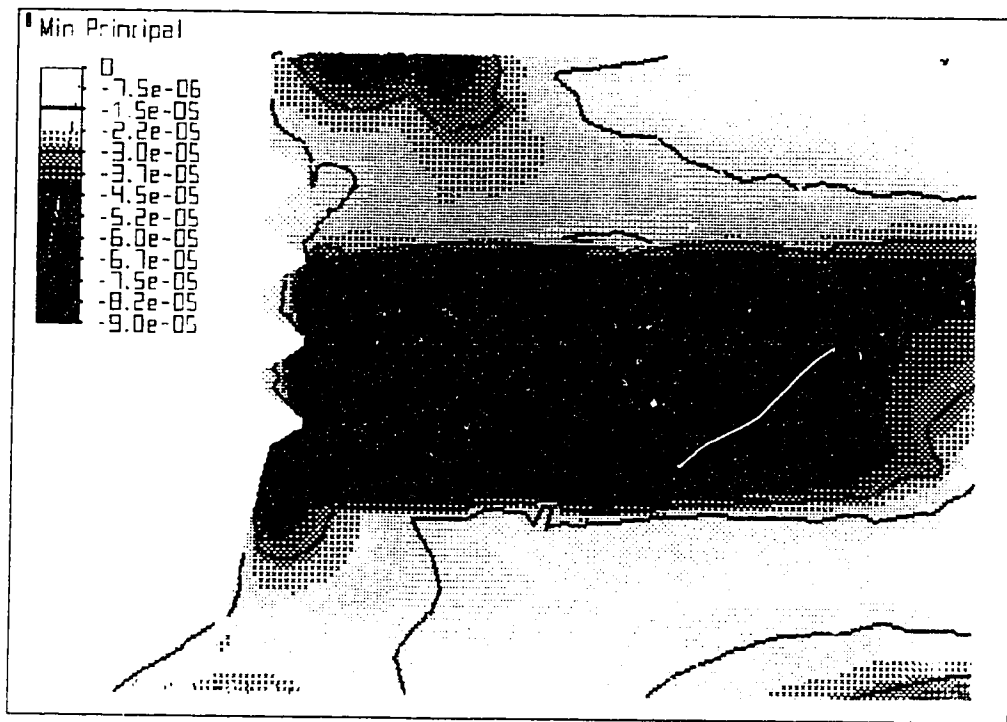


Figure 4-17: Compressive Principal Strain for the Brånemark Implant with a Vertical Load in the Bicortical and Cancellous Bone Configuration.

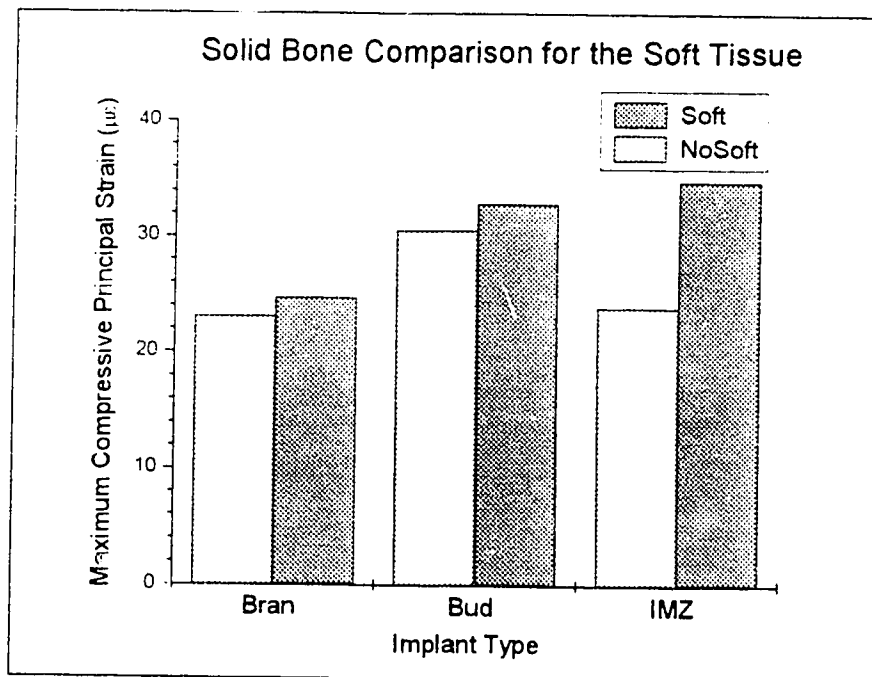


Figure 4-18: Evaluation of the Effects of Soft Tissue on the Minimum Principal Stress for the Solid Bone Configuration and the three Implants with a Vertical Load

compressive principal strain for the IMZ implant in all three of the bone configurations. This figure suggests that for the IMZ implant that the soft tissue did consistently reduce the maximum strain on the bone for the three bone configurations but except for the solid bone configuration this decrease was very small. As an example of the overall influence that the soft tissue had on the strain in the bone Figure 4-20 displays the compressive principal strain distribution in the cortical bone for the Bud implant with the soft tissue present. When this figure is compared to Figure 4-3 (the Bud implant in solid bone with no soft tissue present) there are only minor differences noted in the magnitudes and the locations of the strains. Overall it is felt that the soft tissue had very little effect on the magnitude or location of maximum strain in the bone. The somewhat larger effect that was noticed for the IMZ implant in solid bone was peculiar to that implant.

4.2.3 Flange Vertical Load

It appeared that the flange did have some effect on the strains as well as the locations of the maximum strains that occurred in the bone. Figures 4-21 to 4-23 display bar graphs of the compressive principal strain for the three implants in the three different bone configurations. For the solid bone configuration the maximum magnitude of the compressive principal strain was increased on average by 15% when the flange was removed, while for the bicortical and unicortical cases the average increase was 8% and 13% respectively. With respect to the various implants it was noticed that for the Brånemark implant the compressive principal strain increased for the three bone configurations by approximately 20% when the flange was removed, while for the Bud and IMZ implant the increase was 5% and 11% respectively. Figure 4-24 displays the

compressive principal strain picture for the Brånemark implant with the flange no longer in contact with the bone. When this figure is compared to Figure 4-1 it can be seen that the area of highest strain moves from underneath the tip of the flange to the top corner of the bone at the neck of the implant. Also, the strain along the base of the threads in the bone increased by about 14%. Similar results of removing the flange on the location of strains was also seen in the unicortical and the bicortical configurations as well as with the other two implants. Overall it appeared that the flange did alter the distribution of the strain in the bone and reduce the peak strain to some degree.

4.3 Vertical Load and Moment Loading Condition

As mentioned in Chapter 3 this loading condition was modeled using three dimensional elements. The strain pictures shown in this section display only one half of the model which was sliced down the axis of symmetry which is perpendicular to the vector of the moment applied. For some of the strain pictures it may be difficult to see boundaries of the cortical bone when the strain dither is superimposed so it may be necessary to refer to Figures 4-25 to 4-27, which display a view of the cortical bone for the three general bone configurations. Again all of the strain pictures are displayed in unitless strain (mm/mm). Table 4-2 summarizes the tensile and compressive principal strain for all of the models discussed in this section.

As with the previous section all of the comparisons between the models were done based on the compressive principal strain since it had the highest absolute maximum for the given loading conditions. It is again true that if the vertical load placed on these

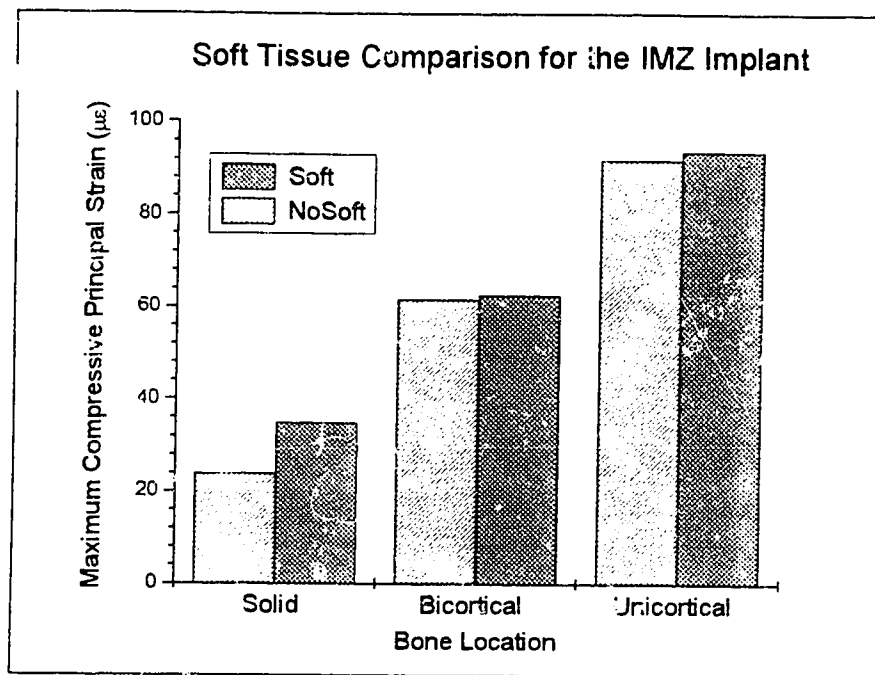


Figure 4-19: Evaluation of the Effects of Soft Tissue on the Compressive Principal Strain for the IMZ Implant in three Different Bone Configurations.

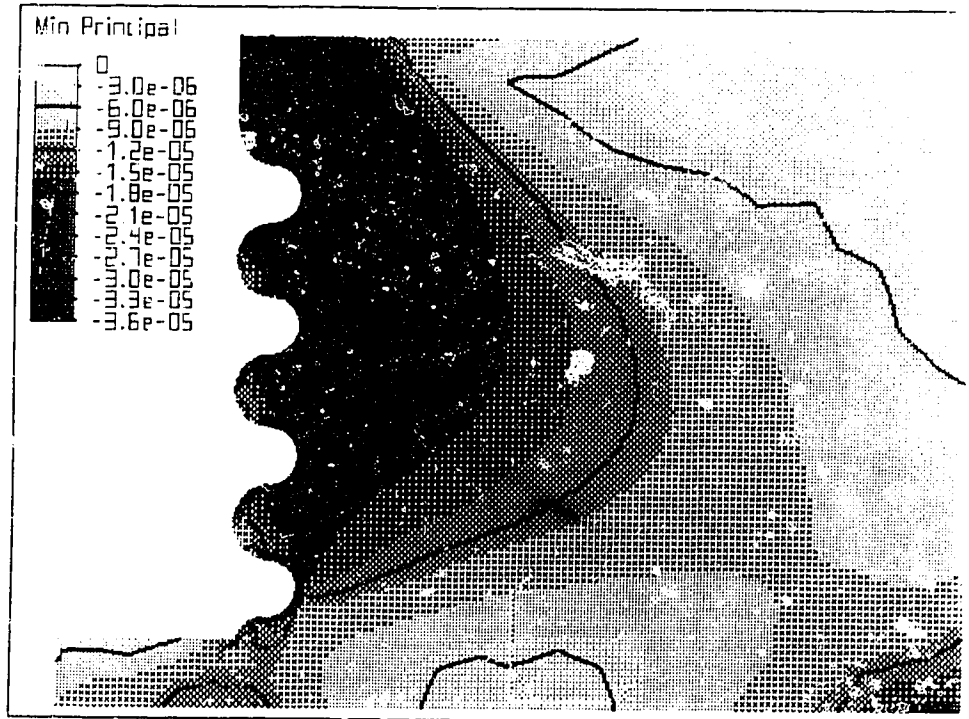


Figure 4-20: Compressive Principal Strain for the Bud Implant in Solid Bone with Soft Tissue and the Vertical Force Loading Condition.

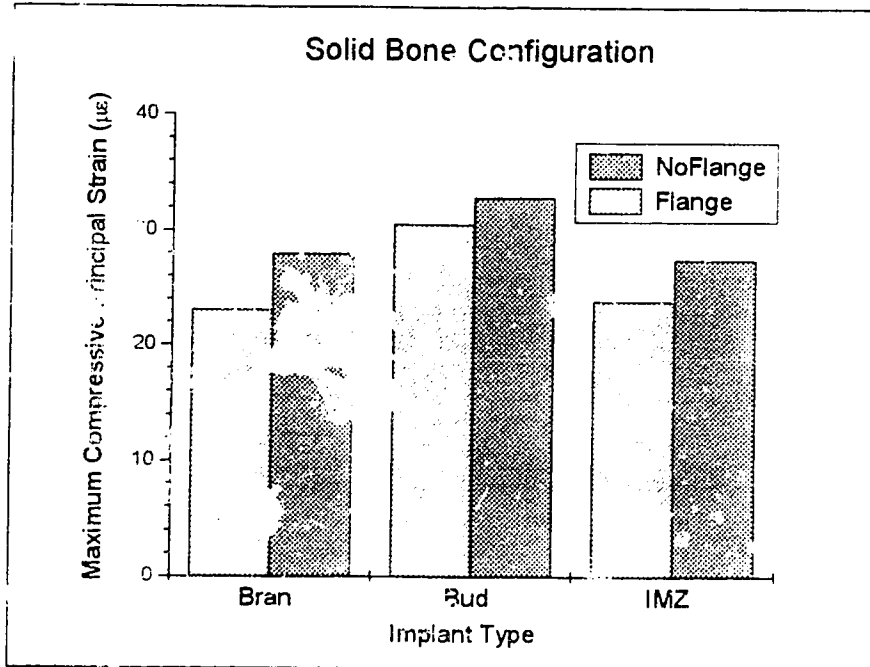


Figure 4-21: Comparison of the Compressive Principal Strain for the three Implants in Solid Bone with a Vertical Load with and without the Flange

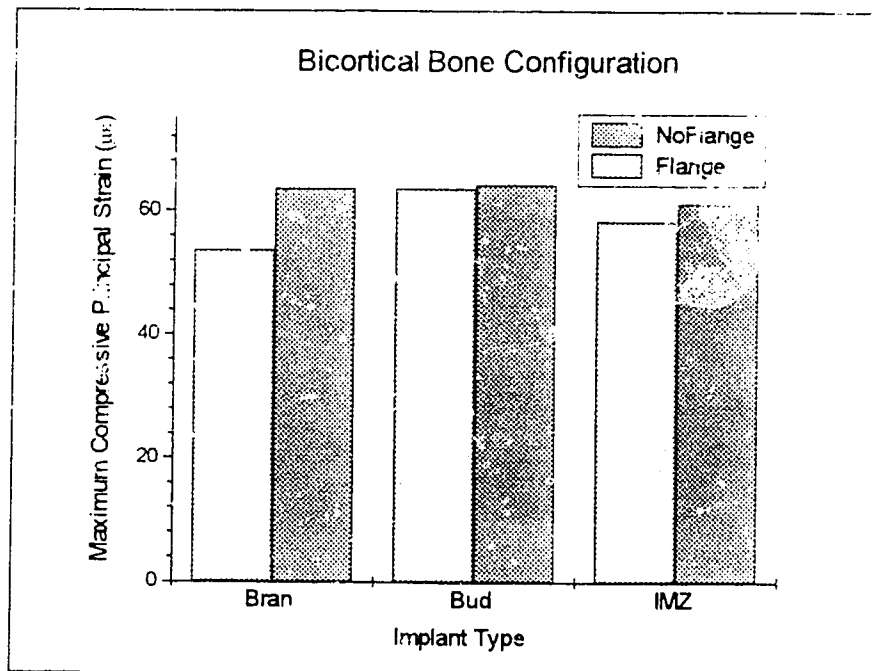


Figure 4-22: Comparison of the Compressive Principal Strain for the three Implants in Bicortical Bone with a Vertical Load with and without the Flange

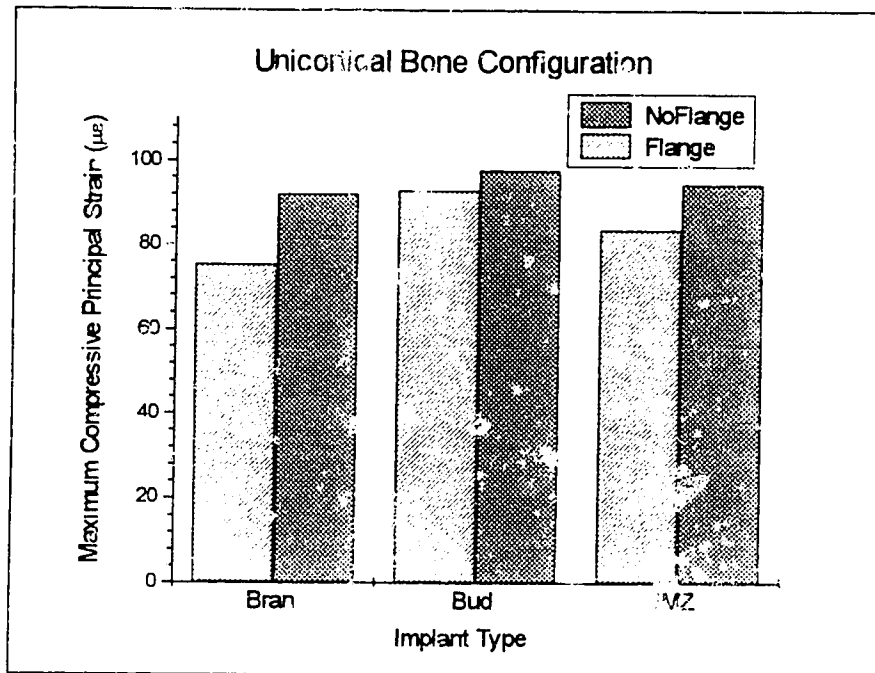


Figure 4-23: Comparison of the Compressive Principal Strain for the Three Implants in Unicortical Bone with a Vertical Load with and without the Flange

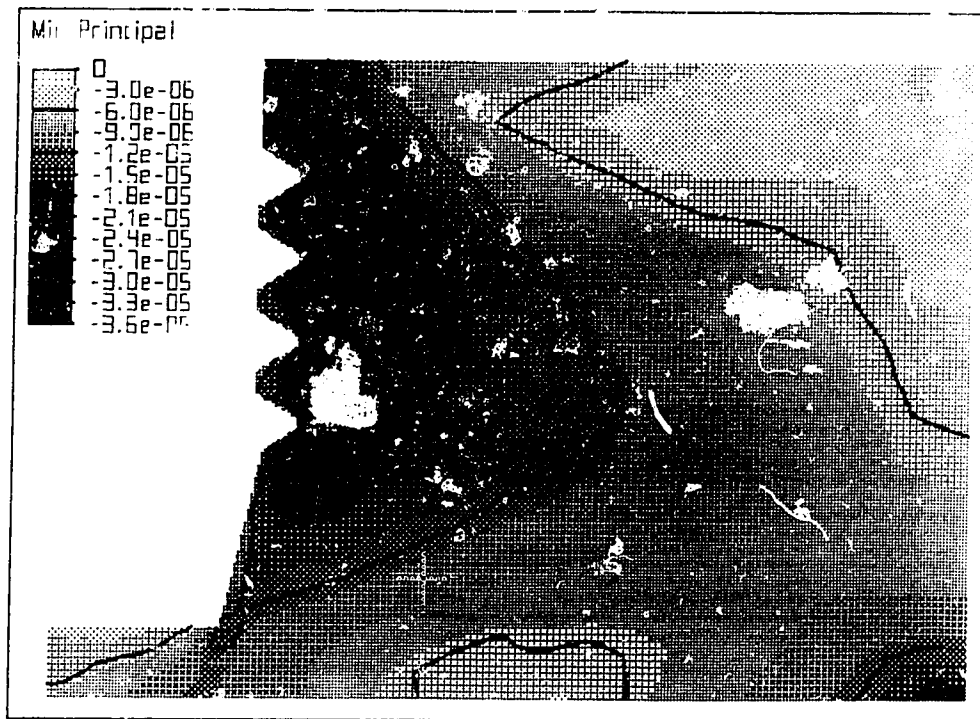


Figure 4-24: Compressive Principal Strain for the Brånemark Implant in Solid Bone with a Vertical Load and No Flange

models was reversed so that it was directed upward that the tensile principal strain would have had the highest magnitude. As with the vertical only loading condition the compressive principal strain represents the highest magnitude of the principal strain (compressive or tensile) that would occur if the vertical load was cycled from positive to negative. It should also be noted that there is nothing unique about high strains that seem to occur on only one side of the implant since the moment placed on the implant could also be reversed which would cause the high strains to appear on the opposite side.

4.3.1 Implant Design: Force and Moment

For the vertical load and a moment loading condition there was a significant difference noticed between the three implants. Figure 4-28 displays the maximum value of the compressive principal strain for the three implants in the three bone configurations. The major feature of these results indicate that the Bud implant produced strains in the bone that were about 33% higher than the other two implants. Figures 4-29 to 4-31 display the strain distributions for the three implants in solid bone. These Figures again indicate the higher strain levels that were associated with the Bud implant, but also show that the general regions of higher strains were approximately the same. The maximum strain for each implant was near the neck of the implant and under the flange. The strain levels decreased with increasing radius from the implant and also as the vertical distance from the bone surface increased.

4.3.2 Bone Configuration: Vertical Load and Moment

4.3.2.1 Unicortical, Bicortical and Solid Bone Comparison

As shown in Figure 4-28 there was a noticeable difference in the strain produced in the bone for the three implants in the unicortical bone configuration versus the solid and the bicortical bone. The strain values on average in the bicortical bone were 20% higher than the solid situation while the unicortical bone on average had a maximum strain that

Table 4-2: Summary of the Maximum Tensile and Compressive Principal Strains for all of the Models Loaded with a Force and Moment.

Implant Type	Bone Configuration	Flange	Cancellous Bone	Soft Tissue	Max. Principal Strain ($\mu\epsilon$)	Min. Principal Strain ($\mu\epsilon$)
Brånemark	solid	yes	no	no	115.8	-150.1
Brånemark	solid	no	no	no	141.0	-174.1
Brånemark (5.0mm diam.)	solid	yes	no	no	59.5	-96.5
Brånemark	unicortical	yes	no	no	335.0	-344.0
Brånemark	unicortical	no	no	no	442.7	-449.7
Brånemark	unicortical	yes	yes	no	255.2	-289.0
Brånemark	bicortical	yes	no	no	151.3	-184.8
Brånemark	bicortical	no	no	no	191.1	-215.8
Brånemark	bicortical	yes	yes	no	145.6	-191.3
Bud	solid	yes	no	no	204.7	-240.7
Bud	solid	no	no	no	205.0	-238.4
Bud (3.26 mm diam.)	solid	yes	no	no	124.0	-158.1
Bud	unicortical	yes	no	no	489.6	-501.5
Bud	unicortical	no	no	no	562.4	-567.0
Bud	bicortical	yes	no	no	237.6	-273.0
Bud	bicortical	no	no	no	240.0	-264.3
IMZ	solid	yes	no	no	119.4	-155.1
IMZ	solid	no	no	no	141.1	-172.8
IMZ	solid	yes	no	yes	143.6	-174.2
IMZ	unicortical	yes	no	no	380.8	-393.7
IMZ	unicortical	no	no	no	464.2	-471.0
IMZ	unicortical	yes	no	yes	390.7	-407.1
IMZ	bicortical	yes	no	no	168.0	-198.5
IMZ	bicortical	no	no	no	192.6	-217.2
IMZ	bicortical	yes	no	yes	184.8	-215.9

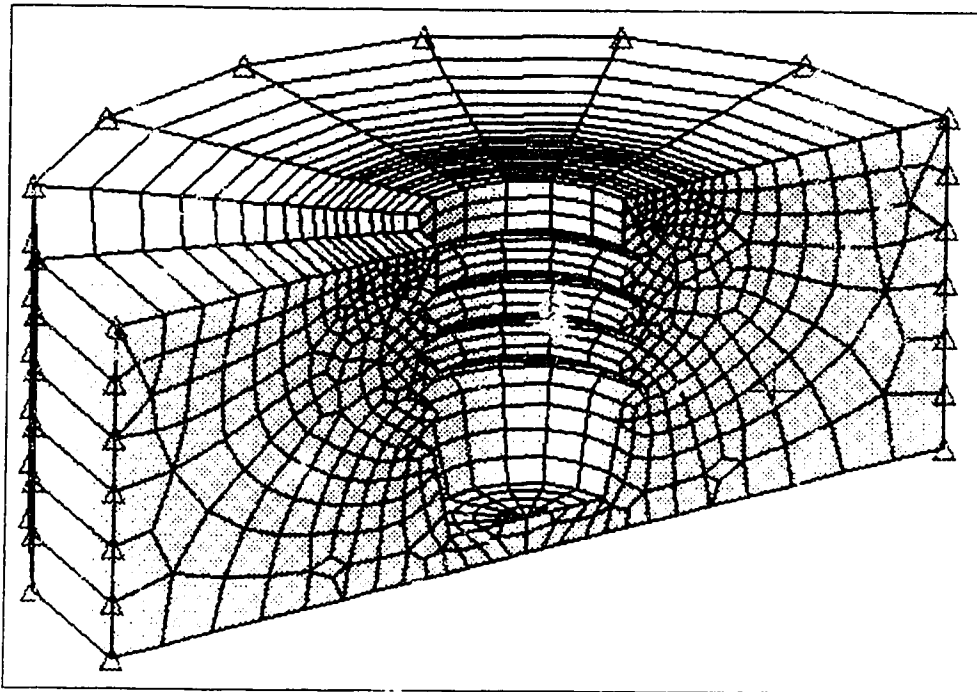


Figure 4-25: Sample View of the Finite Element Mesh of Cortical Bone for the Brånemark Implant in Solid Bone.

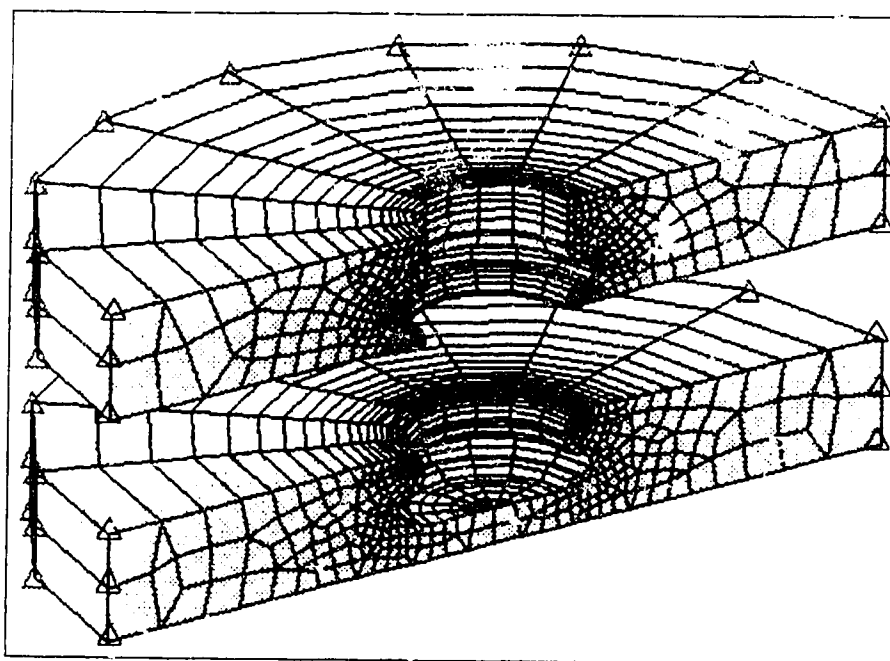


Figure 4-26: Sample View of the Finite Element Mesh of Cortical Bone for the Bud Implant in Bicortical Bone.

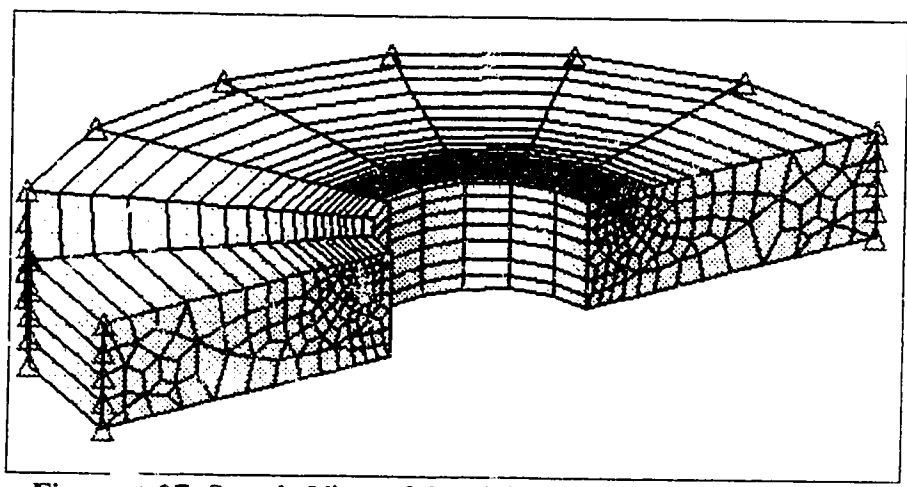


Figure 4-27: Sample View of the Finite Element Mesh of Cortical Bone for the IMZ Implant in Unicortical Bone

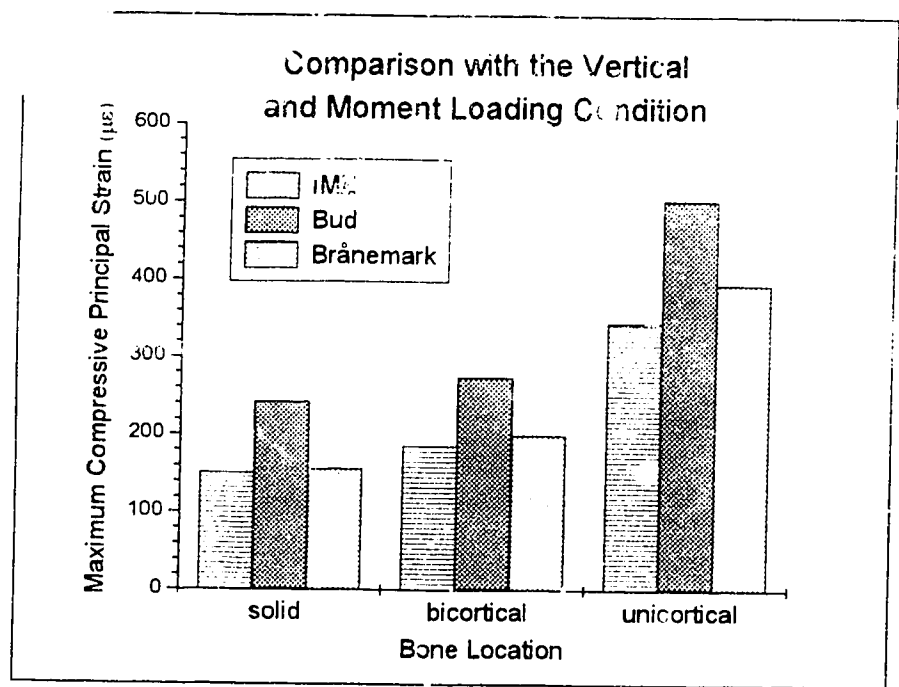


Figure 4-28: Minimum Principal Strain for the Three Implants in the Three Bone Configurations for the Force and Moment Loading Condition

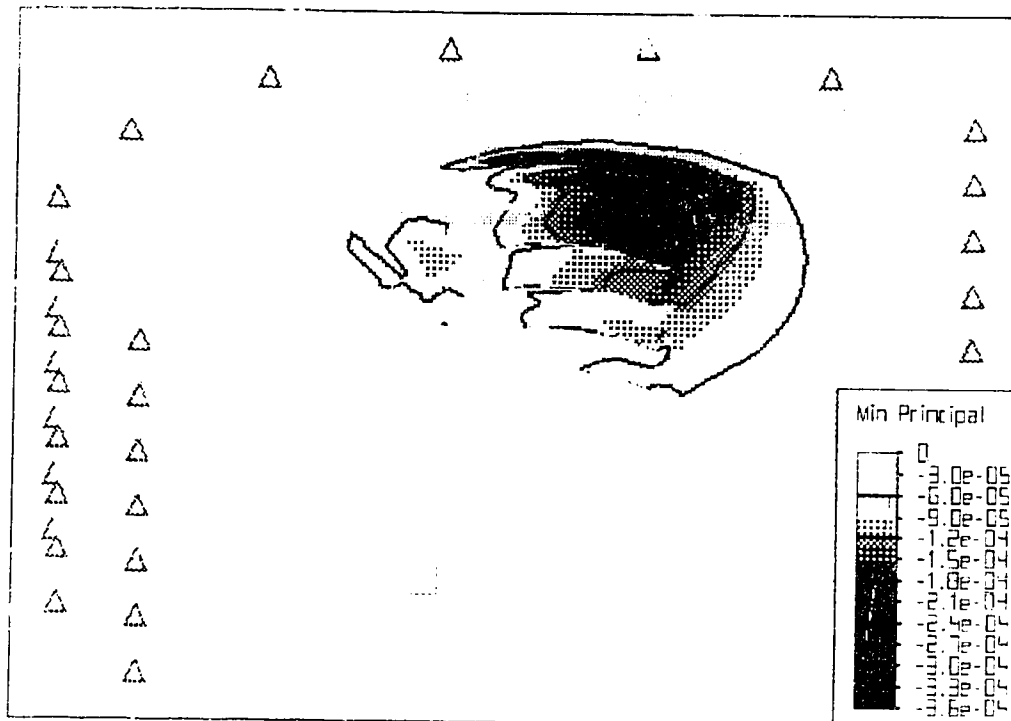


Figure 4-29: Minimum Principal Strain for the Brånemark Implant in Solid Bone with the Force and Moment Loading Condition

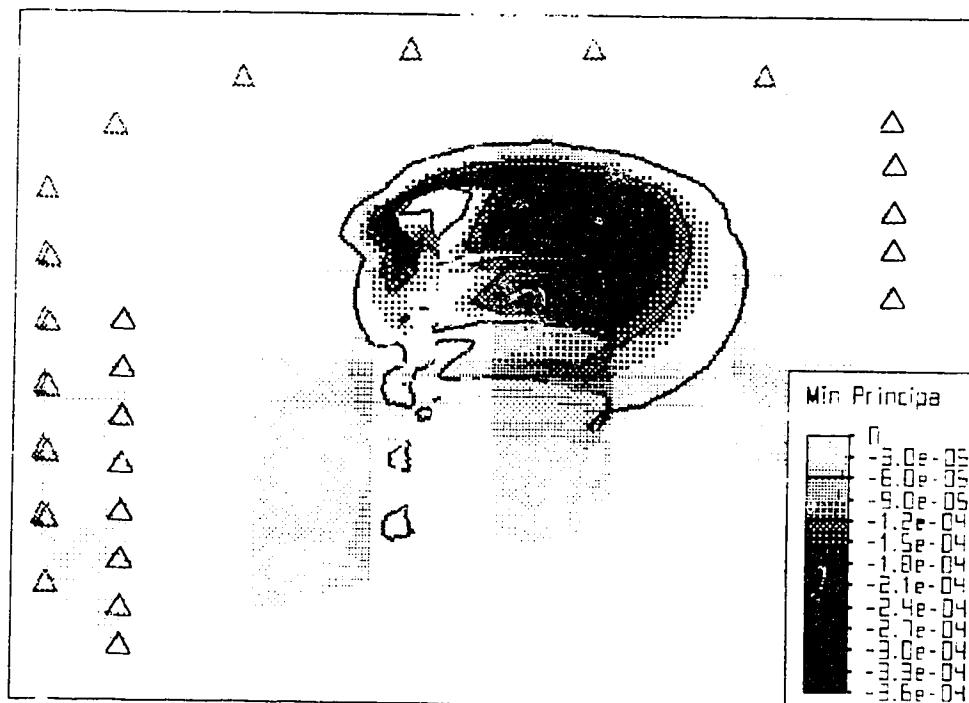


Figure 4-30: Minimum Principal Strain for the Bud Implant in Solid Cortical Bone with a Force and Moment Loading Condition.

was 2.4 times larger than the solid bone. As an example Figures 4-31, 4-32 and 4-33 displays the compressive principal strain for the IMZ implant in the solid, bicortical and unicortical configurations. It should be noted that the scale for the unicortical bone strain picture is 2.5 times that of the other two cases.

As with the vertical load case the strain pattern produced by the force and moment loading condition were quite similar for the three bone configurations. Figure 4-34 displays the deformation of the bicortical bone for the IMZ implant and gives an indication of the regions of compression and tension in the bone. Figures 4-35 to 4-37 display the strain states in the radial, hoop and vertical directions for the Brånemark implant in bicortical bone. These figures confirm the locations of tension and compression in the bone. An examination of the solid bone and unicortical bone configurations showed a similar types of displacement and strain patterns as shown in the previous figures. The only major difference that would be noticed is the magnitudes of the strains that occur for the unicortical bone and the Bud implant.

4.3.2.2 Effects of Cancellous Bone for the Unicortical and Bicortical Bone Configurations

From Table 4-2 it can be seen that the addition of the cancellous bone increased the maximum value of the compressive principal strain in the cortical bone for the Brånemark implant in the bicortical configurations from 184.8 to 191.3 micro-strain. While for the unicortical bone and the Brånemark implant the addition of the cancellous bone reduced the maximum compressive principal strain from 344.0 to 289.0 micro-strain. In general the addition of the cancellous bone for the force and moment produced only

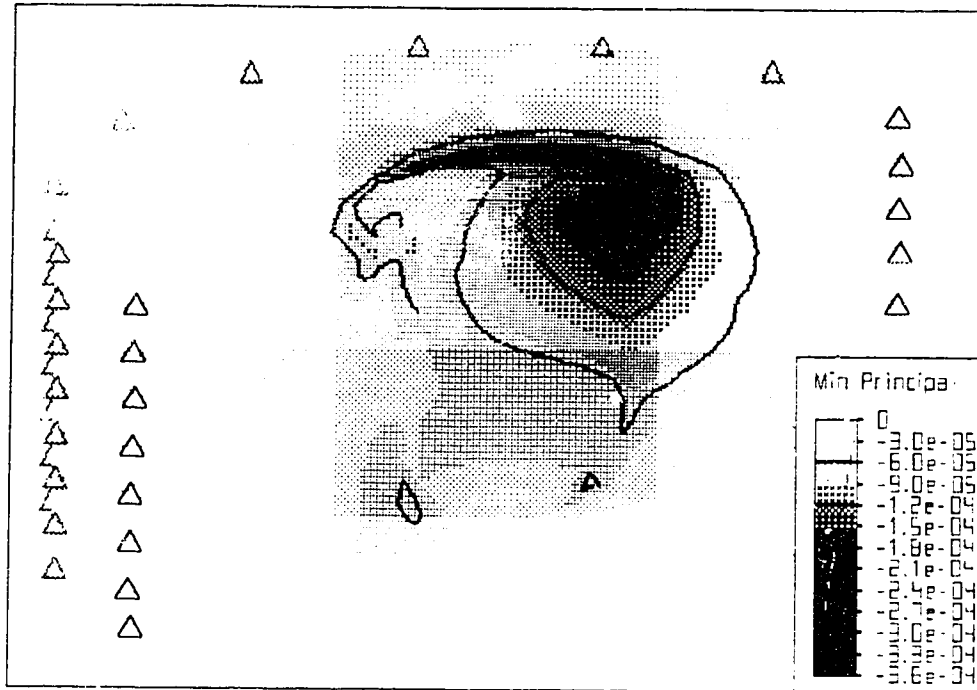


Figure 4-31: Minimum Principal Strain for the IMZ Implant in Solid Cortical Bone with a Force and Moment Loading Condition.

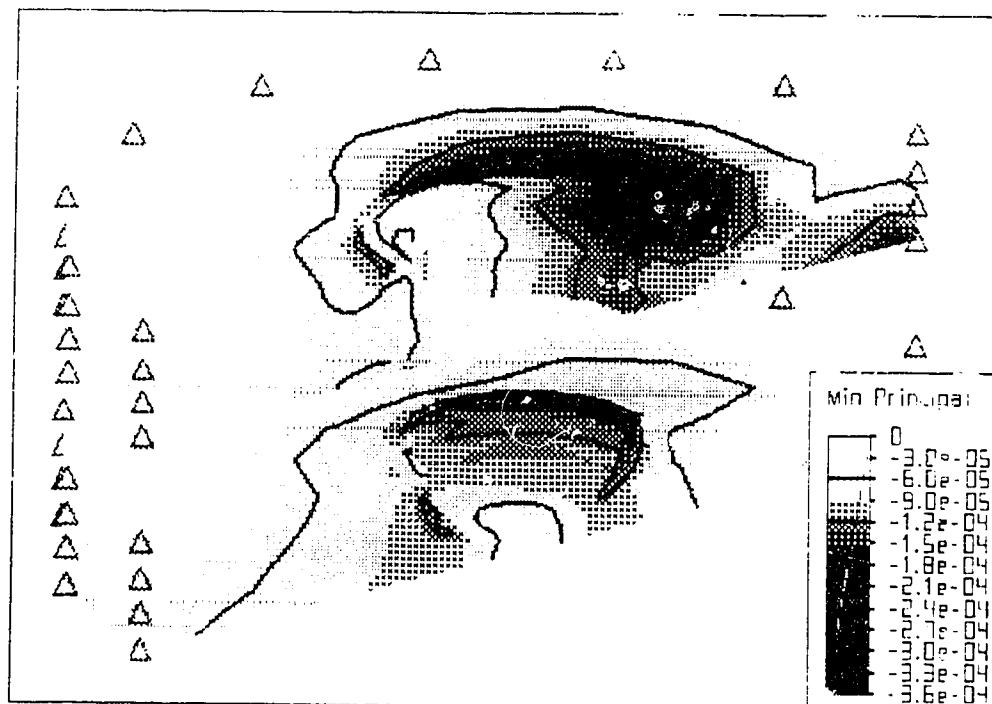


Figure 4-32: Minimum Principal Strain for the IMZ Implant in Bicortical Bone with a Force and Moment Loading Condition.

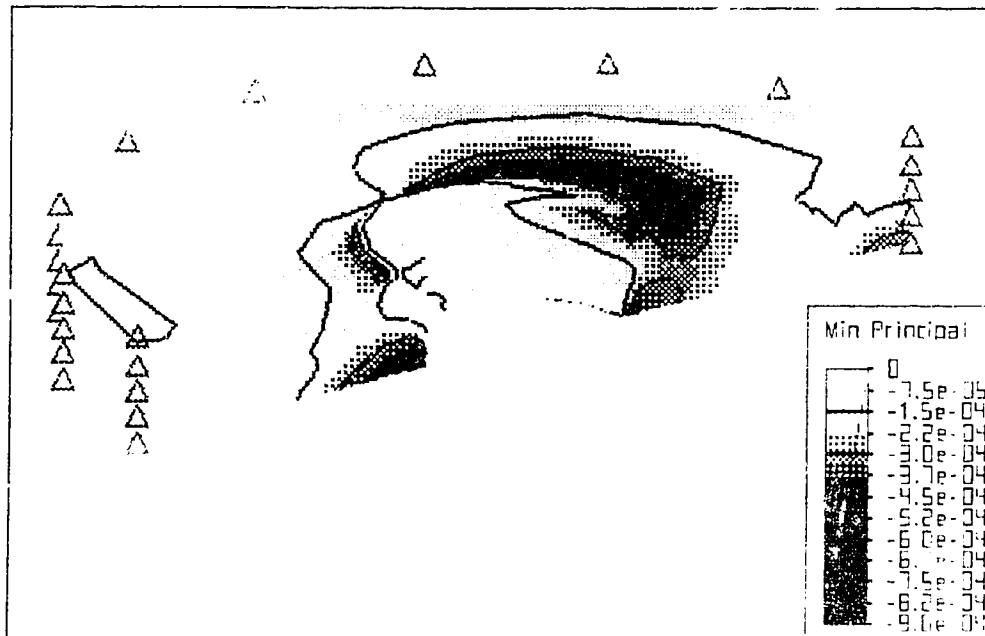


Figure 4-33: Minimum Principal Strain for the IMZ Implant in Unicortical Bone with a Force and Moment Loading Condition.

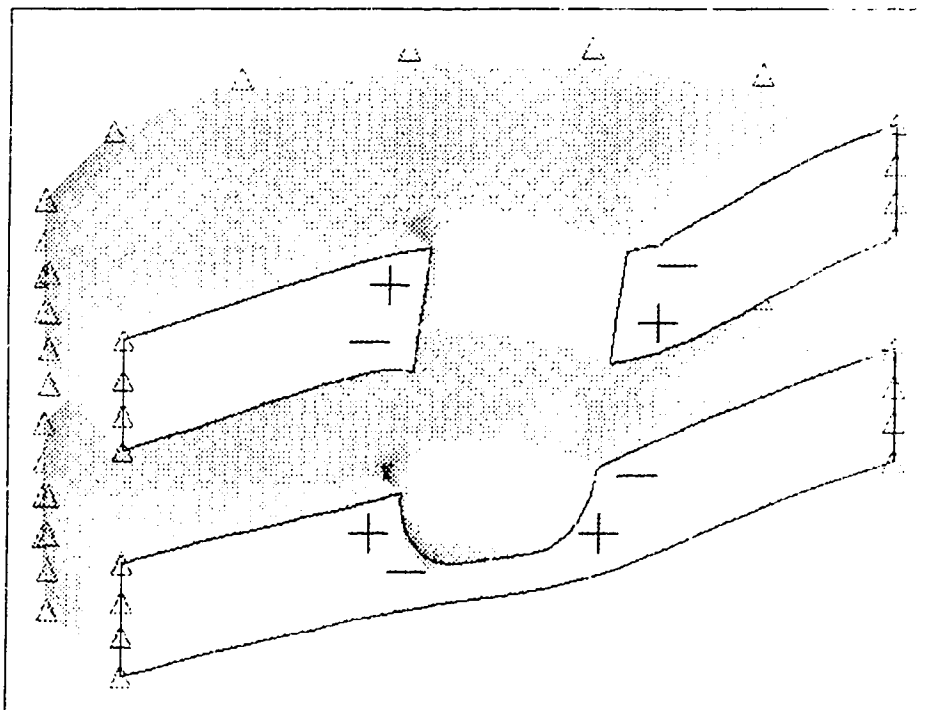


Figure 4-34: Displacement of the Bicortical Bone with an IMZ implant and a force and moment loading condition with regions of compression (-) and tension (+) highlighted. (Scale Exaggerated by a 1000)

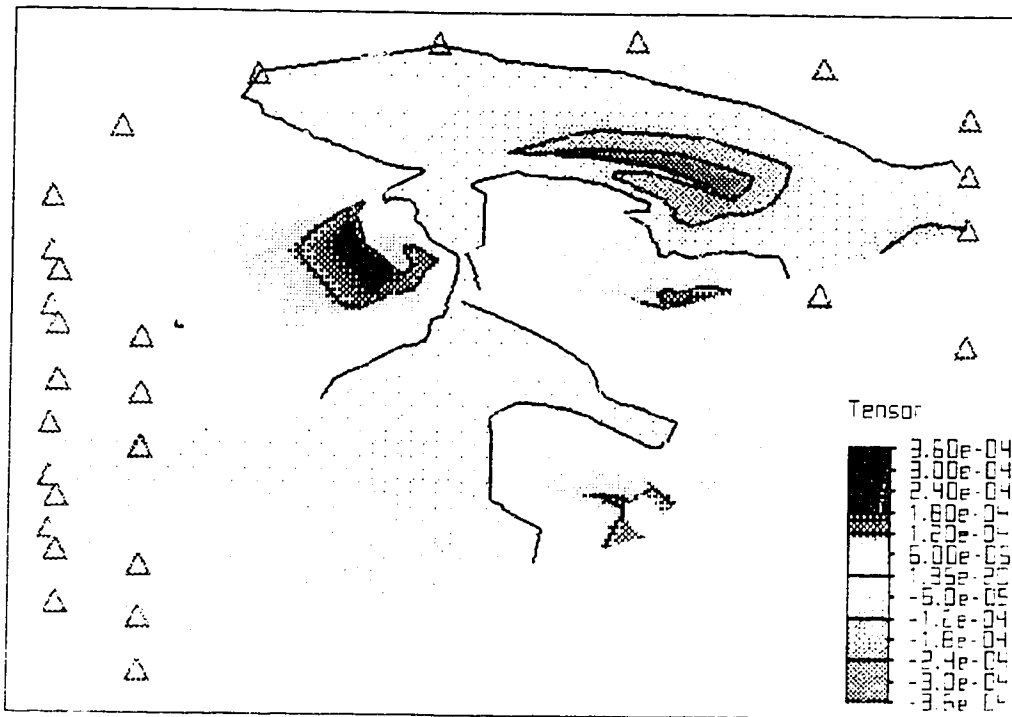


Figure 4-35: Radial Strain for the Brånemark Implant in Bicortical Bone with a Force and Moment Loading Condition.

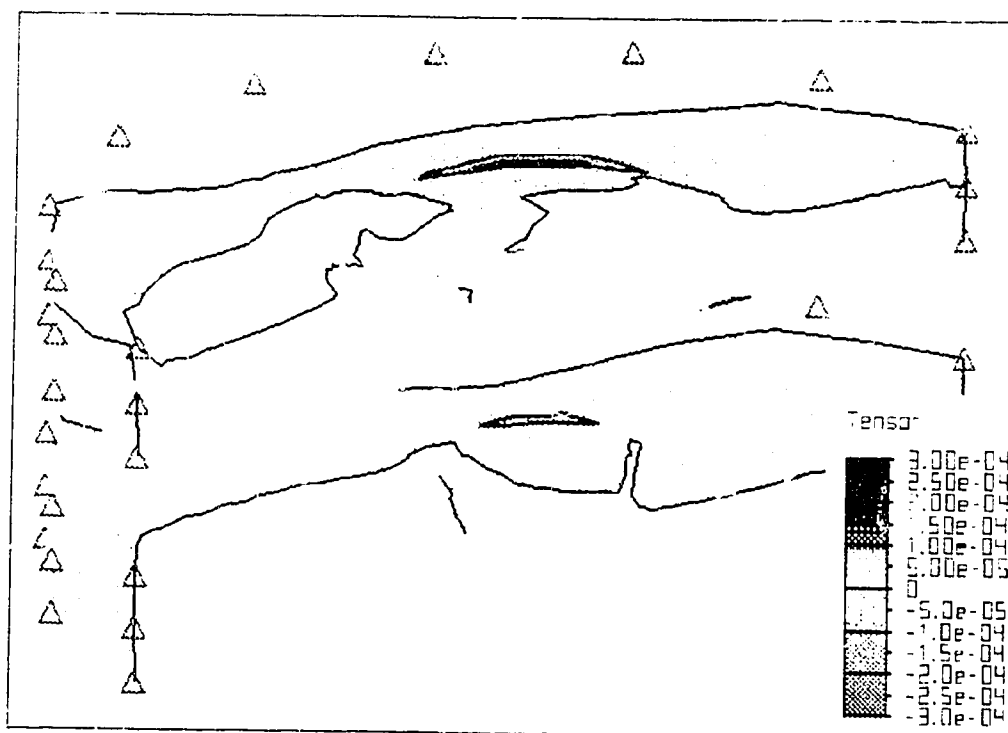


Figure 4-36: Hoop Strain for the Brånemark Implant in Bicortical Bone with a Force and Moment Loading Condition.

small changes in the strain in the cortical bone. It should be noted that like the vertical load loading condition that the strain in the cancellous bone was quite high, as shown in Figure 4-38.

4.3.2.3 Effect of Intervening Soft Tissue

Figure 4-39 displays the maximum magnitude of the compressive principal strain for the IMZ implant in the three bone configurations where the soft tissue has been added. It appears from the figure that there was very little difference in the strain with the introduction of the soft tissue. On average the maximum strain values for the three bone configurations only decreased by 7%. As with the vertical load only case, there were only minor differences in the general locations and distribution of the strains in bone when the soft tissue layer was added.

4.3.3 Flange: Vertical Load and Moment

The overall effect of the flanges under vertical load and moment is shown in Figures 4-40 to 4-42 which display the maximum compressive principal strain for the three implants in the three general bone configurations. It should be noted that the flanges for three implants were substantially different (see Figure 3-2). The Brånemark implant had the flange with the greatest contact area while the Bud implant had the least. In general it was noticed that the maximum strain was increased when the flange was removed, but the Bud implant in the solid and bicortical situation did display a slight decrease in the maximum strain when the flange was removed. These differences were

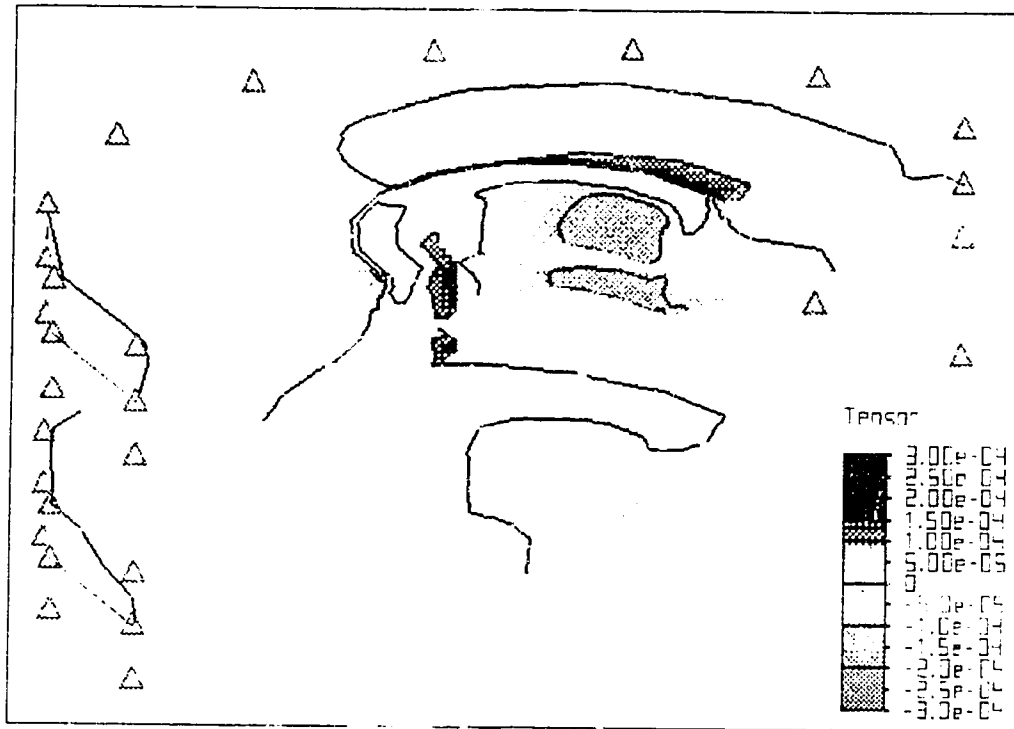


Figure 4-37: Vertical Strain for the Brånemark Implant in Bicortical Bone with a Force and Moment Loading Condition.

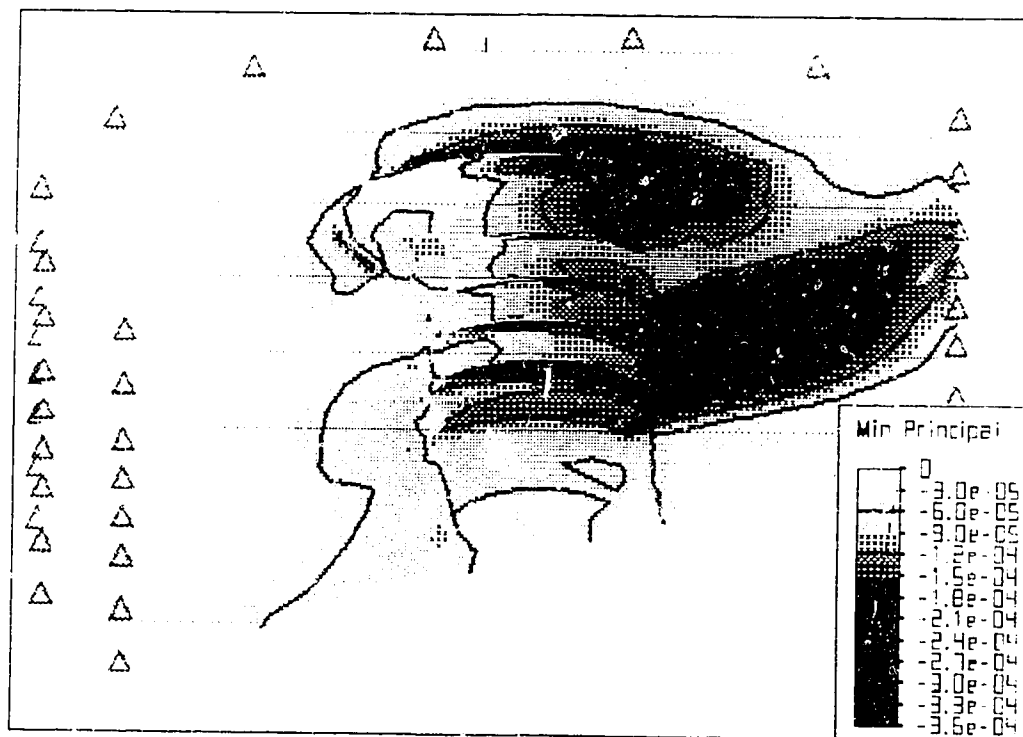


Figure 4-38: Minimum Principal for the Brånemark Implant in Bicortical Bone with Cancellous and a Force and Moment Loading Condition.

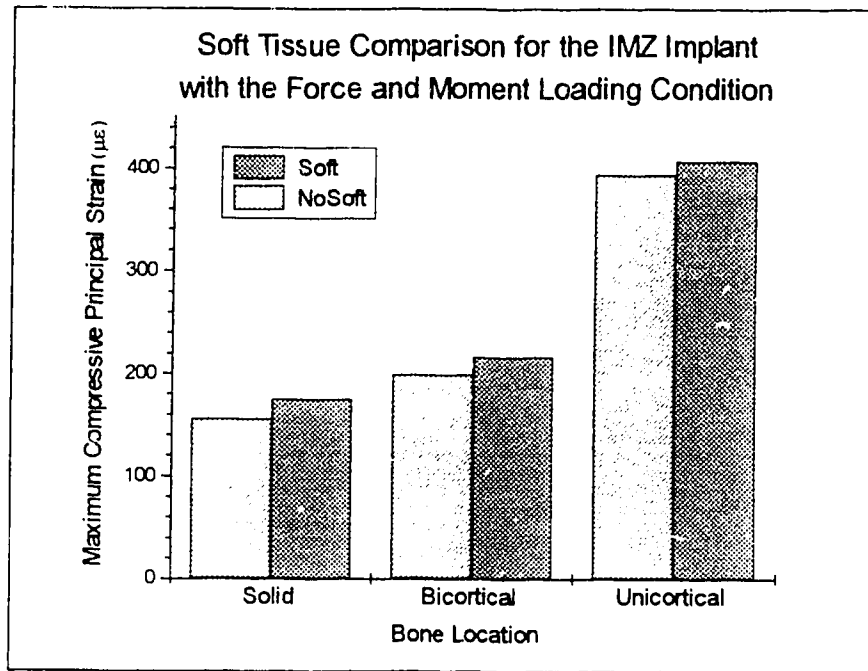


Figure 4-39: Soft Tissue Comparison for the IMZ Implant in the three Bone Configurations for the Force and Moment Loading Condition.

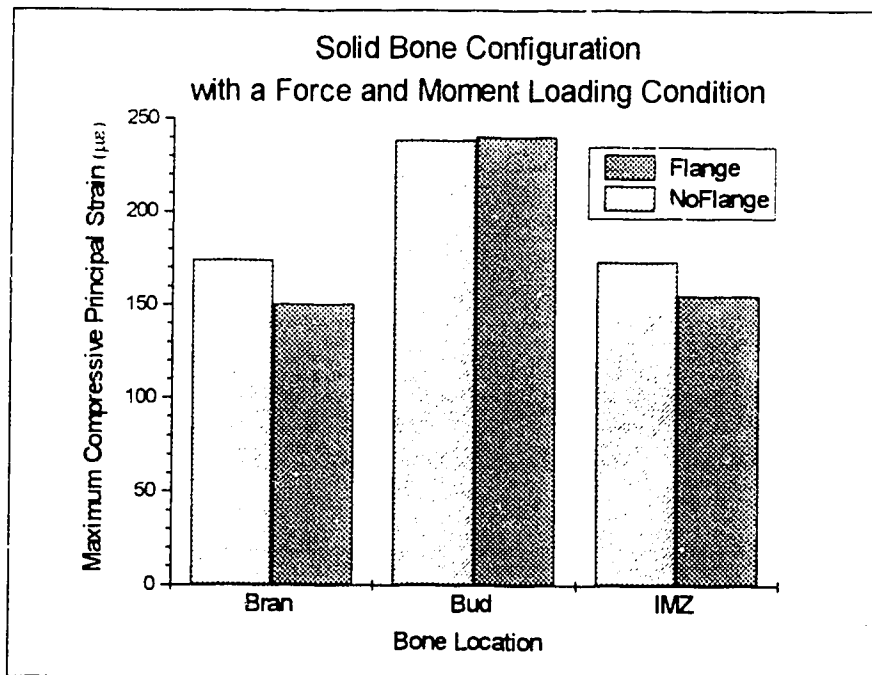


Figure 4-40: Comparison of the Minimum Principal Strain with and without the Flange for the Three Implants in Solid Bone with the Force and Moment Loading Condition

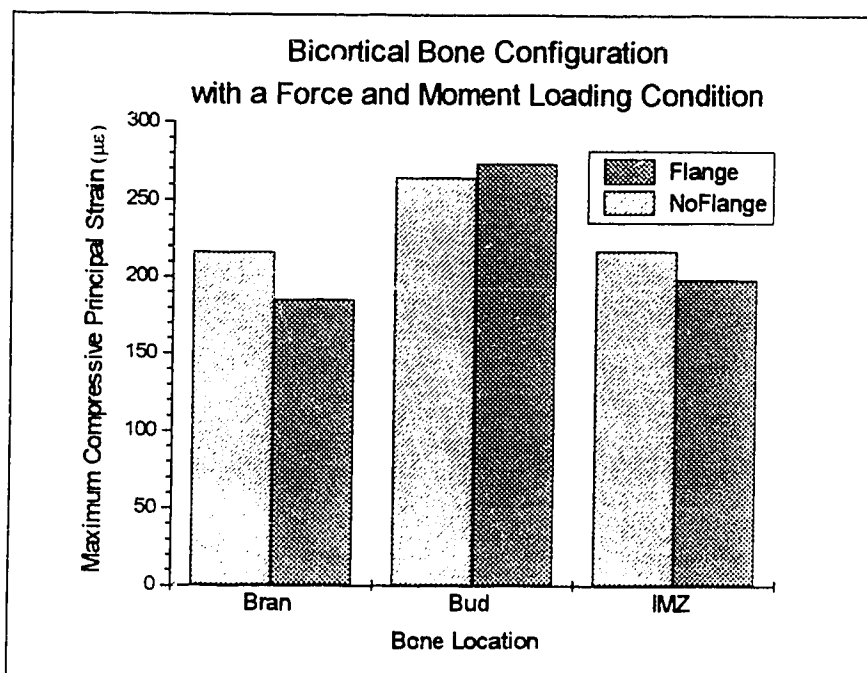


Figure 4-41: Comparison of the Minimum Principal Strain with and without the Flange for the Three Implants in Bicortical Bone with the Force and Moment Loading Condition

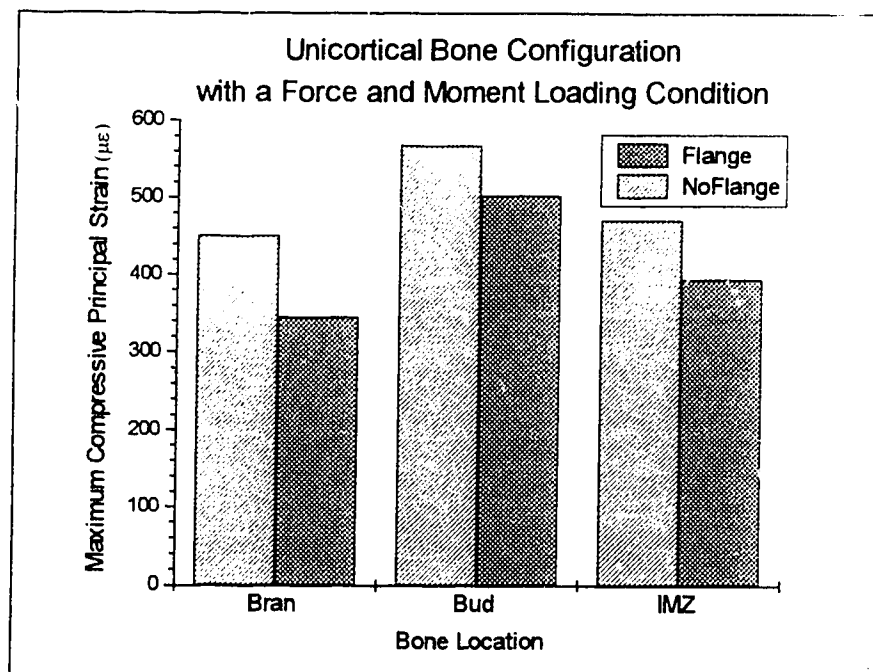


Figure 4-42: Comparison of the Minimum Principal Strain with and without the Flange for the Three Implants in Uncortical Bone with the Force and Moment Loading Condition

very small and may not be significant compared to the accuracy of the model which is discussed later.

On average the compressive principal strain in the cortical bone, averaged for the three bone configurations, increased by 21% for the Brånemark implant, while the Bud and IMZ implants displayed an increase of 7% and 13% respectively. As an example Figure 4-29 and Figure 4-43 display the compressive principal strain distribution for the Brånemark implant with and without the flange. These figures show a slight increase in strain when the flange was removed along with a relocation of areas of maximum strain from under the tip of the flange to the top of the bone near the neck of the implant. It was also noticed that the strain along the bone near the side or threads of the implant increased when the flange was removed. Overall the flange did seem to decrease the maximum strain slightly and had an effect on the distribution of strain in the bone.

4.3.4 Comparison of the Two Loading Conditions

In general it was noticed that the vertical load with a moment loading condition produced significantly higher strains for all of the implants in all of the bone configurations when compared to the vertical load with no moment loading condition. When Figure 4-5 is compared to Figure 4-28 it can be seen that the maximum magnitude of the compressive principal strain increased significantly when the moment was added. On average the strain on the solid bone configuration increased by approximately 6.9 times, while for the bicortical and unicortical configuration the increase was approximately 3.5 and 4.6 times respectively. The vertical load with a moment loading condition also produced a significant difference in the location of tension and compression in the bone. For example

Figure 4-13, which displays displacement and general regions of tension and compression for the IMZ implant in unicortical bone with a vertical load, shows that the cortical plate under the flange was under compression while areas near the bottom of the cortical plate next to the implant was under tension. These areas of compression and tension were of course identical along any path in the hoop direction. For the vertical load and a moment loading condition there was only one plane of symmetry for the strain fields in the bone. The deformation illustrated in Figure 4-34 displays the regions of tension and compression under the flange for the IMZ implant in bicortical bone as well as the change from compression to tension as you move in the hoop direction.

4.4 Discussion

4.4.1 Examination of Stress in the Bone.

In general terms the comparisons that have been done based on the strain in the bone give a good overall picture of the differences that occur for the various loading conditions, implant designs and bone configurations. If these comparisons were redone using stress instead of strain as a basis there would be very little difference noticed in the results. For example it was mentioned that the strain in the solid bone, averaged for the three implants, increased by 6.9 times when the loading condition was changed from the vertical load only to the vertical load and moment loading condition. If this comparison was based on stress instead of strain a similar increase of 6-7 times would have been noticed in the levels of stress between the two loading conditions.

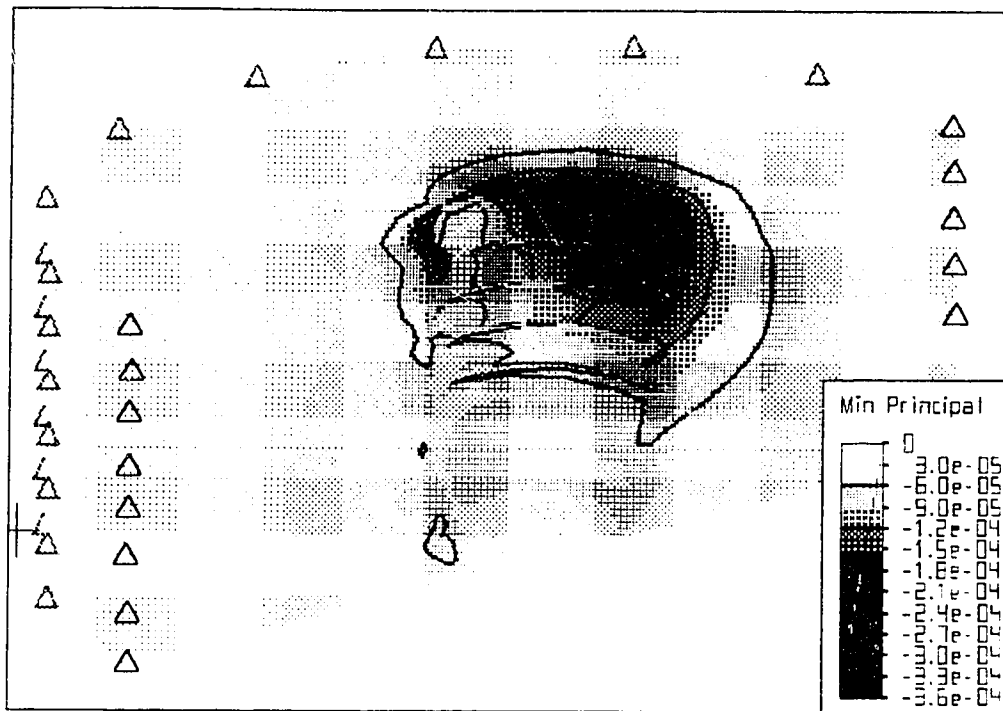


Figure 4-43: Minimum Principal Strain for the Brånemark Implant in Solid Bone with the Flange Removed for the Force and Moment Loading Condition.

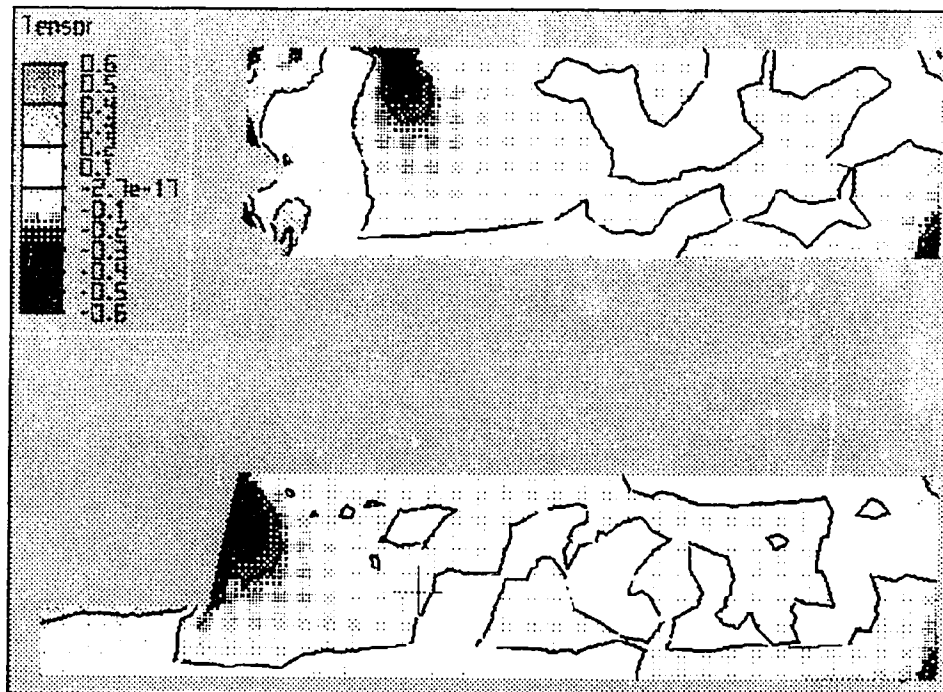


Figure 4-44: Vertical Stress (measured in MPa) for the Brånemark Implant in Bicortical Bone with the Flange in Contact and the Vertical Force only Loading Condition

Some details, however, are more easily defined by examining the stress instead of the strain in the bone. For example Figure 4-44 displays the vertical stress picture for the Branemark implant in bicortical bone with a force only loading condition (the units used are MPa). This figure shows much more clearly the vertical load that is transferred to the bone from the flange. It also illustrates that the vertical stress is concentrated at the tip of the flange.

The stress picture also clearly shows the fact that the cancellous bone for the unicortical and bicortical configurations does not carry much load. Figure 4-45, which displays the Von Mises stress picture for the Brånemark implant in bicortical bone with a cancellous bone layer loaded with a force and a moment, shows that the cancellous layer which appeared highly strained in Figure 4-38 is not highly stressed. The high strains in this layer are therefore due to its low modulus of elasticity.

4.4.2 Overall Effects of Variables

The variables that seemed to have the most effect on the strain in the bone were the loading conditions and the configuration of the cortical bone. For the force and moment loading condition the design of the implant was also important. The force with a moment loading condition produced strains of 3 to 7 times higher than the vertical load only loading condition. As this loading is equivalent to the vertical load applied 10 mm from the axis, this result was expected. The additional stresses were caused by the addition of the couple placed on the system. For both loading conditions the magnitudes of the forces and moments were set at values that were considered reasonable (see Chapter 2). Given the linear elastic nature of the models it should be noted that if the

vertical load was changed the strains in the bone for both loading conditions would change in a similar proportion. In a similar way if the moment arm was changed for the force and moment loading condition the strains produced in the bone from the couple would change in a similar proportion. Therefore using the principal of superposition for the vertical load and the moment the magnitudes of the strains produced in the models could be linearly scaled up or down to estimate the strain produced for a variety of loading conditions.

The configuration of the cortical bone (i.e. the solid, bicortical and unicortical bone) was also a major factor that affected the strain state in the bone. For the vertical load alone the relationship between the strain in the bone and the three different bone configuration showed that increasing the amount of cortical bone at the site decreased the magnitudes of the strains. As expected, when the thickness of the bone was increased or a second plate was added the volume of material able to carry the load increased and the displacements and strains in the bone were reduced. For the vertical load and a moment loading condition the influence of the amount of bone on the strain was also a function of the distribution of the bone. In general the thickness of the solid bone was around 4.6 mm which was about 50% greater than the combined thickness of 3.0 mm for the bicortical plates but the two bone configurations had similar maximum strain magnitudes. This result is similar to the situation for a beam in pure bending as shown in Figure 4-46. Axial tension is induced by the moment at the top of the beam and compression at the bottom. The center portion of the beam, however, is not highly stressed and does not carry much of the load. If the center portion was removed the magnitudes of the tension and

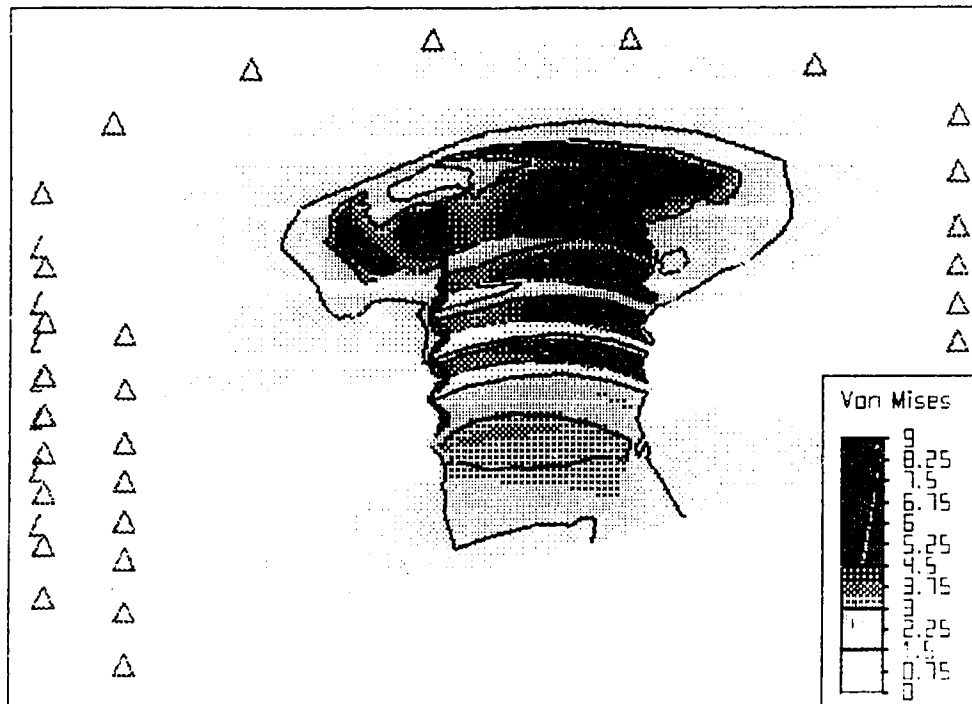


Figure 4-45: Von Mises Stress Picture (measured in Mpa) for the Brånemark Implant in Bicortical Bone with a Cancellous Bone Layer and the Force and Moment Loading Condition.

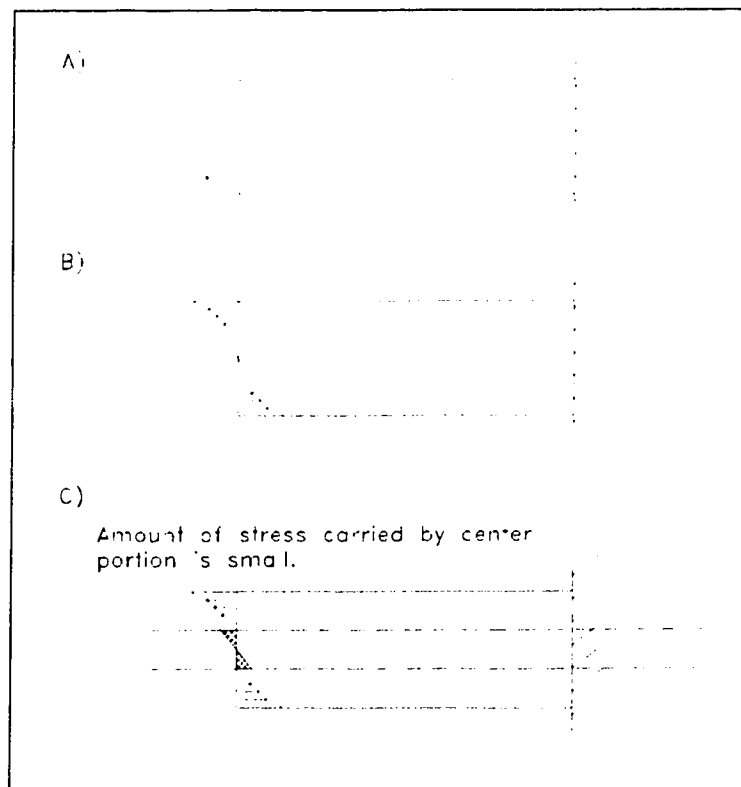


Figure 4-46 Axial Stress Placed on a Beam in Pure Bending

compression at the top and bottom of the beam would have to increase by only a small amount to compensate. In a similar way, when the center portion of the solid bone was removed to form the bicortical configuration, there was very little change noticed in the maximum strain because the center portion was not carrying a significant portion of the load. In general it is expected that having the top and bottom of the implant engaged in cortical bone will help reduce the stresses and strains caused by any moments placed on the implant.

As previously mentioned the type of implant used for the force and moment loading condition also had a large effect on the state of strain in the bone. It was noticed that the Bud implant induced strains in the bone that were approximately 33% more than the other two implants when loaded with a force and a moment. It was noted that the diameter of the Bud implant at its neck was around 2.43 mm while the Brånemark and IMZ implants had diameters of 3.15 mm and 3.3 mm respectively. Since the maximum strains in the bone usually occurred near the neck of the implant, a finite element model was tested with a modified Bud implant that had a diameter of 3.26 mm at its neck while the length and the threads on the implant were not altered. Figure 4-47 displays the compressive principal strain for the modified Bud implant in solid bone with the force and moment loading condition. When comparing this figure with Figures 4-29 to 4-31 it can be seen that the strain in the bone for the modified implant was greatly reduced. In fact, as listed in Table 4-2, the maximum magnitude for the compressive principal strain was for the modified implant in solid bone was -158.1 micro strain which was reduced by about 30% and more in line with the strains produced by the other two implants. From the

Figures 4-29 to 4-31 it can also be seen that increasing the diameter of the Bud implant did not greatly effect the locations of high strain in the bone. The strains remained highest near the neck of the implant under the flange and along the plane of symmetry. As a point of interest the same type of modification was done on the Brånemark implant. Its neck diameter was changed from 3.15 to 5.00 mm. As shown from Figure 4-48, the strain were reduced from the original case but like the Bud the general strain patterns remained the same. It therefore appears that the difference noticed for the Bud implant was almost entirely due to its smaller diameter neck. While it still may be argued that implant thread design influences bone remodeling the above analysis did not show appreciable differences in either the maximum strains developed or the distribution of strains in the bone neighboring the implant. The implication is that factors other than simply mechanical loading may be responsible for the degree of bone remodeling that occurs near the threads.

Other variables that had a smaller effects on the strain in the bone were the removal of the flange, the introduction of cancellous bone and the introduction of the soft tissue.

The removal of the flange increased the strain in the bone anywhere from 5% to 21% depending on the implant, loading and bone configuration. It was noted that the differences in the flange designs on the implant resulted in a variety of effects on the strain in the bone. The Bud implant, which has the smallest flange, had on average only 5% - 7% increase in the strain of the bone when the flange was removed. Removal of the flange for the Brånemark implant, which had the largest flange, showed increases of only about 20% in the maximum magnitude of the compressive principal strain for the various loading

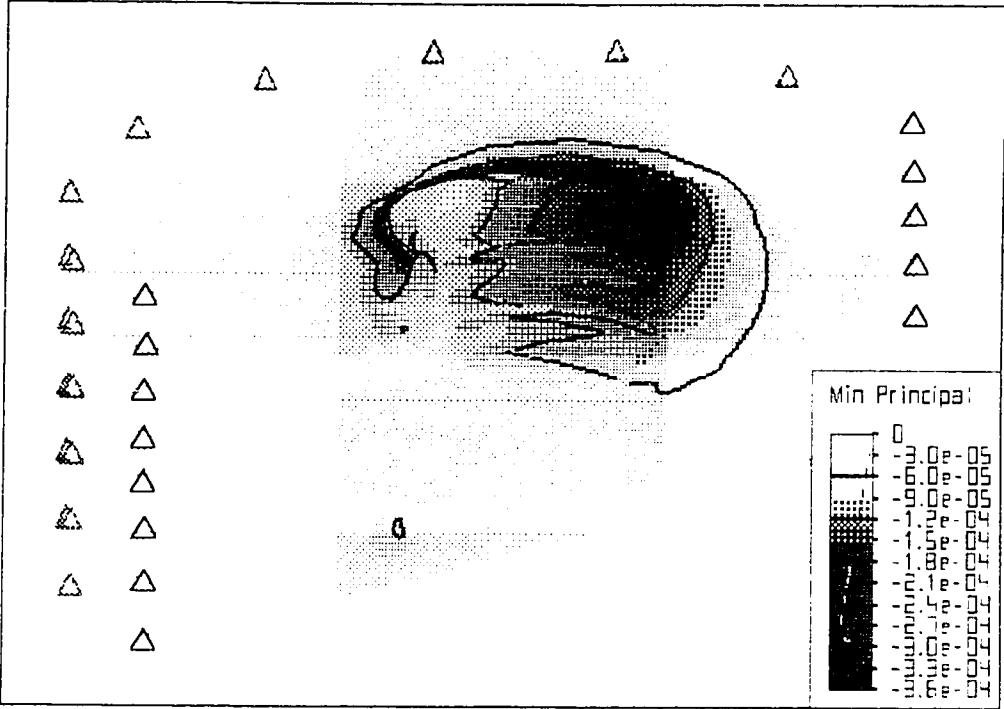


Figure 4-47: Minimum Principal Strain for the Modified Bud Implant in Solid Bone with the force and Moment Loading Condition

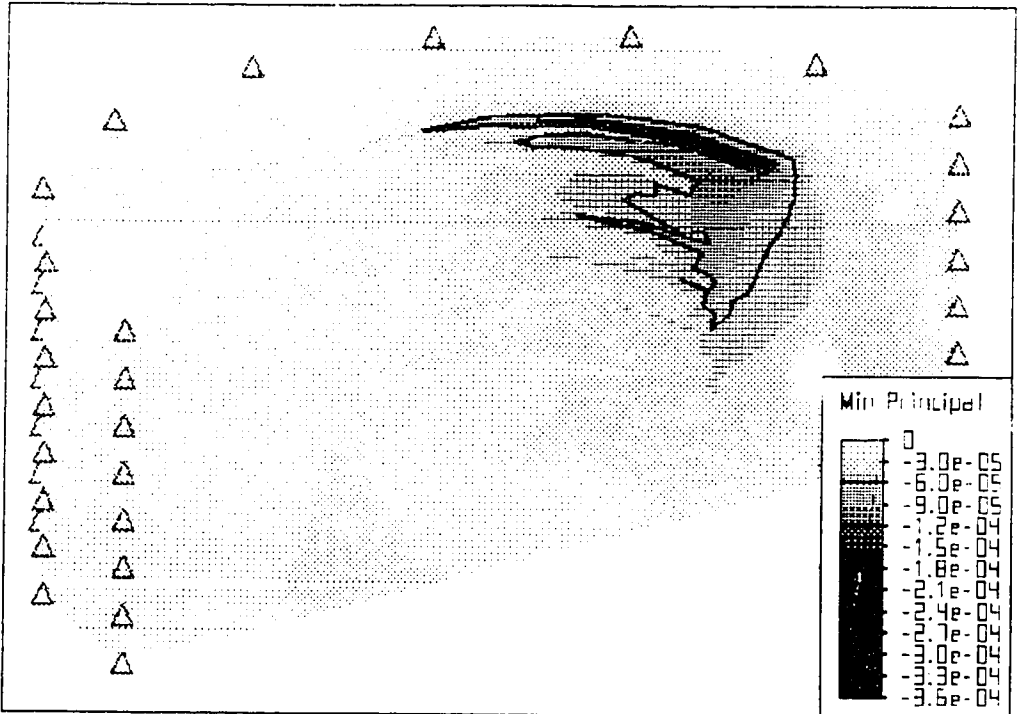


Figure 4- 48: Minimum Principal Strain for the 5.0 mm diameter (at the neck) Brånemark Implant in Solid Bone with a Force and Moment Loading Condition.

conditions and bone configurations. It was noticed, however, that in all of the cases that the removal of the flange did relocate areas of high strain in the bone from under the tip of the flange to the neck of the implant.

An additional factor that produced a small but significant change in the strain of the bone was the introduction of cancellous bone in the bicortical and unicortical bone configurations. As mentioned the compressive principal strain in the cortical bone was reduced by only 21% to 8% in the unicortical and bicortical configuration when the cancellous bone was introduced. The high strains, however, that were noticed in the model for the cancellous bone layer may provide insight into how the cancellous layer and the cortical bone together remodel under load.

The introduction of the soft tissue around the implant resulted only in a small change in the magnitudes and locations of strain in the bone. The introduction of the soft tissue decreased the magnitude of the strain in the bone by approximately 7% - 12%. The distribution and locations of high strains in the bone were almost completely unaffected by the soft tissue. As mentioned in Chapter 3 the properties and thickness of the soft tissue were only a rough estimate of the actual soft tissue that might occur at the implant site. In general it is felt that further study into the implant and bone interface and the tissues that develop at this interface is needed to improve the accuracy of current computer models.

4.4.3 Discussion of Model Limitations

The computer models used were an approximation to the mechanical behavior of real bone. Unlike many of the finite element analyses reported in the literature the current models were constrained only along the outer edge and not along the bottom. This is

believed to be a more realistic situation as constraining the model along the bottom implies that the material under the bone is more rigid than the bone itself. In addition our models included bone configurations with thickness for cortical layers which are more representative of those found in craniofacial applications.

The implant-bone interface was given a "welded" or joined type bond which is probably an overestimation of a true osseointegrated interface. As a result areas of high radial tension in the bone at the implant interface (like the one displayed in Figure 4-10) may indicate regions where the bone and implant could separate. A separation in a region such as this would cause a redistribution of the strain field.

The bone was assumed to be linear elastic, homogenous and isotropic. Although these assumptions are currently accepted they do impose a certain degree of uncertainty in the model. For example the model of the cortical bone, which is better described as an orthotropic material with properties that can vary between patients and bone location, could produce strain patterns that are different to some degree than the ones observed. Also, areas of compression and tension were not treated differently in the model but the bone probably responds differently to compressive and tensile loads. The above assumptions may also produce a much larger inaccuracy for the cancellous bone models. This due to the orientated structure of the bone which is made up of slender lamellae. Therefore the current method of modeling this bone as a uniform and isotropic structure with a reduced modulus is probably over simplistic. In addition it was assumed that the bone filled in all of the space next to the implant and its threads and that all of the bone had similar properties throughout the model for a given bone type, i.e. cortical or

cancellous bone. Further experimental evidence on the structure of the bone and its material properties, especially for the craniofacial region, would help to improve understanding on how these assumptions affect the accuracy of the model and how the models could be improved. In addition a majority of the comparisons were done based on the compressive principal strain in the cortical bone. As indicated in Chapter 1, current theories on bone remodeling point to the strain as a factor in bone remodeling but it is generally felt that bone remodeling is quite complex and that all of the factors that could come into play are not completely understood.

It should also be noted that the bone plug radius of 6.5 mm radially was an approximation of what might occur clinically. A test was done to determine what effect the radius had on the strain in the bone. It was found that as the radius was increased the magnitudes of the strains increased slightly and when the radius was decreased the strain in the bone decreased slightly. For example when the bone radius for the IMZ implant in solid bone with a vertical load was increased from 6.5 to 7.5 mm the maximum magnitude of the compressive principal strain was 24.6 micro strain which was an increase of 3% from the standard bone radius. A similar result was noticed for the IMZ implant in unicortical bone with the force and moment loading condition, when the bone radius was increased from 6.5 to 7.5 mm the maximum magnitude of the compressive principal strain increased by 4% from 393.7 to 411.1 micro strain. In general the changes in the strain due to changes in the bone radius were quite small so that the results of the comparisons done in the study would not have changed significantly if different bone radii were used.

5. CONCLUSIONS AND IMPLICATIONS

5.1 Conclusions

The objectives of the present study were to improve the understanding of the mechanical loads applied to craniofacial osseointegrated implants and to examine how these loads are carried by the surrounding hard tissue. With respect to the first objective it was found in Chapter 2 that the force required to remove a prosthesis from an implant was about 4 - 11 N for a single attachment. The magnitude of this force is quite significant when it is compared to the 25 N peak load that was recorded for implant loading in the oral environment during mastication (see Chapter 1). The load is even more significant considering that the bone volume surrounding the implant in the mandible and maxilla is far greater than that found in the craniofacial environments. These experimental observations also made apparent the obvious benefits of using implants over adhesives for improved strength and reliability for retaining facial prostheses.

The forces determined experimentally were used in a finite element study of various implants and bone configurations of typical craniofacial environments. This study attempted to determine how various factors, such as implant design and bone structure, affected the state of strain in the bone. It was found that the bone configuration (i.e. solid, bicortical and unicortical) and the type of load had the largest influence on the state of strain in the bone. For example, it was found that the strain in the bone for the Brånemark

implant in solid bone with a vertical load increased by a factor of 15 when the implant was placed in unicortical bone and loaded with a force and a moment.

Surprisingly, there were very few differences in the strain produced in the bone for the various implant designs. The only design factors that seemed to cause a large effect were the flange and the diameter of the implant at its neck when it was loaded with a force and a moment. In general the flange did reduce the maximum strain in the bone by about 7 to 21% and relocated some of the strain from near the neck of the implant to the tip of the flange. It was noticed that the flange on the Brånemark implant, which was the largest, seemed to have a greater effect on the strain in the bone than did the other flanges.

The neck diameter of the Bud implant was 32% smaller than the other two implants and it produced strains that were on average 33% higher when loaded with a force and a moment. The reason for the discrepancy in the strains would appear to be almost entirely due to the differences in the neck diameter since it was noted that the Bud implant produced strain levels that closely matched the other two when its diameter was increased.

5.2 Implications of the Results

As discussed in Chapter 1 it is felt that the bone has a variety of responses for different levels of strain. Frost's theory explains that there are regions of strain that induce bone resorption and bone formation. Frost gives an estimation of the strain levels that will induce the various responses but, these levels probably change significantly between patients and bone locations. For example it may be anticipated that the mandible, which is used to constant loading, will respond differently for a given strain level than the mastoid

region which does not normally receive direct loading. It may also be speculated that regions treated with radiation therapy (for cancers) could have different strain responses due to the nature of radiated bone. It is known that implants in the craniofacial region have a good degree of long term success. Although there are many factors that determine the success rate of osseointegrated implants it can therefore be assumed that the level of strain that is present in the bone is probably in the region that induces equilibrium or bone resorption and formation. It is important then to determine what the strain response levels are for the craniofacial environment and to ensure that the strain in the bone is maintained at the appropriate levels.

In Chapter 4, the uncertainty present in the models is certainly of some concern especially if exact strain levels are required. It is very difficult to determine the exact degree of uncertainty that is present in the finite element results. As an example, changes in material properties and boundary conditions could easily change the results by approximately 10-20%. Consequently it is proposed that the benefit of the finite element study was not in predicting the exact strain levels in the bone but rather in comparing how various implants and bone configurations changed the state of strain. The results show the clinician that both the magnitudes of the moments and the amount of bone at an implant site is critical to the amount of strain that is present in the bone and that factors such as the thread design may have very little mechanical effect. Observations of the various bone responses to different moment magnitudes and bone thickness will aid in providing a better model for bone strain responses for craniofacial environments.

REFERENCES

- [1] Brånemark, P., Zarb, G. A., Albrektsson, T. *Tissue-Integrated Prostheses Osseointegration in Clinical Dentistry*. Chicago, London, Berlin, Sao Paulo and Tokyo, Quintessence Publishing Co., Inc 1985
- [2] Cowin, S.C. *Bone Mechanics*. CRC Press Boca Raton, Florida 1989
- [3] Hoshaw, S.J. *Investigation of Bone Modeling and Remodeling at a Loaded Bone-Implant Interface*, Ph.D. Thesis, Rensselaer Polytechnic Institute, 1992
- [4] Clelland N.L., Ismail Y.H., Zaki H.S., Pipko D. "Three Dimensional Finite Element stress Analysis in and Around the Screw-Vent Implant". *International Journal of Oral & Maxillofacial Implants*, Volume 6, Number 4, Pages 391 - 398, 1991
- [5] Meroueh K. A., Watanabe F. and Mentag P. J. "Finite Element Analysis of Partially Endentulous Mandible Rehabilitated with an Osteointegrated Cylindrical Implant" *Journal of Oral Implantology*, Volume 8, Number 2, Pages 215 - 237, 1987
- [6] Rieger M.R., Adams W.K., Kinzel G.L., Brose M.O. "Finite Element Analysis of Bone-Adapted and Bone-Bonded Endosseous Implants", *Journal of Prosthetic Dentistry*, Volume 62, Number 4, Pages 436-440, 1989
- [7] Frost, H. M. "The Mechanostat: a Proposed Pathogenic Mechanism of Osteoporoses and the Bone Mass Effects of Mechanical and Nonmechanical Agents." *Bone and Mineral*. Volume 12, Pages 73-85 1987
- [8] Rieger, M.R., Mayberry, M., and Brose, M.O. "Finite Element Analysis of Six Endosseous Implants." *The Journal of Prosthetic Dentistry*. Volume 63, Number 6, Pages 671-676, 1990
- [9] Clelland, N.L., Ismail, Y.H., Zaki, H.S., Pipko, D. "Three Dimensional Finite Element Stress Analysis in and Around the Screw-Vent Implant." *The International Journal of Oral and Maxillofacial Implants*. Volume 6, Number 4, Pages 391-398, 1991
- [10] Maatsushita, Y., Kitoh, M., Mizuta, K., Ikeda, H., Suetsugu, T. "Two-dimensional FEM Analysis of Hydroxyapatite Implants: Diameter Effects on Stress Distribution." *Journal of Oral Implantology*. Volume 16, Number 1, Pages 6-11, 1990
- [11] del Valle V. R., Faulkner, M.G., Wolfardt J. F., Rangert B. "Mechanical Evaluation of Craniofacial Osseointegration Retention Systems" *The International Journal of Oral and Maxillofacial Implants*. In Press.

- [12] Tam, V. Faulkner, M.G., Wolfaardt, J.F. "Apparatus for the Mechanical Testing of Maxillofacial Prosthetic Adhesives." *The Journal of Prosthetic Dentistry*; Volume 67, Pages 230-235, 1992
- [13] Wolfaardt, J.F., Tam, V., Faulkner, M.G., Prasad, N. "Mechanical behavior of three maxillofacial prosthetic adhesive systems: a pilot project." *The Journal of Prosthetic Dentistry*; Volume 69, Pages 943-949, 1992
- [14] Glantz, P.O., Rangert, B., Svensson, A., Stafford, G. D., Arnvidarson, B., Randow, K., Linden, U., Hulten, J. "On Clinical Loading of Osseointegrated Implants: A Methodological and Clinical Study." *Clinical Oral Implants Research* Volume 4, Pages 99 - 105, 1993
- [15] Robinson, J. *Understanding Finite Element Stress Analysis*, Robinson and Associates Wimborne Dorset England, 1981